AD-A034 262

MECHANICAL PROPERTIES OF CERAMICS FOR HIGH TEMPERATURE APPLICATIONS

ADVISORY GROUP FOR AEROSPACE RESEARCH AND
DEVELOPMENT, PARIS, FRANCE

DECEMBER 1976

DISCLAIMER NOTICE

THIS DOCUMENT IS BEST QUALITY
PRACTICABLE. THE COPY FURNISHED
TO DTIC CONTAINED A SIGNIFICANT
NUMBER OF PAGES WHICH DO NOT
REPRODUCE LEGIBLY.

REPORT DOCUMENTATION PAGE

1. Recipient's Reference	2. Originator's Reference	3. Further Reference	4. Security Classification of Document
	AGARD-R-651	ISBN 92-835-1232-5	UNCLASSIFIED

5. Originator	Advisory Group for Aerospace Research and Development North Atlantic Treaty Organization 7 rue Ancelle, 92200 Neuilly sur Seine, France

6. Title	MECHANICAL PROPERTIES OF CERAMICS FOR HIGH TEMPERATURE APPLICATIONS

7. Presented at	the 43rd Meeting of the Structures and Materials Panel of AGARD, in October 1976.

8. Author(s)	9. Date
Various	December 1976

10. Author's Address	11. Pages
Various	60

12. Distribution Statement	This document is distributed in accordance with AGARD policies and regulations, which are outlined on the Outside Back Covers of all AGARD publications.

13. Keywords/Descriptors

Ceramics	Fracture properties
Mechanical properties	Creep properties
High temperature tests	Design criteria

14. Abstract

The Structures and Materials of AGARD has been actively involved in high temperature materials and their mechanical properties for a number of years. The Panel organized a Working Group on High Temperature Material Testing in 1966, and in 1971 published its results on a cooperative creep testing program as AGARD Report 581. The Panel followed up that activity by forming a Working Group on Low-Cycle High Temperature Fatigue. The Group first undertook a survey of current activities and test methods used in this field, published as AGARD Conference Proceedings 155. The Panel's current Sub-Committee on High Temperature Materials is conducting, as its primary activity, a cooperative program on the characterization of low-cycle, high temperature fatigue by strainrange partitioning techniques. In view of the current interest in ceramics for use in high temperature turbine engine applications in many of the NATO nations, however, the Sub-Committee has undertaken several activities in this area as well.

Two invited papers on analytical techniques for the determination of localized stresses and strains and the application of fracture mechanics, proof testing, and life prediction techniques to ceramics were presented at the Panel's 40th Meeting in April 1975 and published as AGARD Report 634. Three additional papers were invited for presentation at the 43rd Panel Meeting in October 1976 and are published in this report. These papers covered in greater detail the fracture mechanics, high temperature creep properties, and design aspects of ceramic materials.

014059

AGARD

ADVISORY GROUP FOR AEROSPACE RESEARCH & DEVELOPMENT

7 RUE ANCELLE 92200 NEUILLY SUR SEINE FRANCE

AGARD REPORT No. 651

on

Mechanical Properties of Ceramics
for High Temperature Applications
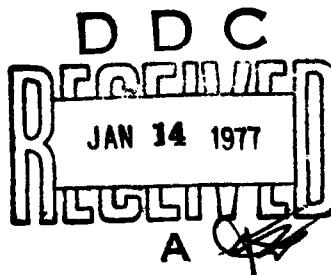
DDC

RECEIVED

JAN 14 1977

A

NORTH ATLANTIC TREATY ORGANIZATION

**DISTRIBUTION AND AVAILABILITY
ON BACK COVER**

DISTRIBUTION STATEMENT A

NORTH ATLANTIC TREATY ORGANIZATION

ADVISORY GROUP FOR AEROSPACE RESEARCH AND DEVELOPMENT

(ORGANISATION DU TRAITE DE L'ATLANTIQUE NORD)

AGARD Report No.651

MECHANICAL PROPERTIES OF CERAMICS FOR

HIGH TEMPERATURE APPLICATIONS

THE MISSION OF AGARD

The mission of AGARD is to bring together the leading personalities of the NATO nations in the fields of science and technology relating to aerospace for the following purposes:

- Exchanging of scientific and technical information;

- Continuously stimulating advances in the aerospace sciences relevant to strengthening the common defence posture;

- Improving the co-operation among member nations in aerospace research and development;

- Providing scientific and technical advice and assistance to the North Atlantic Military Committee in the field of aerospace research and development;

-- Rendering scientific and technical assistance, as requested, to other NATO bodies and to member nations in connection with research and development problems in the aerospace field;

- Providing assistance to member nations for the purpose of increasing their scientific and technical potential;

- Recommending effective ways for the member nations to use their research and development capabilities for the common benefit of the NATO community.

The highest authority within AGARD is the National Delegates Board consisting of officially appointed senior representatives from each member nation. The mission of AGARD is carried out through the Panels which are composed of experts appointed by the National Delegates, the Consultant and Exchange Program and the Aerospace Applications Studies Program. The results of AGARD work are reported to the member nations and the NATO Authorities through the AGARD series of publications of which this is one.

Participation in AGARD activities is by invitation only and is normally limited to citizens of the NATO nations.

Published December 1976

ISBN 92-835-1232-5

PREFACE

The Structure s and Materials Panel of AGARD has been actively involved in high temperature materials and their mechanical properties for a number of years. Increasing performance requirements for military aircraft o· er the years have imposed harsh high temperature strength and creep resistance requirements on materials, particularly for turbine engine construction. More recently there has also been increasingly widespread concern about the reliability and durability of high temperature components in service. This has been accompanied by an increasing interest not only in improved materials, but also in improved methods for describing their behavior under complex engine environments and in improved means of predicting material and component lifetimes.

In response to these needs, the Panel organized a Working Group on High Temperature Material Testing in 1966, and in 1971 published its results on a cooperative creep testing program as AGARD Report 581. The Panel followed up that activity by forming a Working Group on Low-Cycle High Temperature Fatigue. The Group first undertook a survey of current activities and test methods used in this field, published as AGARD Conference Proceedings 155.

The Panel's current Sub-Committee on High Temperature Materials is conducting, as its primary activity, a cooperative program on the characterization of low-cycle, high temperature fatigue by strainrange partitioning techniques. In view of the current interest in ceramics for use in high temperature turbine engine applications in many of the NATO nations, however, the Sub-Committee has undertaken several activities in this area as well.

Two invited papers on analytical techniques for the determination of localized stresses and strains and the application of fracture mechanics, proof testing, and life prediction techniques to ceramics were presented at the Panel's 40th Meeting in April 1975 and published as AGARD Report 634.

To assist member nations in guiding their current efforts in the mechanical property testing and use of ceramics and to assist the Panel in its formulation of future activities in this area, three additional papers were invited for presentation at the 43rd Panel Meeting in October 1976. These papers covered in greater detail the fracture mechanics, high temperature creep properties, and design aspects of ceramic materials. They were very well received and generated extensive discussion. They are offered here in the hope that they will stimulate others in their efforts to develop high temperature ceramic structural components.

The Panel is deeply indebted to the authors for their efforts in preparing and presenting these papers.

Norman M.TALLAN
Chairman
High Temperature Materials
Sub-Committee

iii

CONTENTS

CREEP OF CERAMIC MATERIALS FOR
GAS TURBINE APPLICATION

by

Prof. Dr. Fritz Thümmler
Dipl.-Ing. Georg Grathwohl
Institut für Werkstoffkunde II
der Universität (TH) Karlsruhe,
Institut für Material- und Festkörperforschung
des Kernforschungszentrums Karlsruhe
Postfach 3640
D-7500 Karlsruhe 1

SUMMARY

The creep properties of silicon nitride and silicon carbide are important with respect to their possible application in gas turbines. After introductory chapters on general aspects of creep including creep mechanisms common and unusual testing procedures and evaluations are outlined. The creep of different types of Si_3N_4, Sialons and of SiC is reviewed and compared, considering the important influences of purity, microstructure and environment. Relations of creep to fatigue and to the delayed fracture phenomenon have been mentioned. In the last paragraph some open questions and future research requirements are discussed.

1. INTRODUCTION

The possible use of ceramics for high performance engineering applications is one of the most exciting approaches in today's material science and technology. In gas turbines the gas inlet temperatures could be raised as high as to 1300° or 1350°C by use of silicon nitride or silicon carbide for the main turbine parts. It is well known that the main difficulties to be overcome are related to the brittleness of ceramics, i.e. the impossibility of stress relaxation by microplastic flow at low temperatures. The application of these materials at high temperatures raises also other material problems mainly with respect to creep and chemical reactions. An adequate creep resistance is mainly important for the rotating turbine parts. A high creep rate leads not only to unallowed elongations but also to uncontrolled stresses in the transition zones between crept and non crept material after cooling down. In spite of the general agreement with respect to use creep resistant materials for turbine construction it is difficult to get definite figures of tolerable creep strain from the designer. For reaction bonded silicon nitride (RBSN) less than 0.5% creep at 1260°C, ~70 MN/m² and 200 hrs was sheduled for turbine components /1,2/. Nevertheless, the relevance of the creep phenomenon with respect to material specifications seems not to be fully established so far.

Creep properties have been investigated extensively by many researchers during the last decade or even before, but very different and in some cases hardly comparable results have been achieved. This is true for the hot-pressed Si_3N_4 (HPSN) as well as for the RBSN material and also for SiC. Nevertheless some consistency has been achieved recently with respect to important aspects. Considering the chemical behaviour we must take into account the system: nonoxide ceramic – turbine gas as highly unstable in terms of thermodynamics. Thus, oxidation starting from the surface occurs, depending strongly on the temperature regime as well as from the materials quality.

In this paper, at first some general aspects of creep in ceramics will be lined out, followed by a paragraphe of creep testing. The most important creep results of HPSN, RBSN, Sialons and SiC will be reviewed. A special purpose of this paper is to point out the numerous parameters being important for the creep properties, including impurity and environmental influences. In addition some related or competitive phenomena to creep (fatigue, delayed fracture) will be mentioned shortly. Last, some proposals for further research will be summarized.

2. GENERAL ASPECTS OF CREEP AND CREEP MECHANISMS CONSIDERING CERAMIC MATERIALS

The phenomenon of creep as the most important aspect of the high temperature plasticity of matter is a slow plastic deformation under all sorts of stresses. It is observed in many types of engineering materials: metals and alloys, ceramics, glasses and polymers. Only short paragraphes can be devoted to the general aspect, comprehensive reviews are

available, e.g./3,4/.

The parameters involved in a creep experiment with a constant stress or a constant load excluding the sample itself are commonly: stress (σ), temperature (T) and time (t), the figures characterizing the creep behaviour are the plastic strain (ε) and the strain rate $d\varepsilon/dt = \dot{\varepsilon}$. Generally, the simple creep curve ε vs t ($\varepsilon(t)$) at a constant stress and temperature (Fig.1) can be divided into 3 parts: the primary or transient creep with a decreasing creep rate and the strain ε_t, the secondary or steady state creep (ε_s) with a constant (minimum) creep rate ($\dot{\varepsilon}_s$) and the tertiary creep (ε_{tt}). The latter is the part of the curve with an enhanced creep rate indicating the fracture of the sample in the near future. In Fig. 1 also the initial strain (ε_o), i.e. the elastic deformation (ε_{el}) plus some plastic strain during the time of loading is included. This initial strain is hard to define exactly. Thus, the summarized deformation during the experiment considering all the stages is

$$\varepsilon(t) = \varepsilon_o + \varepsilon_t + \varepsilon_s + \varepsilon_{tt} \qquad (1)$$

The summarized _creep_ deformation of the sample is

$$\varepsilon_{cr}(t) = \varepsilon(t) - \varepsilon_{el} \qquad (2)$$

or, with only little failure in many cases

$$\varepsilon_{cr}(t) \approx \varepsilon(t) - \varepsilon_o \qquad (2a)$$

The absolute and the relative extension of the three stages of the creep curve can be very different depending on material and experimental parameters.

TRANSIENT CREEP

The time dependence of ε_t have been formulated by different equations e.g. /5/ :

$$\varepsilon_t = a \cdot t^{1/3} \qquad (3)$$

This $t^{1/3}$ term allows to describe adequatly transient creep results of Cu, Ni-Co-alloys and steels between $\varepsilon_t = 1$ and 10%. Another approach was developed containing an e^{-mt}-term /6/. It was proved by creep results also found with different metals showing little difference to a plot after eq. (3). A logarithmic equation

$$\varepsilon_{t'} = a' \ln(1 + \frac{t}{t_o}) \qquad (4)$$

or in the simple form

$$\varepsilon_{t'} = a'' \log t \qquad (4a)$$

has been observed mainly at low temperatures ($T < 0.3 T_m$) and up to relatively small strain values in metals. Also graphite follows this equation below 1500°C /6/. Due to the strain and temperature limitations one can consider the logarithmic law to describe only a part of the transition creep curve /3/. For this reason the symbol $\varepsilon_{t'}$ has been choosen.

The most reasonable interpolation of the $\varepsilon(t)$ values during transient creep is given by the general parabolic form

$$\varepsilon_t = b \cdot t^{1-c} \qquad (5)$$

This form includes eq. (3). The differentiation leads to the creep rate

$$\dot{\varepsilon}_t = A \cdot t^{-c} \qquad (5a)$$

$$\text{with } b = \frac{A}{1-c}$$

Many experimental results on metals as well as on ceramics follow this equation. The value of c can vary, ranging e.g. from 0.4 to 0.8 /7/. From a basic point of view, the initial $\dot{\varepsilon}_t$ should be proportional to $\dot{\varepsilon}_s$ and the total strain in the primary range (ε_t) should be independent from σ and T /3/. According to /8/ primary as well as steady state creep should be controlled by the same constants and by the same elementary steps. Results on oxide nuclear fuel materials /10/ seem to meet this statement to some extent. On the other hand, the independence of ε_t from stress could not be verified in some metallic systems (for data s./3/), but the ε_t range increases with the stress. The same seems to be true for the ε_t range of RBSN as demonstrated by several $\varepsilon(t)$-curves up to 50 hrs /7/. This problem must not be confused with the dependence of $\dot{\varepsilon}_t$ on σ, both correlate at any rate. This was demonstrated also in /7/ and a relation

$$\dot{\varepsilon}_t \sim e^{B\sigma} \qquad (6)$$

has been observed. An equation, which includes time, temperature, stress and grain size (a) was proposed in / 9 /:

$$\dot{\epsilon}_t = (A \cdot \frac{\sigma}{a^{1.5}} \cdot \exp \frac{-Q}{RT}) \; t^{m-1} \qquad (7)$$

being compatible with (5a). The constant m was found to be 0.7 ± 0.1 for UO_2 with a grain size of 10 to 30 μm.

A discussion of the mechanisms of primary creep as proposed for metals would be of little value here, because it involves dislocation reactions in any case. In this stage hardening reactions are dominating over recovery and the main process seems to be the formation of sub-grains, in metals as well as in ceramics. In the ceramic material discussed below dislocation motion is very probably of small importance, especially during primary creep.

Nevertheless, the principal statement that the duration of primary creep is as long as considerable microstructural changes occur must be valid also for these substances. In oxide nuclear fuels /10/ a considerable grain growth, thermally activated as well as stress induced, has been found to be responsible for the decrease of $\dot{\epsilon}$ during transition creep. These processes could be clearly separated from the built-up of a dislocation network.

The microstructural changes in ceramics can occur due to at least one parameter more than in metals, namely the porosity. There is strong evidence, that ceramics with a higher pore volume exhibit a more extended ϵ_t-range than those with lower porosity, but such systems can undergo densification during creep by hot pressing effects.

An evaluation of the extension of primary creep due to grain boundary sliding combined with diffusion processes has been given by Raj and Ashby /19/. In a model of a dense polycrystalline material with hexagonal, purely elastic, grains and viscous boundaries a very limited sliding displacement of about 50 Å can occur when crack formation and grain boundary separation is not considered. The process stops when the internal stresses have built up to a sufficiently high level.

A transition creep range should not occur, if the creep process follows a pure diffusional Nabarro-Herring mechanism.

STEADY STATE CREEP

The steady state range ϵ_s is the most investigated part of the creep curve in metals and ceramics. The constant rate $\dot{\epsilon}_s$, i.e. the minimum rate which the material can undergo, is of principal engineering importance. The definition of the rate

$$\dot{\epsilon}_s = \frac{d\epsilon_s}{dt} \qquad \text{leads to the time}$$

dependence
$$\epsilon_s = \dot{\epsilon}_s \cdot t \qquad (8)$$

The exact evaluation of the onset of $\dot{\epsilon}_s$ is difficult, because $\dot{\epsilon}_t$ turns over in $\dot{\epsilon}_s$ continously. In addition, the beginning of $^s\dot{\epsilon}_s$ depends on the accuracy of the measurements as well as on the graphical representation ^{s}/11,12/. In tensile tests a difficulty arises due to sample cross section diminishing, resulting in a raise of the stress. In compression tests stress at constant load is decreasing during deformation. This must be considered mathematically, at least at larger strains /10/.

The extension of the ϵ_s range (as well as the creep properties in general and especially $\dot{\epsilon}_s$) depends mainly from microstructural parameters of the sample. After evaluation of precise creep measurements of stainless steel an influence of temperature and stress on the duration of $\dot{\epsilon}_s$ could not be observed, as long as microstructure is unchanged /13/. The onset of $\dot{\epsilon}_s$ indicates, that microstructure has reached something like an equilibrium and the substructure reached does not change during further creep. The end of $\dot{\epsilon}_s$ indicates the occurence of special types of (dangerous) microstructural changes.

Of course, the creep rate $\dot{\epsilon}_s$ is strongly influenced by temperature and stress as well as by structural parameters. The general equation[x)]

$$\dot{\epsilon}_s = A \cdot \sigma^n \cdot \exp (-Q/RT) \qquad (9)$$

seems to be valid for all creep mechanisms, discussed below and includes:

- structural parameters involved (mainly grain and subgrain size, character of "cells", porosity), in the factor A
- stress dependence, in the stress exponent n

[x)] more detailed: $\dot{\epsilon}_s = A \cdot (\frac{\sigma}{\mu})^n \cdot \sin h(\frac{V\sigma}{KT}) \cdot \exp (-Q/RT)$, see also eq. (16) (17) (18).

- temperature dependence, in the Arrhenius term exp $(-Q/RT)$

- Q being the activation energy of the rate controlling step.

This equation holds in many practical cases for certain ranges of stresses, strains and temperatures (provided structural parameters being unchanged during experiment). On the other hand, A, n and Q are no constants in principle: A and Q may be also a function of stress, strain and temperature, n (depending mainly from creep mechanism) may be a function of stress /3/. Thus a limited validity range of eq. (9) can be stated.

TERTIARY CREEP

The transition of $\dot{\epsilon}_s$ into $\dot{\epsilon}_{tt}$ occurs continously in a similar manner as the $\dot{\epsilon}_i$-$\dot{\epsilon}_s$ transition. The time of the beginning $\epsilon_{tt}(t_2)$ should be reciprocal to $\dot{\epsilon}_r$

$$t_2 \sim 1/\dot{\epsilon}_s \qquad (10)$$

if the independence of the ϵ_s-range on stress and temperature is valid /3/. Tertiary creep introduces fracture due to the growth of cracks in the critical size range. The total time to fracture (t_f) is found in many materials similar to eq. (10), namely

$$t_f = C \cdot {}^1/\dot{\epsilon}_s \qquad (10a)$$

This is a result of the principal geometrical similarity of most of the creep curves. It seems to be difficult to find a time dependence of ϵ_{tt} with broader validity for the entire tertiary range, because crack formation and growth under creep conditions are too complex processes. The equations

$$\epsilon_{tt} = a \cdot t^{4/3} \qquad (11)$$

and
$$\epsilon_{tt} = a \cdot \exp(p \cdot t) \qquad (12)$$

(a and p being constants) have been found experimentally for the first and for the second part, resp., of this range /3/. All these results have been achieved with metals and alloys.

CREEP MECHANISMS AND RATE DEPENDENCE ON STRESS, GRAIN SIZE AND POROSITY
IN THE STEADY STATE RANGE

At first, it is worthwhile to have a look on a so-called deformation mechanism map. Such general views have been established for metallic and nonmetallic materials during the last years. Fig. 2 represents this map for nickel and fig.3 for spinel. In these stress-temperature-plots one finds a number of fields, each with a certain mechanism which controlls the deformation process under these conditions. Further some curves for certain measured creep rates can be seen. The comparison of these figures show, that in metals and ceramics the same mechanisms of deformation occur, at least in principle. The importance of a single mechanism, on the other hand, with respect to the stress-temperature field can be different in ceramics and in metals, indeed.

At high temperatures and low stresses or even over a large stress range the <u>Nabarro-Herring creep</u> /15,16/ dominates. It is a purely volume diffusion controlled process, initiated by stress, resulting in a directed diffusional flow in order to relax the stress. The creep rate $\dot{\epsilon}$ is deviated as

$$\dot{\epsilon} = B \cdot \frac{\Omega \cdot D_v}{K \cdot T \cdot a^2} \cdot \sigma \qquad (13)$$

with B = a constant in the order of 10, depending on the geometry of the grains

Ω = volume of a point defect responsible for diffusion

D_v = volume diffusion coefficient

a = grain size (boundaries acting as sinks for vacancies)

σ = effective stress

The most important feature in this mechanism is the proportionality of $\dot{\epsilon}$ and σ, the characterizing relation of the viscous flow process. The $\dot{\epsilon} \sim 1/a^2$ relation is also significant for this mechanism. The temperature dependence of this process is controlled by the figure of D_v. In principle, this mechanism may occur during all three stages of creep, but it gets unimportant at such stresses, when considerable dislocation motion occurs. Due to their high dislocation mobility in metals it is very difficult to observe Nabarro-Herring creep in metallic materials, but it has been found in many ceramics and often investigated in Al_2O_3 /17/. With respect to a calculation of D_v-values from such creep experiments one must consider, that in ionic crystals anions and cations cannot diffuse independently into one direction, due to charge separation and production of an internal electric field. Ambipolar coupling occurs and the rate is controlled by the slower diffusion species along its fastest path, including grain boundaries.

A similar model, where the diffusion flow occurs only through the grain boundaries, was developed by Coble /18/ (Coble creep). The creep rate according to this model is:

$$\dot{\varepsilon} = B_1 \cdot \frac{\Omega \cdot D_B \cdot \delta}{K \cdot T \cdot a^3} \cdot \sigma \qquad (14)$$

with B_1 = a constant

δ = the effective cross section of a grain boundary

D_B = the grain boundary diffusion coefficient

Eq. (14) includes $\dot{\varepsilon} \sim 1/a^3$ but also the $\dot{\varepsilon} \sim \sigma$ relation.

Generally, volume and boundary diffusion occur simultaneously, and the diffusional creep rate can be written /19/

$$\dot{\varepsilon} = B \cdot \frac{\Omega \cdot D_v \ \sigma}{K \cdot T \cdot a^2} \ (1 + \frac{\P \cdot \delta}{a} \cdot \frac{D_B}{D_v}) \qquad (15)$$

Due to the small δ-value the term in brackets is only in fine grained material much higher than unity. Otherwise diffusion round the grain boundaries is unimportant and the Nabarro-Herring process dominates. At high temperatures D_B/D_v tends to decrease due to the lower activation energy of D_B, also favouring the Nabarro-mechanism.

Important ideas for the materials discussed below have been worked out by Gifkins and Snowdon /20,21,22/. Their model is based on a boundary diffusion or sliding mechanism without a deformation of the individual grains. This leads to accomodation processes in the grain boundary wedges, necessary for geometrical reasons. In this model again a

$$\dot{\varepsilon} \sim \frac{1}{a^3}$$ relation is claimed which could not always be con-

firmed by the results. This relation seems to depend on the grain size itself. It has been shown several times /reviewed e.g. in 4/, that these accomodation processes give raise to wedge cracks, void formation and grain boundary separation, especially in the case when the diffusional or viscous flow directed to these triple points is not fast enough to reach full accomodation.

Cavity formation and growth may occur after two principle mechanisms: The model of void growth envisages the diffusion of grain boundary vacancies to a highly stressed sink within this boundary as the rate controlling step. This is something like a "negative sintering", with the driving force due to a chemical potential gradient caused by the tensile stress /23/. Another possibility is the formation of the cavity as a shear crack, which grows by grain boundary sliding /22/. There is strong evidence for both mechanisms, depending on materials and experimental parameters involved. For gas turbine ceramics the latter mechanism is of special relevance. One has to consider the important fact, that crack and cavity formation and growth can occur in all stages of creep, not only within the tertiary range, particularly in materials with individual grains of low plasticity.

Gifkins formula for the boundary sliding process is very similar to eq. (14), including also $\dot{\varepsilon} \sim \sigma$. Stress exponents in ceramic substances have been found often higher than unity, e.g. n = 1,3 to 2 and the simultaneous operation of at least two principles, including dislocation mechanism nave been argued (s. below). On the other hand it was stated that the rate dependence on stress can raise to higher values (n = 2 or even more) without participation of dislocation processes, when considerable grain boundary separation occur /24/. As a consequence care must be taken with the explanation of such stress exponents.

Most of the crystalline materials undergo creep deformation under a broad field of experimental conditions by dislocation motion. This holds for polycrystalline ceramics mainly at higher stresses and at temperatures, where dislocations are mobile. In a creep process, where the grain boundary accomodation is controlled by dislocation climb but the principle mechanism is still grain boundary sliding, an equation has been derived /19/

$$\dot{\varepsilon} = B_2 \frac{\mu \cdot b \cdot D_v}{KT} \cdot (\frac{\sigma}{\mu})^n \qquad (16)$$

where B_2 = a constant

μ = shear modulus

b = Burgers vector

The stress exponent n is higher than unity in this case, depending on specific dislocation mechanism operating during creep.

In the large amount of experiments, where n has been found between 4 and 5, a strong evidence for dislocation processes as the principle mechanism is given. At higher and

6

very high stresses n values of 7 or even 10 to 40 have been reported /3/, figures empiri-
cally found on the basis of these power functions but without any realistic respect. Thus,
a function

$$\dot{\varepsilon} = B_3 \cdot \exp\,(\beta\sigma) \qquad\qquad (17)$$

has been proposed. Experimental verification has been reported also for this equation
(being not valid for $\sigma \to 0$, because of a residue creep rate at $\sigma = 0$). It was suggested that
perhaps all models for a thermally activated creep lead to a sin h-function of the first
power, following the equation

$$\dot{\varepsilon} = B_4 \cdot \sigma^{n-1} \cdot \sin\,h\,(\beta\sigma) \qquad\qquad (18)$$

where $\beta = \dfrac{V}{KT}$, V being an activation volume.

At low stresses, eq. (18) passes over to the power function $\dot{\varepsilon} \sim \sigma^n$, normally fit by the
experiments.

It was emphasized, e.g. in /25/, that all creep processes with dislocation climb as
a main principle must be reducible to volume diffusion processes and the relevant dif-
fusion coefficients are the basic rate controlling figures. On the other hand, disloca-
tion glide cannot be completly excluded during creep, mainly at high stress levels and in
metallic systems /26/. In this case a correlation to diffusion data is no longer valid.
In ceramics however the upper stress limit for high temperature deformation may be deter-
minded by brittle fracture, rather below the stress level of pure dislocation glide.

Equations (13)(14)(15) include the creep rate dependence on grain size. The diminis-
hed creep rate in a coarse grained material is of considerable practical importance. It
holds for all cases of diffusion or grain boundary sliding as the creep mechanism con-
trolling and can be easily understood. This effect is in contrast to the grain size de-
pendence of the yield strength (Hall-Petch). However, the coarser grain sized materials
obviously exhibit a smaller creep strain at fracture /27/. It is difficult to realize the
$\dot{\varepsilon}_s \sim 1/a^2$ and $\dot{\varepsilon}_s \sim 1/a^3$ relations experimentally, especially to distinguish them.

It seems to be doubtful, whether a dislocation controlled creep rate can also be in-
fluenced by grain size variations. The path of dislocation motion should be limited by
the substructure (formed during transition creep) or generally by the threedimensional
dislocation network and only to a much lower extent by large-angle grain boundaries. Ne-
vertheless, the grain size effect seems to occur in many ceramic and metallic materials.
Although dislocation controlled creep is widely accepted in metallic systems a marked
contribution of grain boundary sliding cannot be excluded, at least in fine grained ma-
terials /3/.

Also the porosity may influence $\dot{\varepsilon}_s$ as investigated in a few examples and discussed
in /28/. Of course a higher porosity leads to an enhanced creep rate. The equation pro-
posed is:

$$\frac{\dot{\varepsilon}_{s,p}}{\dot{\varepsilon}_\sigma} = 1 + a \cdot p^2 \qquad\qquad (19)$$

$\dot{\varepsilon}_{s,p}$ being the creep rate of the porous sample, a is a constant, (0,044 /28/ or 0,125 /29/)
and p the porosity in %. A marked influence of the stress exponent n on the $\dot{\varepsilon}_s$
dependence on porosity was stated /30/. This - certainly important - porosity influence
may in practice often be superimposed by grain size effects because materials of high
porosity normally have a smaller grain size than dense materials, otherwise doping sub-
stances were used during fabrication.

3. EXPERIMENTAL METHODS

In a normal creep test a specimen is heated up to the temperature provided which has
to be controlled to a constant value during the experiment. After reaching a constant
temperature distribution in the test equipment a constant stress is mechanically induced
in the specimen. The sample answers the stress by deformation as a function of time which
has to be continuously measured and registered. In special cases a constant deformation
speed (constant cross head velocity) was used, followed by building-up of the deforma-
tion stress in the sample /57/.

TEMPERATURE AND ATMOSPHERE

The furnaces for creep testing of ceramics are normally equipped with heating ele-
ments which allow the operation under oxidising conditions. These elements are commonly
made from SiC but also platinum or Kanthal wound furnaces are used. In order to investi-
gate the atmosphere influence on the creep behaviour of silicon nitride some creep tests
under inert atmospheres, i.e. vacuum /31/ and He /32/ have also been performed. The tempe-
rature in the furnace is normally measured by using thermocouples and maintained constant
to better than ± 5°C at creep temperatures up to 1400°C. Because of the thermal expansion
of the testing arrangement and the specimen, especially tensile creep tests, are very
sensitive to temperature instability. With the present standard of temperature control-
ling systems the sensitivity limit for continuous tensile strain measurement is supposed
to be in the order of 10^{-4} h^{-1} /3/.

As an important feature of the considered engineering ceramics the creep rate under the exposure to oil combustion products would be of high interest. Up to this point the knowledge about the creep behaviour under gas turbine typical environments is very limited. Another approach has been started in /2/, where with an oxyacetylene torch along the gauge length of a tension specimen extremely rapid heating to the creep temperature has been attained. A constant specimen surface temperature distribution, e.g. at 1350°C has been achieved after less than 10 seconds. This very high heating rate meets another aim of gas turbine ceramics. Temperature measuring by optical pyrometer gives here a reproducibility of approximately 15°C. The temperature distribution over the gauge length seems to be reasonable with respect to the highly difficult testing arrangement. A much more unsatisfying temperature distribution with a temperature gradient of 80°C across the gauge length has been achieved with a different torch configuration for torsion creep tests /2/.

LOADING

In creep testing of ceramics the bending load system is widely favoured in contrast to other loading methods as tension, torsion or compression. The reasons are mainly of experimental or economical nature: The bending specimen is normally a simple bar with parallel surface sides, which needs very much lower manufacturing costs than e.g. a tension or torsion specimen. In the bending system no problem with the definition of a gauge length arises; moreover the deflection signal can be measured by feelers (leading to the linear working differential transformators (LVDT) which are in direct contact e.g. to the tension side of the specimen. A very high sensitivity of the strain measurement can be reached by this method, which is needed for the highly creep resistant ceramics discussed below. The difficulties to guarantee true axial loading in a tension specimen are a further disadvantage of the tension loading method.

From a performance point of view the 3-point bending system is the most uncritical method, but the resulting load distribution leading to a maximal moment under the point of loading makes the 4-point bending system more preferable. One obtains here an uniform load distribution between the two (inner) loading points and so a larger volume of the sample tested under the maximal stress. By most investigators the outer-fiber tensile stress is calculated by the elastic beam equation and this maximal stress has been taken as the nominal stress for bending creep. This stress has been termed the simple beam stress /33/ and is obtained from the bending load as

$$\sigma = \frac{P \cdot l}{J} \cdot \frac{h}{2} \qquad (20)$$

with P = applied load by one of two loading points

l = distance between a loading and a supporting point

$J = \frac{b \, h^3}{12}$ = moment of inertia of the beam with a rectangular cross section

h = specimen thickness

` = specimen width

Eqn. (20) may be rewritten as

$$\sigma = \frac{6 \, P \, l}{b \, h^2} \qquad (20a)$$

Although this calculation originally stays for the elastic case it may also be used without a big failure for the plastic behaviour up to a small amount of plastic deflection. Nevertheless, a failure always arises, if the stress exponent n in eqn. (9) is larger than unity (no viscous flow). For n = 1 the linear stress distribution over the specimen cross section derived from elastic loading remains linear. The case n > 1 means a stronger stress dependence of the strain rate what leads to a fast relaxation of the outer-fiber (maximum) stress because of the fact that the strain in any fiber is linear dependent on the fiber distance from the neutral axis. In the steady state creep range this behaviour results in changing of the stress distribution from the linearity $\sigma \sim y$ to a function $\sigma \sim y^{1/n}$, y being the fiber distance from the neutral axis. At least for lead at room temperature it has been shown /34/ that this new stress distribution is achieved in a very short time ($\approx$ 12 min) and stays unchanged during further creep. For the steady state creep stage the outer-fiber stress after the stress redistribution is obtained /35/ as

$$\sigma = \frac{6 \, P \, l}{bh^2} \cdot \frac{2 \, n + 1}{3 \, n} \qquad (21)$$

This redistributed stress will be constant if n does not change its value during the experiments. During the time to reach this constant stress distribution the outer-fiber stress will be decreasing which brings a further element to the primary creep phenomenon. If the value of n is known, e.g. from tension creep tests, the redistributed stress calculated by eqn (21) is by 17% lower for n = 2 than the simple beam stress. This leads to a tensile strain rate reduced by 31% in the outer fiber, using again the relation $\dot{\epsilon} \sim \sigma^n$.

When the primary creep stage also has to be considered, a much higher effort is needed for the calculation of the stress redistribution. An approach has been given /35a/, where a time dependent (m < 1), non-elastic (n > 1) deformation of a beam according to $\epsilon = A \, \sigma + B \, \sigma^n t^m$ is assumed. Again it is noted that for these conditions the outer-fiber stresses, strains and strain rates decrease compared with the values expected for a con-

stant stress uniaxial test. The resulting creep behaviour of the beam is considered to be found between two boundaries: first, the deformation response of the beam, i.e.the stress strain behaviour is the same under tension and compression, second, the compressional side of the beam deforms only by an elastic mode. Calculated results (with n = 2, m = 0.5) for the first case show, that the resulting creep rate of the beam initially stressed to the same elastic value as a tension specimen becomes only 60% from the creep rate of the tension specimen in the uniaxial constant stress test. The calculation shows that after the elastic loading part a rapid drop of the outer-fiber stress occurs, which is followed by a further continuous decrease with time. In the second case the stress-strain relation remains linear (according to the presumption) but goes on to higher values on the compression side, while the outer-fiber stress on the tension side is dropping down very rapidly. An eventual ratio between the resulting creep rate of the tension compared with the bending specimen under initially the same elastic stresses is obtained as approximately 7 : 1, resp. Of course, the experimental ceramic materials should normally exhibit a behaviour between these two boundaries. An evaluation considering primary and secondary creep has been given in /35b/. However, the material constants, e.g. n in eqn (9) or B in eqn (6)have to be known for any approach. For this purpose the tension creep test with the definite unaxial stress over the total cross section of the specimen has been appreciated by several authors /2,32,53/.

The tension creep specimen is normally an uniform cylindrical body as the gauge length with two conical heads to be retained in the gripping arrangement. The surface finishing of the gauge length section of the specimen should be perfectly conducted in order to avoid any stress concentrations. The grips for transmitting the load to the specimen should exhibit high refractoriness which make their cooling avoidable, first because of the high specimen test temperature and second to provide a high uniformity of the temperautre along the gauge length. As mentioned before exact axial loading which avoids additional bending moments is very difficult. By the use of several strain gauges distributed around the gauge section and measuring the strain following a small preload the misalignment could be reduced to less than 3% bending strain /32/. For the considered engineering ceramics the stress in this tension specimen can simply be taken as the relation of the load to the specimen cross section, P/F. Any stress increase because of the decrease of the specimen cross section during creep can be neglected up to a strain of at least 1%. Considering higher creep strain this stress changing should be taken into account. An evaluation is suggested for the compression creep test, which allows simpler experimental procedures.

A specimen for torsion creep tests has been described in /2/. The specimen with the gauge diameter r ends in two square heads for accomodating the gripping arrangement. The stress will be induced by a torque moment M and can be taken /3/ as

$$\tau = \frac{3 \, M}{2 \pi r^3} \qquad (22)$$

Similar as for the bending system the stress dependence of the strain rate (described by n) may be considered, what leads to a slightly different stress in the plastic case as

$$\tau = \frac{3 \, M}{2 \pi r^3} \cdot \frac{3 \, n + 1}{3 \, n} \qquad (23)$$

A short notice has been given in /36/ about a compression creep test of HPSN with a very high stress of 690 MN/m^2. For ceramics the compression creep test seems to be useful with respect to many applications in practice (but not for turbine wheels!); it further seems to be preferable because of the less complex experimental equipment and performance combined with a broadly valid evaluation of the stress status. Nevertheless, additional tangential and radial stresses are commonly neglected. The stress in a compression creep specimen is simply calculated as the initial relation P/F. In the real creep performance the stress is decreasing because of the increase of the specimen cross section. The measured creep strains (resulting from this decreasing stress) should normally be corrected to strain values which would be initiated by a constant stress (s.below). The creep test can be conducted up to strains as high as 40% /10/, before at higher strains the deviation of the originally cylindrical to a ton-shaped specimen has to be considered.

STRAIN MEASUREMENT

As mentioned in the previous chapter the measured strain in a compression creep test (for tension creep tests the equivalent evaluation is valid) should be corrected taking into account the decrease of the stress during the experiment. The corrected strain which results from a virtually constant stress is obtained /10/ as

$$\varepsilon = \frac{1}{n}\left[\left(\frac{l_o}{l}\right)^n - 1\right] \qquad (24)$$

with

l_o = original specimen length

l = actual " "

n = stress exponent (on the basis of $\dot{\varepsilon} \sim \sigma^n$).

As to be seen this correction can only be made, if n is known. By a further evaluation with a numerical solution /37/ this problem can be overcome and the material parameters A, n and Q e.g. from eqn. (9) can simultaneously be obtained.

The experimental realisation of the continuous measurement of the specimen deformation is mostly attained by the use of LVDT's . The signal will be read by an extensometer which brings it to these electronic transducers mounted outside the furnace. Mainly for discontinuous strain measuring some optical systems, e.g. a telescope - cathetometer arrangement are in use for compression /10/ as well as for bending /38/ tests. Both methods, the mechanical-electronic and the optical system, have nearly the same sensitivity, which is limited for a compression test with ±2 μm /10/. In order to check the validity of the in-situ-measured strains some investigators compare these results with the total strain obtained after the experiment by measuring the curvature or the elongation of bending /31,38/ or tension specimens /32/, resp.

For the bending specimen the outer-fiber tensile strain i· calculated from the deflection at the center of the beam relative to the two inner loading points, f, resulting in

$$\epsilon = \frac{4\ h\ f}{a^2} \qquad (25)$$

with a = distance between the two (inner) loading points. This relation is given by means of geometrical reasons considering the existence of a constant radius of curvature between the inner loading points. Thus eqn. (25) allows its application up to small strains of approximately 2% /28/. If, because of experimental reasons only the loading point deflection or the central deflection relative to the (outer) supporting points can be measured, the calculation has also to consider the stress exponent n. Thus, an evaluation is given /39/ based on two models describing the curvature of the specimen section betweer the loading and supporting points as straight line or as part of the circle from the central specimen part under the constant moment.

The surface shear strain γ of a torsion creep specimen is received as

$$\gamma = \frac{r\ \psi}{l} \qquad (26)$$

During the experiment the twist angle ψ has to be measured from indicator points which mark the two ends of the gauge length, l. Eqn. (26) stays only, if l remains constant during the experiment by fixing both ends of the specimen in the axial direction. Because of volume constancy the radius of the gauge section, r, remains constant as well.

4. RESULTS

4.1 HOT PRESSED Si_3N_4

HPSN is - in contrast to RBSN - a material of nearly full density and high bend strength. Its creep properties are strongly influenced by the amorphous phase formed mainly due to the MgO additions, necessary for the successful densification during hot pressing. This leads in many cases to considerable creep strains, as well in the primary as in the secondary range. The figures for $\dot{\epsilon}_s$ are generally higher than those for RBSN (discussed in the next paragraphe) at least comparing high quality material. Fig. 4 summarizes important data of $\dot{\epsilon}_s$, but not all the data published so far, could be included. The chemical composition of different types of HPSN is presented in Table 1. With HPSN material, flexure as well as tension creep tests are available /2,40,41,42,43,44/ a very important feature. These values are - as expected theoretically - considerably higher than the bend test values, the differences being nearly $1^1/2$ orders of magnitude. The values can be compared mainly at the test temperature of 1260°C. One has to take into account, that sample heating during tensile test was partly performed by direct action of an oxyacetylene torch /2/, leading to temperature profiles and sharp gradients at the ends of the gauge length. Thus, a thorough comparison seems to be difficult so far. Also torsion creep tests have been performed /2 /, not considered in this figure. The data show a relatively consistent picture with respect to stress and temperature dependence. In Fig. 4 no experiments performed in helium atmosphere are included. $\dot{\epsilon}_s$ in He is about one order of magnitude lower than in air /40/. This result is similar, at least in principle, to the creep experiments with RBSN, performed in air and vacuo, resp.

Fig. 5 illustrates results on time to reach 1% plastic strain. This time decreases with increasing temperature and increases with purity, being consistent with the results reported before.

Many of the creep tests have been extended up to fracture, so, stress rupture life data are available. It is obvious from fig. 6 and Table 1, that a small decrease of Ca content results in a significant increase in stress rupture life. The life time in helium in considerably shorter than life in air and the failure occurs generally at less than 1% total strain, in contrast to 3% or more total strain in air /40/. This seems to be a principle strain limit for the HPSN developed so far. Very similar results have been reported by /2/ .

The marked influence of the impurity content, mainly Ca is agreed for all the high temperature mechanical properties. The effect was investigated in detail by Kossowsky /32/, who found an $\dot{\epsilon}_s$ of $4\cdot10^{-7}$/h at a Ca content of 0.05%, raising to $1\cdot10^{-3}$/h at 0.5% Ca, both at 1150°C(fig. 7). Even a reduction of Ca content from 0.06 - 0.08% (NC 130 A) to 0.03 - 0.05% (NC - 130 B) seems to have a marked influence /1/. The grain boundary phase was identified as a Mg silicate containing Ca, Al and alkali metals. It

was shown, that CaO is present in the grain boundaries of the Norton HS-130 up to 12 mole % and even more in the HS-110. Consequently, Kossowsky /40/ claims to lower the Ca impurities to below 100 ppm, a figure, which should result in a still better creep resistance.

Selected impurity additions as oxides or carbonates lead to a similar result for Li and Na /45/, but the high volatility during hot pressing resulted in a reduced concentration in the billets, thus minimizing their deleterious influence. Fe_2O_3 and Al_2O_3 did not give a marked effect on the high temperature mechanical properties.

Note that the latest types of HPSN don't contain large amounts of Mg, e.g. less than 1 percent (Tab.1), but the chemical analyses are subject to considerable scatter.

Turning over to the creep mechanism, obviously all the experiments exhibit a primary and secondary creep range, the former often extended up to 50 hrs are even more. In a few cases /40/ also tertiary creep has been observed. This stage of accelerated creep is rather short and in many cases not detected at all. It is difficult to extract from the published data the experimental conditions, where tertiary creep occur, because very probably sample failures are responsible in some cases, at least for an early observation of this stage. On the other hand a creep strain limitation of generally a few percent is claimed for HPSN material.

Stress exponents for $\dot{\varepsilon}_s$ in air have been measured near n = 1,7, /41/ 2,0 to 2,2 /32,40/ activation energies[s] in the range of 585 KJ/mol ($\sim$140 Kcal/mole) /41/ and 627 KJ/mole ($\sim$150 Kcal/mole) /40/. The principle creep equation agreed is eq (9). Both the pre-exponential term A and the activation energy Q are functions of structure, stress, temperature and environment. At high stresses (100 MN/m^2 at 1150°C) or high temperatures (1350°C at 40 MN/m^2) even n-values higher than 4 and in helium, n $\approx$ 3,0 has been observed. Also the activation energies observed are variable, depending from purity as well as from atmosphere (fig. 8). The value is higher (630 KJ/mol) for tests conducted in helium than for tests in air and decreases with increasing impurities of the material. On the other hand, the activation energy is in principle agreement with the figures measured for viscous flow of silicate glasses ($\approx$ 600 KJ/mol) /46/.

It is generally agreed that creep deformation is controlled by grain boundary sliding, depending on the amount and the viscosity of the glass phase. Crack and void formation and growth, i.e. grain boundary separation, occurs during this process. (Fig.9) It has been shown by several researchers that wedge cracks have to open at the grain junction due to geometrical reasons in order to maintain the straining process during grain boundary sliding in a polycrystalline material. The growth rate was formulated in /47/, being a function of stress, strain rate and other parameters. When strain reaches a limiting value, unstable cracks are formed by linking of grain boundary single separations, which rapidly grow, marking the start of accelerated creep or fracture.

Explanations for the n-values observed have been offered by several investigators. Stress exponents between 1 and 2 can be caused by operation of non-Newtonian sliding processes. A value of 2 can be relevant for grain boundary sliding in fine grained materials . A more general treatment of this matter was reported in /24/, with respect to creep of glass ceramics. It was shown that the void formation during creep modifies the rate dependence of stress to higher n-values, mainly if a free flow of the glass phase is inhibited and not enough glass phase is available to refill the voids. The reason for this is an effective decrease of area supporting the load. Thus, it was followed in /40/, that the observed differences in the creep rates of RBSN in air (n $\approx$ 2) and helium (n $\approx$ 3) are due to the amount of glass phase present: In air a continous formation of new glass phase occurs, migrating along grain boundaries into the material. This is a somewhat similar approach for the explanation of atmosphere dependent creep as the inner oxidation concept for RBSN (s. below). As a consequence, an exposure in air can provide a valuable mechanism to heal surface cracks.

Even the high values of n > 4 are not explained by a plastic behaviour of the Si_3N_4 grains due to dislocation motion: This process should occur to a considerable extent not below 1700°C /40/. At temperatures below 1400°C, only 1/1000 of the strain observed (up to 10^{-2}) can be contributed by dislocation motion. Although a very limited plastic deformation of the grains have been observed, the micrographs indicate that deformation and failure during creep are caused directly by deformation and failure of the grain boundary phase. It is claimed further, that failure in creep always originates from external surface, using grain boundaries for its growth.

4.2 REACTION BONDED Si_3N_4

The creep properties of this material published by different authors exhibit very large scatter, indeed. This is true for the strain vs. time curves as well as for the secondary creep rate ($\dot{\varepsilon}_s$). In fig. 10 a collection of data is presented including own measurements. This plot contains results of recent experiments but also data from earlier materials, thus, representing a development of more creep resistant materials during the last years. A creep rate $\dot{\varepsilon}_s = 10^{-7}$ to 10^{-6}/h is really at the limit of measurable creep rates at all, perhaps below it in many cases, depending on the equipment used. Inspite of the large uncertainities in this range such figures indicate highly creep resistant materials, especially if they were received under high stresses and at temperatures above 1250°C.

Another difficulty is the definition of the steady state value $\dot{\varepsilon}_s$. Secondary creep is not observed in many cases before times of 50 hrs or even longer, especially at high strains. Additionally, this evaluation is very dependent on the strain measurement accuracy. This is a similar effect as with HPSN, but the longer duration of exposure often used in creep experiments with HPSN make it easier to evaluate a minimum creep rate as $\dot{\varepsilon}_s$. Nevertheless, in fig. 10, an $\dot{\varepsilon}_s$ Value was defined in any case, resulting in some uncertainty of only moderate practical relevance.

Fig. 10 contains results from materials with differences in fabrication methods (e.g. starting powder, powder preparation, forming procedure, reaction sintering shedule, atmospheres used), impurities, porosity, pore size and size distribution, α/β-ratio and other variables.

A few results of stress rupture life data are available, ranging at a lower level than HPSN /2,48/. Most of the creep experiments did not run up to fracture. Investigators agree /48,51/ that impurities, mainly Ca have a deleterious effect on creep resistance. Thus, a material with 0.02 to 0.05% Ca behaves much better than with 0.1 of even 0.4%. The reasons for this behaviour should be similar as for HPSN: The viscosity of the glass phase at creep temperatures decreases with increasing Ca contents.This was deduced from the relevant phase diagrams /52/, which exhibit lower liquidus temperatures if phases with high Ca content are involved. Especially the phase $CaO-2Al_2O_3-2SiO_2$ is described as deletrious for creep resistance /48/.

A high α/β-ratio seems to be favorable for creep resistance /49,51/, although this is not investigated in detail. This was followed from creep experiments together with the lack of plastic deformation observed in α-grains in comparison with the observation of dislocations in (hot pressed) β-Si_3N_4.

With respect to the influence of bulk density, several investigators found a higher creep resistance of the more dense materials (7,49,53), like in other ceramic materials. The density range of the materials investigated was 2.05 to 2.6g/cm^3. Not all the investigators gave figures of the density values. Engel and Thümmler /7/ observed pure primary creep in experiments lasting up to 50 hrs (fig.11). From their data a preliminary formula (known from other creep experiments /29/

$$\frac{\dot{\varepsilon}_p}{\dot{\varepsilon}_o} = 1 + 0,125 \ p^2$$

($\dot{\varepsilon}_p, \dot{\varepsilon}_o$ = creep rate of the porous and dense material, resp.,

p = porosity in %)

can be derived. A physical meaning of this equation is not given. It should be emphasized, that this density influence gives an incomplete picture due to the marked influence of pore size and size distribution (s. below), even at the same bulk density.

An interesting phenomenon is the influence of H_2 in the N_2-atmosphere during reaction sintering on creep /48/. The steady state creep rate and the plastic strain after 1000 hrs are shown to reach a minimum with a 1v/o H_2 addition and to remain nearly constant for higher H_2 concentrations. The material sintered in an N_2 - 1.8% H_2 atmosphere was studied in detail. The reason for better creep resistance was claimed to be a microstructural effect: The as-nitrided samples without H_2 show a larger grain size and an overall structure being more open. In contrast, the samples nitrided with the H_2-N_2-mixture have an increased contact area between grains, requiring more force to be applied to the sample to generate an equivalent stress condition at the grain boundaries. Such a material with only 0.04% plastic strain after 200 hrs at 1260°C and ~70 MN/m^2 meets the initial design goals, a statement that one can agree with.

In this laboratory /54,55/, the surprising effect of severe inner oxidation of RBSN during creep experiments was detected. We observed this phenomenon not only after creep, but also after simple annealing tests, depending on the time-temperature regime. The inner oxidation is very dependent also on structural parameters, mainly on porosity and pore size distribution. Fig. 12 compiles results of x-ray measurements of the cristobalite profiles in crept samples over the whole cross section in the loaded area. Fig. 13 collects measurements of pore size distributions, obtained by Hg-porosimetry, of several RBSN qualities. Fig. 14 compares creep curves of the same materials used for the measurements in fig. 12 and 13. The RBSN samples used for these experiments are described in table 2. The following clear correlation can be observed: After a creep experiment the inner oxidation is much more severe in materials with a broader pore spectrum including larger pores than with a narrow pore distribution. This leads to high creep strains of highly oxidized samples, while materials with very limited inner oxidation exhibit excellent creep resistance. This result is confirmed by comparative creep tests of the same RBSN quality in air and in vacuo resp./31/. The vacuum tests$^{x)}$ lead to a very low and difficult measurable creep strain, being a factor of at least 30 lower than the tests in normal atmosphere. The lack of inner oxide phases was responsible for this creep resistance in vacuo. We believe that a "high quality" RBSN shows a very low and nearly identical creep rate in air as well as in vacuo.

x) The vacuum test temperatures shall be chosen not higher than 1350°C, otherwise a considerable dissoziation occurs.

These figures include another possibility to get a high creep resistance, namely surface treatment by exposure in air (e.g. 1 h at $T \geq 1250^\circ C$) or by CVD-coatings of SiC or Si_3N_4. Obviously in both cases the inner oxidation is diminished and nearly avoided in the CVD coated material. Nevertheless, the strength properties of such a material are not investigated so far.

Considering the results with respect to the creep mechanism many authors observed both primary and secondary-stage creep. No evidence of tertiary creep occured, even in the case of fracture, besides of a few exeptions /7/. Generally, the long term tests did not run longer than 100 to 200 hrs or even shorter and have been concluded before fracture occured. During secondary creep, the equation (9) was generally fulfilled and stress exponents between 1.2 and 1.4 /48,51/ , 2.0 in the very fine grained material /48/ and activation energies around $\sim$ 540 KJ/mole ($\sim$130 kcal/mole) have been found. In the case of constant creep rate stress exponents as well as activation energies have been measured by stress-change and temperature-change experiments, resp., with one sample. At moderate changes no considerable alteration of microstructure must be taken into account.

The extended primary creep range was investigated in /7/. A time dependence according to eq. (5) and a stress dependence according to eq. (6) have been derived from experimental results. A log-log-plot shows no constant creep rate during the experimental time. In this case the evaluation of an activation energy is somewhat more difficult and we found values between $\sim$ 500 and 700 KJ/mole ($\sim$ 120 - 167 kcal/mole). Here it is not possible to take the value from temperature change experiments and one needs more than one sample. In order to eliminate structural features, only samples with similar strain values have been used for the $\dot{\varepsilon}$ vs $1/T$ plots. Lower activation energies have been found at higher stress and lower strain values and vice versa.

There is general agreement, that the dominating creep mechanism is not a true plasticity of the Si_3N_4 crystals under experimental creep conditions, but a viscous mechanism along the grain boundaries /48,51/. This is in agreement with the stress exponents measured as well as with the triple point voids observed in crept samples. The importance of glass phases at boundaries is stressed. The vacuum creep tests discussed above show very clearly the dominative role of oxidation products formed in-situ during the creep test. Experiments in this laboratory make clear, that an important part of the inner oxidation products is formed during the heating up period, providing the phases responsible for the creep rate measured. The x-ray measurements (fig. 12) show a considerable part of these products being crystalline in nature as a consequence of the amorphons-crystalline transformation during exposure. The contribution of the cristobalite together with the glass phase to the grain boundary viscosity has not been investigated.

One can speculate, that certain impurities (e.g. Ca) enhance the process of inner oxidation, forming sinks for oxygen due to their high affinity. This can be in addition to the diffusion of these atoms to the surface and should be true in the case, when the impurities in the as-manufactured state are not fully oxidized.

4.3 SIALONS

The substitution of Si and N in the β-Si_3N_4-lattice by Al and O is possible up to high concentrations and a serie of new compounds is resulting in this way. Although sialon parts can be fabricated by normal cold pressing and sintering procedure (at least in principle) this paper considers only hot pressed material. Some properties of the sialons are most interesting, e.g. the extremly good oxidation resistance. It seems somewhat difficult to get monophase products, being free from other crystalline and amorphous phases. Considerable progress was reached during the last years /44/.

The creep properties of sialons are influenced as well by impurities including amorphous phases as by the Al/Si-ratio. Osborne has published four point bending creep results of Lucas material (fig. 15) showing a very broad range of creep behaviour. It is difficult to take figures for $\dot{\varepsilon}_s$ from these curves; a rough estimation leads to values ranging from $\dot{\varepsilon}_s \approx 1 \cdot 10^{-5}$/h for the low creep resistant and $\dot{\varepsilon}_s \approx 5 \cdot 10^{-7}$/h for highly creep resistant material. Many of the materials developed have exhibited less than 0.06% creep in 100 hrs. Obviously it is possible to manufacture Sialon with a low creep rate, probably better than HPSN, nearly as good as the best qualities of RBSN. This material must be very near the monophase Si-Al-O-N composition, but the effect of glass content and/or composition has not been published in detail. It was found difficult to combine a high room temperature strength and a good creep resistance in the same material. The best combination is reported to have the sialon 144 with a room temperature strength of 790 MN/m^2, a Weibull modulus of 21 and a creep strain of 0.113% in 100 hrs at $1227^\circ C$ and 77 MN/m^2.

Some of the most creep resistant sialons were selected for testing at $1370^\circ C$, 77 MN/m^2. The results show an extremly wide range of creep curves. The differences between the materials are more apparent at this temperature and the surface strains range between 0.13 and more than 0.3% in 100 hrs, an order of magnitude higher than at $1227^\circ C$. The best $\dot{\varepsilon}_s$ seems to be in the order of 10^{-5}/h, but generally no steady state creep can be seen in the relevant figure. All sialons with a modulus of rupture strength at $1200^\circ C$ higher than at room temperature exhibit very good creep resistance, but the best creep resistant type has low room temperature strength (450 MN/m^2) and low density (3,08 g/cm^3).

4.4 Sic

The results on creep of silicon carbide published so far concern experiments under very different experimental conditions and with different materials.

Deflection vs time plots at 1000 and 1235°C have been reported in /56/ and data at 900° to 1200°C in /53/. It is difficult to evaluate these results due to the lack of data with respect to material properties. It was reported in /53/ that the time to promote 0.125% creep strain in bend-creep tests at 30,9 MN/m^2 can be > 300 hrs at 1000°C and at 1100°C,or > 630 hrs and even > 1000 hrs at 1200°C depending on the SiC-material tested.

More recent work is published in /43,57,58,59/. The experimental conditions and some principle results are collected in table 3. One should emphasize, that the results are rather complementary than contradictory and cannot be compared directly. A few other data are reported in /44/.

Due to a lack of data, it is hardly possible to plot them in a similar manner as done for Si$_3$N$_4$. No $\dot{\varepsilon}_s$ values have been reported in /59/ and even no rough estimation could occur from the collected data. Obviously, temperatures higher than 1500°C /57,58/ are not actual for gas turbine applications and must not be discussed here. In fig. 16 and 1/ creep curves of HPSC and Refel SiC are compared with some types of Si$_3$N$_4$. A rough estimation of $\dot{\varepsilon}_s$ leads to values of $\sim 5 \cdot 10^{-7}$/h for HPSC and somewhat higher for Refel, both at 1227°C and 77 MN/m^2. Very low total strain (0.01 to 0.02%) after 100 hrs is visible. The figure for 1370°C is $\sim 2 \cdot 10^{-6}$/h for HPSC with a total strain well below 0.1%. Creep elongation at higher stresses is demonstrated in fig. 18 . Here, somewhat higher strains are observed, but a complete stop of the deformation occurs after a certain time. This is visible for both investigated types, for the Carborundum KT as well as for the Springfields Ref-1. The difficulties of obtaining reproducible measurements of the low levels of strain have been mentioned /43/.

As a preliminary consequence it can be followed, that dense, polycrystalline, pure SiC is a material with outstanding creep resistance, still better than the best qualities of RBSN. Little systematic information is available in the most interesting temperature range of 1200 - 1500°C. A content of free silicon enhances the creep rate considerably and leads to marked irregularities in the $\varepsilon(t)$-curve as well as in the rate sensitivity of strain (n = 2, see table 3).

5. RELATIONS TO FATIGUE AND DELAYED FRACTURE

Kossowsky /32/ has performed creep tests as well as low and high cycle fatigue experiments. He found the higher purity material (HS-130) not exhibiting considerable time dependent fatigue behaviour at 1200°C, in contrast to the lower purity material (HS-110). This is true up to $2 \cdot 10^6$ cycles at 1800 cpm, perhaps up to 10^7 cycles. Neither material displays the phenomenon at 230°C. Failure generally occurs by intergranular cracking. Micrographs show areas of highly localized deformation with dislocation structures, stacking faults etc. Mainly at 1300°C, triple point cavitations and grain boundary separations are indicative of grain boundary sliding. Some of these phenomena are very similar as during creep.

During low cycle fatigue, similar structural features have been observed. It was followed /32/, that a low cycle fatigue test actually subjects the material to an intermittent creep test.

Corrosion effects are claimed to be operative during fatigue: The lifetime of a fatigue specimen, being controlled by the slow crack growth, shall be influenced by the formation of glassy oxidation products from a corrosion mechanism in air. This is a very similar statement as given in /55/ with respect to the creep rate dependence on atmosphere.

In summary, the behaviour of Si$_3$N$_4$ in all three modes of testing is controlled by the same mechanisms, namely the temperature and strain rate dependence of grain boundary sliding. Thus, a high quality material (e.g. with a low impurity level and an optimal microstructure) has a high resistance to creep as well as to fatigue.

Delayed fracture is the catastrophic failure of a material under static load, some times referred as to static fatigue. Experimental results on gas turbine ceramics have been presented in /42,60/. The phenomenon occurs mostly in the absence of considerable creep, i.e. at relatively low temperatures; also the mechanism is not related to creep. On the other hand, both processes seem to be competitive with respect to failure: In HPSN the failure mode in the temperature range of 1200°C depends on the stress level. Different Si$_3$N$_4$- and SiC-materials can undergo very different time dependence of rupture stress. The explanation of delayed fracture considers a stress corrosion effect in air acting at existing flaws until they grow to the critical size for rapid propagation. Although there is no direct proof of this aspect, we must take into account environmental influences also for delayed fracture.

6.   CONCLUSIONS AND FURTHER RESEARCH REQUIREMENTS

Obviously, the gas turbine ceramics described in this paper exhibit very different
creep behaviour, not only between the groups 4.1 to 4.4, but also within each group. To
understand these facts we must take into account the numerous parameters influencing the
low as well as the high temperature properties actually and inprinciple. With these non-
oxide ceramics, which are thermodynamically unstable in air and often porous and multi-
phase a very complex system is operative during creep. The most important parameters with
respect to material and environment are:

- purity and additives

- microstructure (grain size, pore volume, pore size and size distribution,
                  inclusions, amorphous and oxide phases)

- atmosphere   (oxygen potential, humidity, other aggressive constituents)

These parameters are strongly dependent on each other: purity, additives as well as the
atmosphere during creep determine the microstructure, not completely but to a great ex-
tent. Other, very important influences on microstructure are the characteristics of the
raw material and the fabrication shedule, not discussed in this paper. Thus, the micro-
structure is the key problem to obtain a high creep resistant material. It should be em-
phasized that it is not sufficient to have an "adequate" microstructure before creep,
it must be maintained during the whole time of high temperature exposure.

For the HPSN and sialons, the amount and viscosity of the non refractory phases
and their distribution seem to be the most important features. In RBSN, the pore charac-
teristics and the inclusions are the leading parameters. Many of the failures observed
after short exposure times could be initiated by the latter, perhaps also in HPSN. As
shown before, the purity is most important for all types of Si_3N_4. As a very preliminary
statement it seems, that SiC (at least without large amounts   of free silicon) is not
as sensitive to microstructure as Si_3N_4 and lower amounts of oxide phases are present or
formed in the material.

With respect to the total creep deformation after a certain exposure, the RBSN is
generally more creep resistant than HPSN. The outer fibre creep deformation after 100 hrs
at $1300^{\circ}C$ at a 70-100 MN/m^2 stress level for RBSN is $\sim$ 0.1 to 0.2% or even less. Under
these conditions even the latest qualities of HPSN undergoe much higher deformation, say
0.5 - 1%. But this temperature seems too high for the application of HPSN under stress.
The latest qualities of sialons are encouraging with respect to creep properties, on the
other hand it seems doubtful whether a replace of Si_3N_4 by sialons only due to their creep
behaviour should occur. The creep problem of RBSN for practice has apparently been solved
by the development of the latest qualities, with respect to the requirements mentioned in
chapter 1, but the creep behaviour of very thin cross sections(1 mm or less) together
with the influence of burnt fuel components remains still questionable. Some potential
to improve the HPSN can be seen in a further reduction of the impurity level as well as
in special additives (e.g. Cerium oxide /61/). in order to receive the main part of the
amorphous phase occuring only temporarily or to enlarge its viscosity considerably. Under
identical creep conditions, hot pressed SiC shows the smallest summarized creep deforma-
tion.

Very important with respect to fabrication of high quality products in a reprodu-
cible manner is a better understanding of the relations between the relevant fabrication
steps and the resulting microstructure. Of course, this is a function of the growing
fabrication experience combined with careful parameter studies.

Last not least there is strong evidence, that a material of "high quality" exhibits
a good resistance to creep as well as to fatigue and delayed fracture together with a
high stress rupture life and other good properties, possibly with the exception of some
sialons. The demand to high rupture strength and high creep strength may be contradic-
tory in some cases due to the different influence of grain size and flaw size.

With respect to the testing procedure the limited value of flexure creep results
for design purposes should be emphasized. Only at special boundary conditions flexure
data can be transferred into tensile data. Nevertheless, flexure tests have been and will
still be of great importance as a controlling tool for quality improvements.

As an addition to these conclusions in the following paragraphe a number of special
problems are listed as aims for further necessary research work. They may be of more prac-
tical or more basic relevance. resp.

1   - to get a model for transient creep

2   - to elucidate the parameters, where the extension of the transient range depends
       from

3   - the influence of α/ß-ratio on creep

4   - to explain the different $\dot{\epsilon}_s$ rate sensitivities of strain, found by the same class
       of material

5   - to explain failures by fracture after short exposure considering surface and bulk
       flaw

6   - to characterize the microstructure before and after creep with standardized methods

7 - systematic investigation on environmental influences on creep, fracture and fatigue

8 - influence of impurities on internal oxidation of RBSN

9 - study on a stress-induced internal oxidation during creep

10 - investigation of the internal oxidation during creep of HPSN

11 - creep of very thin cross sections of RBSN

12 - further elucidation of the desired pore size distribution of RBSN with respect to internal oxidation and creep

13 - further analytical effort to characterize amorphous and high oxygen containing phases

14 - studies on the influence of doped HPSN with respect to creep and other properties

15 - studies on the composition of Sialons and its influence on the creep behaviour

16 - creep of CVD coated Si_3N_4 (SiC and Si_3N_4 coating), together with rupture strength and delayed fracture measurements

17 - to get more consistent creep results on SiC

18 - the comparison of compression creep with tensile creep results in the primary as well as in the secondary range

19 - the comparison of flexure creep with tensile creep data in the primary as well as in the secondary range in order to get results on the relevance of flexure creep data for engineering purposes

REFERENCES

/1 / A.F. McLean, E.A. Fisher, R.J. Bratton: Brittles materials design, high temperature gas turbine, Interim report, Jan. 1 - June 30, 1974, AMMRC - CTR 74 - 59

/2 / E.M. Lenoe, G.D. Quinn: Preliminary creep studies of hot-pressed silicon nitride, in: Deformation of ceramic materials, ed. by R.C.Bradt, R.E.Tressler; New York, London, Plenum Press 1975, p. 399 - 412

/3 / B. Ilschner: Hochtemperaturplastizität, Springer-Verlag 1973

/4 / J. Gittus: Creep, viscoelasticity and creep fracture in solids, Applied Sci. Publishers London, 1975

/5 / A.H. Cottrell, V. Aytekin: Andrade's creep law and the flow of zinc crystals, Nature 160 (1947) p, 328 - 29

/6 / F. Garofalo: Fundamentals of creep and creep rupture in metals, McMillan, New York, 1975

/7 / W. Engel, F. Thümmler: Kriechverhalten von reaktionsgesintertem Si_3N_4 bei 1200 bis 1400°C, Ber. Dt. Keram. Ges. 50 (1973) p. 204 - 210

/8 / G.A. Webster, A.P.D. Cox, J.E. Dorn: A relationship between transient and steady-state creep at elevated temperatures, Met. Sci. J. (1969) p. 221 - 225

/9 / A.A. Solomon: Relationship between primary and steady-state creep of UO_2 at elevated temperature and under neutron irradiation, in: /2/ p. 313 - 324

/10/ D. Vollath, Nucl. Res. Centre, Karlsruhe: Kriech- und Erholungsvorgänge in Uran Plutonium-Mischoxid, 1973, KFK-1884 and: Strukturänderungen in UO_2 - PuO_2 während des Kriechens, J. Nucl. Mat. 55 (1975) p. 335 - 344

/11/ T.H. Hazlett, E.R. Parker: Nature of the creep curve, J. Metals (1953) p. 318 - 323

/12/ D.A. Woodford: Measurement and interpretation of the stress dependence of creep at low stresses, Mater. Sci. Engng. 4 (1969) p. 146 - 154

/13/ F. Garofalo, R.W. Whitmore, W.F. Domis, F. von Gemmingen: Creep and creep-rupture relationships in an austenitic stainless steel, Trans. Met. Soc. Aime 221 (1961) p. 310 - 319

/14/ M.R. Notis: Deformation mechanism maps - a review with applications, in: /2/ p.1-23

/15/ F.R.N. Nabarro in: Report on a conference on the strength of solids, Physical Soc., London, p. 75-90 (1948)

/16/ C. Herring: Diffusional viscosity of a polycrystalline solid, J. Appl. Phys. 21 (1950) p. 437 - 445

/17/ R.M. Cannon, R.L. Coble: Review of diffusional creep of Al_2O_3, in /2/ p. 61 - 100

/18/ R.L. Coble: A model for boundary diffusion controlled creep in polycristalline materials, J. Appl. Phys. 34 (1963) p. 1679 - 1682

/19/ R. Raj, M.F. Ashby: On grain boundary sliding and diffusional creep, Met. Trans. ASM 2 (1971) p. 1113-1127

/20/ R.C. Gifkins, K.U. Snowden: Mechanism for viscous grain boundary sliding, Nature 212 (1966) p. 916-917

/21/ R.D. Gifkins: Diffusional creep mechanism, J.Amer.Ceram.Soc. 51 (1968) p. 69-71

/22/ R.D. Gifkins: A mechanism for the formation of intergranular cracks when boundary sliding occurs, Acta Met. 4 (1956) p. 98-99

16

/23/ D. Hull, D.E. Rimmer: The growth of grain-boundary voids under stress, Phil. Mag. 4 (1959) p. 673

/24/ R. Morrell, K.H. G. Ashbee: High temperature creep of lithium zinc silicate glass-ceramics, J. Mater.Sci. 8 (1973) p. 1253

/25/ J. Weertman: Dislocation climb theory of steady-state creep, Trans. ASM 61 (1968) p. 681 - 694

/26/ M.F. Ashby: A first report on deformation mechanism maps, Acta Met. 20 (1972) p. 887-896

/27/ R. Lagneborg: Effect of grain size and precipitation of carbides on creep properties in Fe-20% Cr-35% Ni Alloys, J. Iron Steel Inst. 207 (1969) p. 1503-1506

/28/ G. Engelhardt, Nucl. Res. Centre, Karlsruhe: Untersuchungen zum Kriechverhalten von polykristallinem Al_2O_3 und Al_2O_3-Cr-Cermets, 1973, KFK-1753

/29/ D. Brucklacher, W. Dienst: Creep behaviour of ceramic nuclear fuls under neutron Irradiation, J. Nucl. Mater. 42 (1972) p. 285 - 296

/30/ R.L. Coble, W.D. Kingery: Effect of porosity on physical properties of sintered alumina, J. Amer. Ceram. Soc. 39 (1956) p. 377 - 385

/31/ G. Grathwohl, F. Thümmler: Kriechen von Si_3N_4 unter oxidierenden und nichtoxidie-renden Bedingungen, Ber. Dt. Keram. Ges. 52 (1975) p. 268 - 270

/32/ R. Kossowsky: Creep and fatigue of Si_3N_4 as related to microstructures, in: Ceramics for high-performance applications, ed. by J.J. Burke, A.E. Gorum, R.N. Katz; Chestnut Hill, Mass. Brook Hill Publ. Co. 1974, p. 347 - 371

/33/ D.L. Vrooman, J.E. Ritter: Nonlinear behavior of thin beams in four-point bending, Am.Ceram.Soc.Bull. 49 (1970) p. 789

/34/ H.J. Tapsell, A.E. Johnson: An investigation of the nature of creep under stresses produced by pure flexure, J. Inst. Metals (1935) p. 121 - 138

/35/ S. Timoshenko: Strength of materials, part II, Advanced theory and problems, Prince-ton, D. van Nostrand Co. 1968

/35a/ A.F. McLean, E.A.Fisher, R.J. Bratton, D.G. Miller: Brittle materials design, high temperature gas turbine, Interim report, July 1 - Dec. 31, 1974, AMMRC - CTR 75 - 8

/35b/ L.W.Hu, N.H. Triner: Bending creep and its application to beam-columns, J. appl. mech. (1956) p. 35 - 42

/36/ A.F.McLean, A.F. Fisher, R.J. Bratton: Brittle materials design, high temperature gas turbine, Interim report, Jan. 1 - June 30, 1973, AMMRC - CTR 73 - 32

/37/ D. Vollath: Neue Methode zur Auswertung von Kriechversuchen, Ber. Dt. Keram. Ges. 50 (1973) p. 31 f

/38/ J.L. Iskoe, e.a.: Effect of selected impurities on the high temperature mechanical properties of hot-pressed silicon nitride, Westinghouse research lab. (1974), AD/A - 002 251

/39/ G.W. Hollenberg, G.R. Terwilliger, R.S. Gordon: Calculation of stresses and strains in four-point bending creep tests, J. Amer. Ceram. Soc. 54 (1971), p. 196 - 199

/40/ R. Kossowsky, D.G. Miller, E.S. Diaz: Tensile and creep strengths of hot-pressed Si_3N_4, J. Mater. Sci. 10 (1975) p. 983-997

/41/ S.U.Din, P.S. Nicholson: Creep of hot-pressed silicon nitride, J. Mater. Sci. 10 (1975) p. 1375 - 1380

/42/ W. Ashcroft: The tensile and bend strengths of silicon nitride and hot-pressed silicon carbide, in Special Ceramics 6, ed. by P. Popper, Brit.Ceram.Res.Ass. (1975) p. 245 - 260

/43/ J.E. Restall, C.R. Gostelow: A limited assessment of selected low-expansion coef-ficient ceramic materials with potential for high-temperature applications, in: Proceedings of the Brit. Ceram. Soc. 22, ed. by D.J. Godfrey, (1973) p. 89 - 115

/44/ N.J. Osborne: Creep testing of high temperature engineering ceramics, in : Procee-dings of the Brit.Ceram. Soc. 25 (1975) p. 263 - 280

/45/ J.L. Ishoe, F.F. Lange, E.S. Diaz: Effect of selected impurities on the high tempe-rature mechanical properties of hot-pressed silicon nitride, J.Mater.Sci. 11 (1976) p. 908 - 912

/46/ R. Rossin, J. Bersan, G. Urbain: Etude de la viscosité de laitiers liquides appar-tenant au système ternaire: SiO_2-Al_2O_3-CaO, Rev. Hautes Temp. Refract. 1 (1964) p. 159 - 170

/47/ J.A. Williams: A general approach to creep failure resulting from wedge crack growth, Phil. Mag. 20 (1969) p. 635 - 639

/48/ J.A. Mangels: Development of a creep-resistant reaction-sintered Si_3N_4, in /32/ p. 195 - 206

/49/ D.S. Thompson, P.L. Pratt: The mechanical properties of reaction-sintered silicon nitride, in: Proceedings of the Brit. Ceram. Soc. 6 (1966) p. 37 - 47

/50/ G. Grathwohl, F. Porz, F. Thümmler: Beitrag zur Entwicklung von kriechfestem reak-tionsgesintertem Siliziumnitrid, Ber. Dt. Keram. Ges. 53, 9 (1976), in print

/51/ S.U.Din, P.S. Nicholson: Creep deformation of reaction-sintered silicon nitrides, J. Amer. Ceram. Soc. $\underline{58}$ (1975), p. 500 - 502

/52/ E.M. Levin, C.R. Robbins, H.F. McMurdie: Phase Diagrams for Ceramists, ed. by M.K. Reser, Amer. Ceram. Soc. Columbus, 1964

/53/ E. Glenny, R.A. Taylor: The high-temperature properties of ceramics and cermets, Powder Met. (1958) p. 189 - 226

/54/ W. Engel, F. Porz, F. Thümmler: Messung der inneren Oxidation von kriechbeanspruchtem reaktionsgesintertem Si_3N_4, Ber. Dt. Keram. Ges. $\underline{52}$ (1975) p. 296 - 299

/55/ F. Thümmler, F. Porz, G. Grathwohl, W. Engel: Kriechen und Oxidation von reaktionsgesintertem Si_3N_4, in: Science of Ceramics 8, Brit. Ceram. Soc. (1976) p. 133 - 144

/56/ R.D. Chipman: Stress-strain-temperature-time relationships for refractory materials, Atomics International, a division of north American Aviation, Inc. Canoga Park, Calif., (1958), NAA-SR-3205

/57/ P.L. Farnsworth, R.L. Coble: Deformation behaviour of dense polycrystalline SiC, J. Amer. Ceram. Soc. $\underline{49}$ (1966) p. 264 - 268

/58/ T.L. Francis, R.L. Coble: Creep of polycrystalline silicon carbide, J. Amer. Ceram. Soc. $\underline{51}$ (1968) p. 115 f

/59/ P. Marshall, R.B. Jones: Creep of silicon carbide, Powder Met. $\underline{12}$ (1969) p. 193 - 208

/60/ A.G. Evans: High-temperature slow crack growth in ceramic materials, in: /32/ p. 373 - 396

/61/ K.S. Mazdiyasni, C.M. Cooke: Consolidation, microstructure and mechanical properties of Si_3N_4 doped with rare-earth oxides, J. Amer. Ceram.Soc. $\underline{57}$ (1974) p. 536 f

18
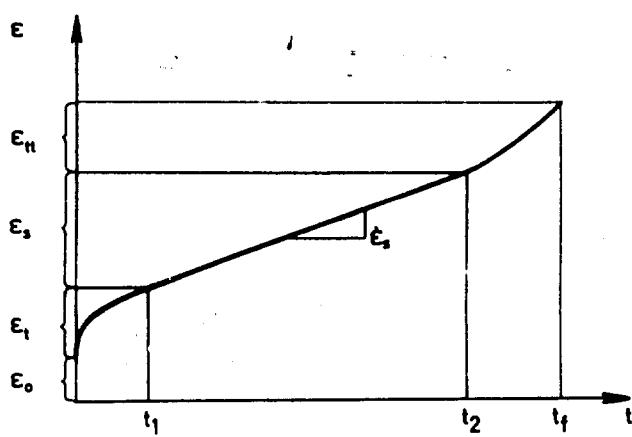
Fig 1:Creep straim vs. time
                (σ,T=const.)
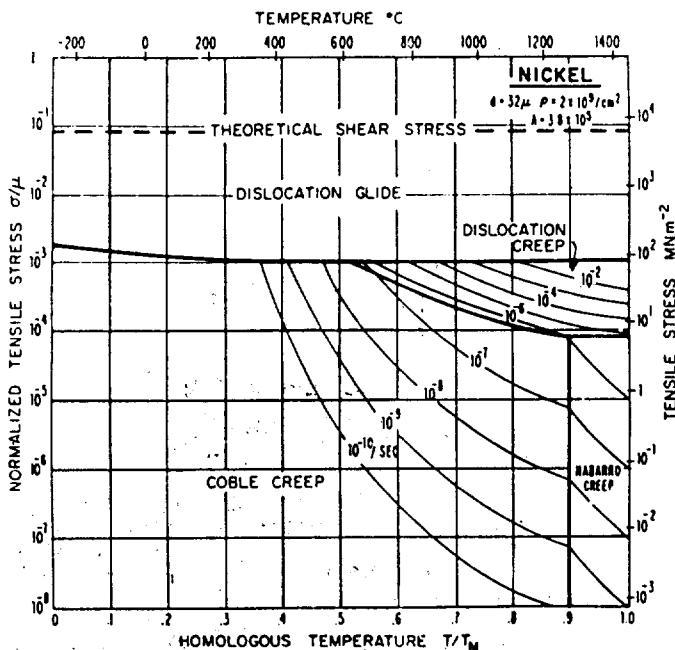
Fig. 2: Deformation map of Ni /26/
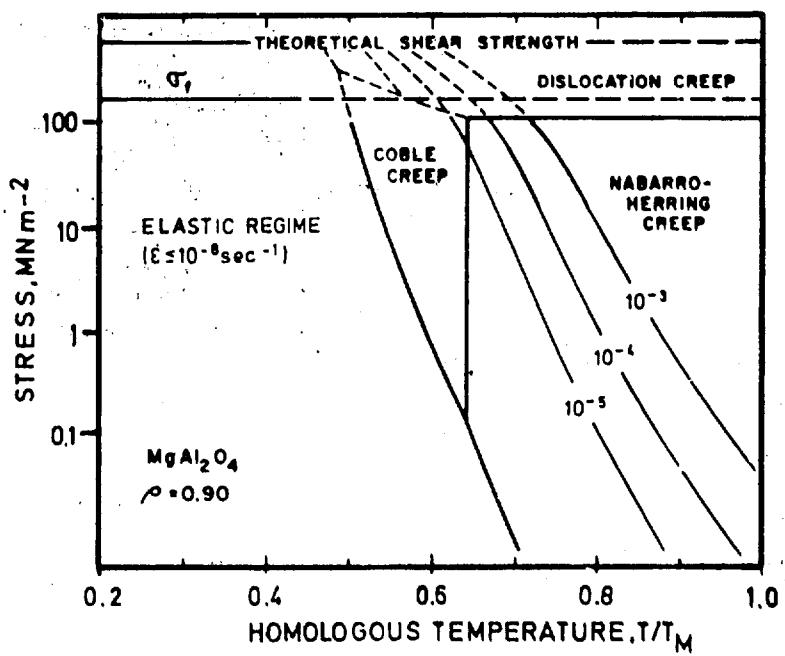

Fig. 3: Deformation map
         of MgAl₂O₄ /26/
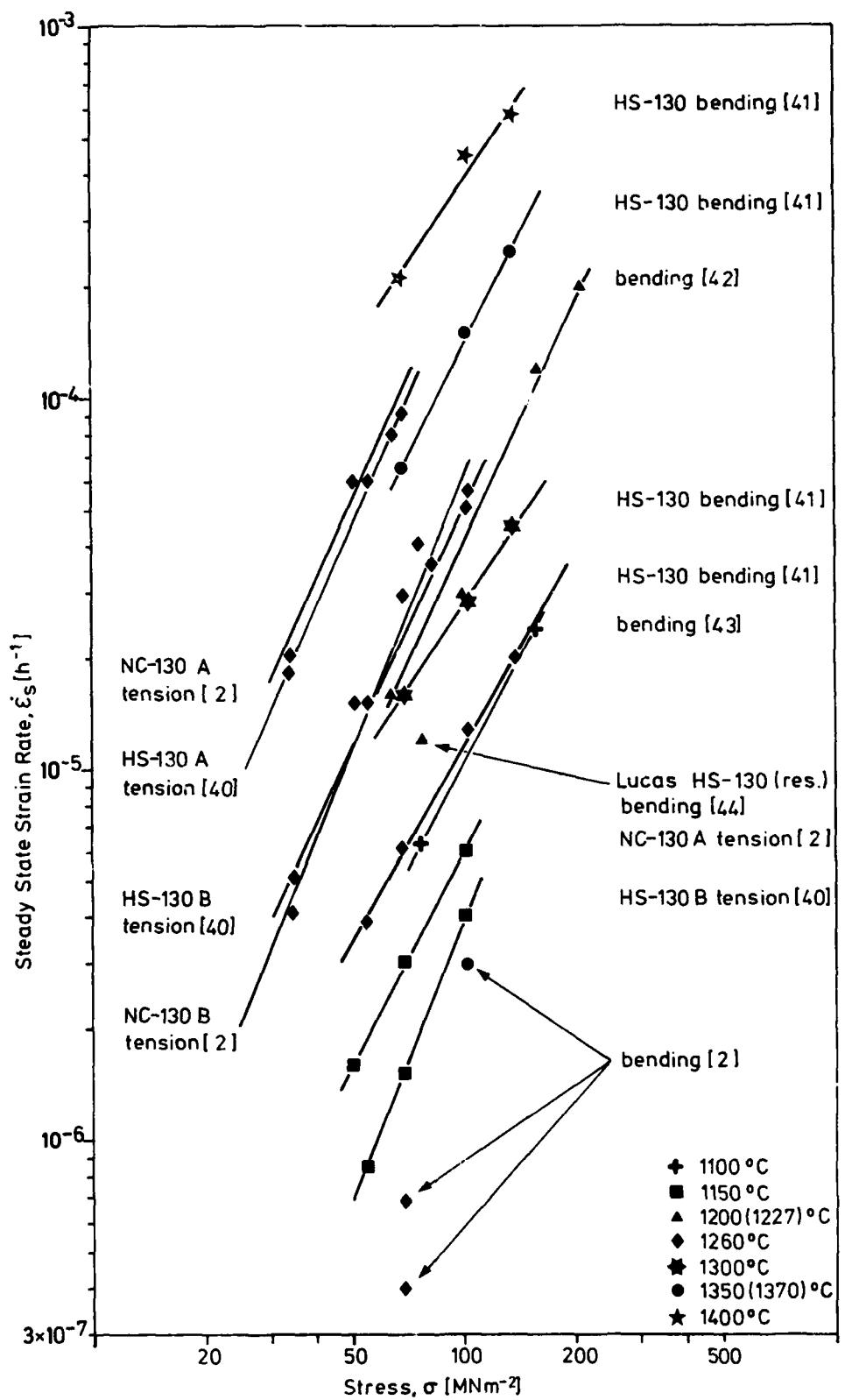
Fig. 4 : Steady state creep rate of various types of HPSN

20

Material	Impurities or additives, resp. (wt-%)						Ref.
	Ca	Na	K	Al	Fe	Mg	
HS – 130	0,04	–	–	0,4	0,4	0,7	/41/
HS – 130A	0,06–0,08	0,006–0,01	0,004–0,008	0,1–0,2	0,5	0,3–0,4	
HS – 130B	0,03–0,05	0,004–0,006	0,004–0,006	0,2	0,5	0,3–0,4	/2,32/

Table 1 : Chemistry of advanced HPSN-qualities
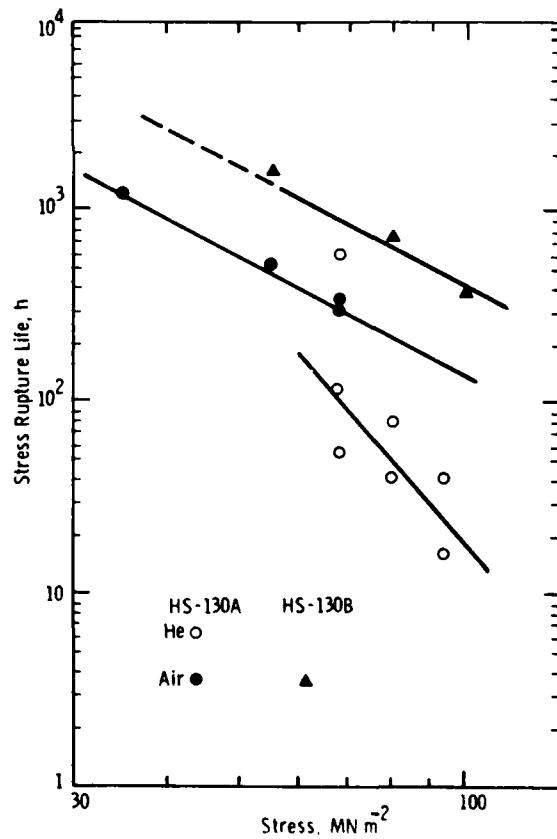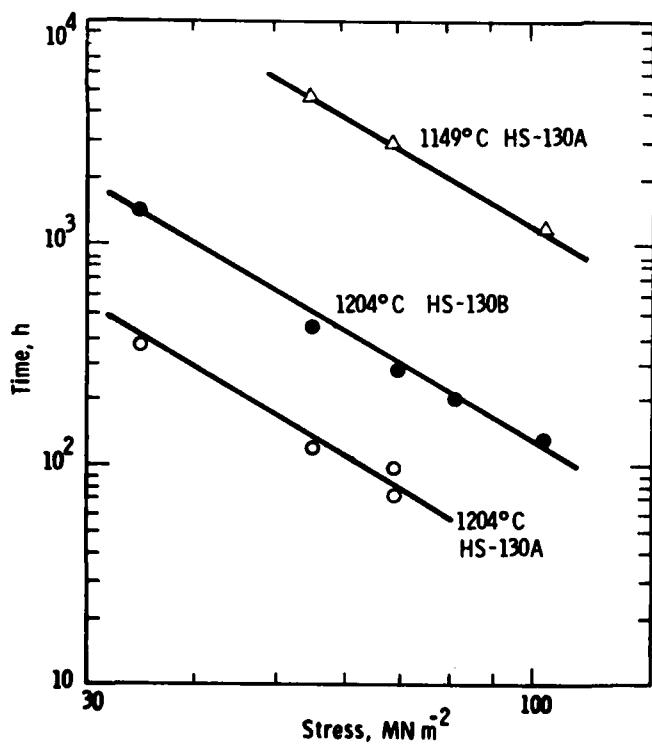
Fig. 5: Time to 1% creep strain as a function of stress in air /40/

Fig. 6 : Stress rupture of HPSN at 1260°C /40/

Fig. 9 : Grain-boundary separation after
deformation /41/

$$\dot{\varepsilon}_s \approx A X_{ca}^n$$

$$n \approx 3.5$$

Steady State Creep Rate, $\dot{\varepsilon}_s$, hr^{-1}

Wt % Ca, Bulk Composition
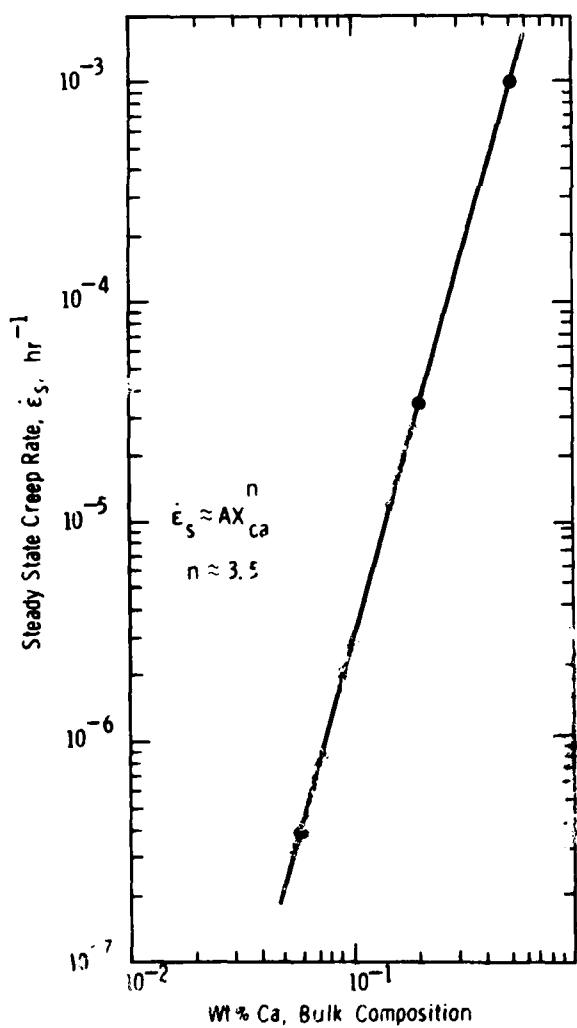
Fig. 7: Dependence of $\dot{\varepsilon}_s$ on Ca content
(qualitative) of HPSN
(1149°C, He, 68,0 MN/m^2)/32/

Temperature °F

▲ HS-130A in He
△ HS-130A in Air
● HS-110B in He
■ HS-110A in He

$\Delta H = 546 \, kJ \, mol^{-1}(\pm 20)$
$(130 \, kcal/mol^{-1})$

$\Delta H = 630 \, kJ \, mol^{-1}(\pm 20)$
$(150 \, kcal \, mol^{-1})$

Steady State Creep Rate $\dot{\varepsilon}_s$, h^{-1}

1/T. 10^{-4} K^{-1}
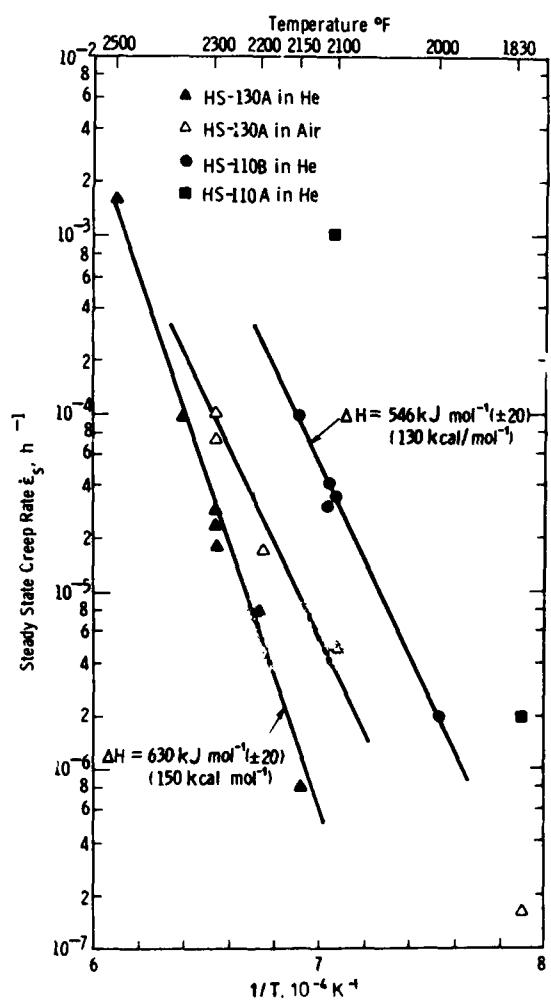
Fig. 8: Arrhenius plots for various types of
HPSN at 70,5 MN/m^2 /40/

22
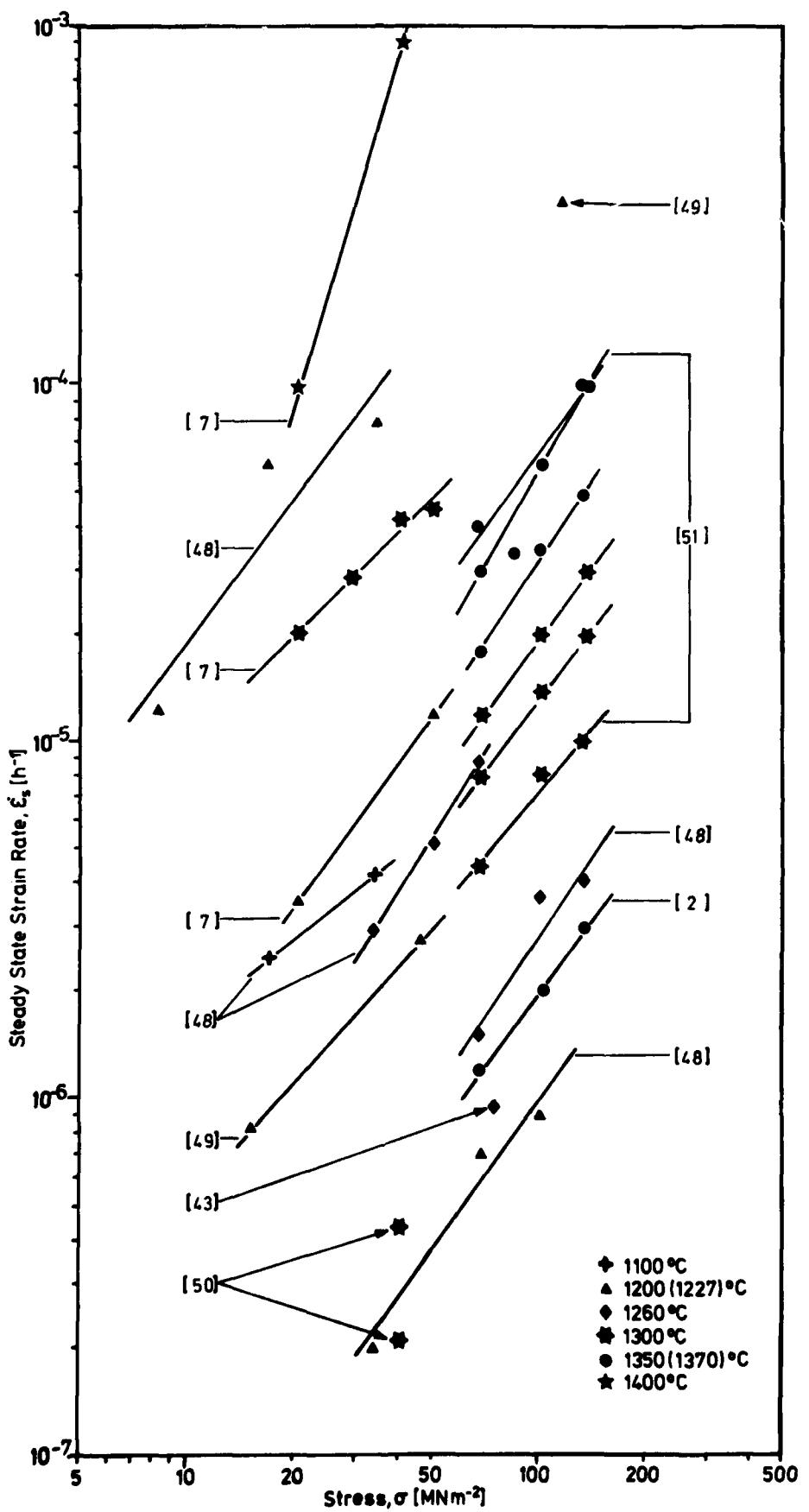
Fig. 10 : Steady state creep rate of various RBSN materials
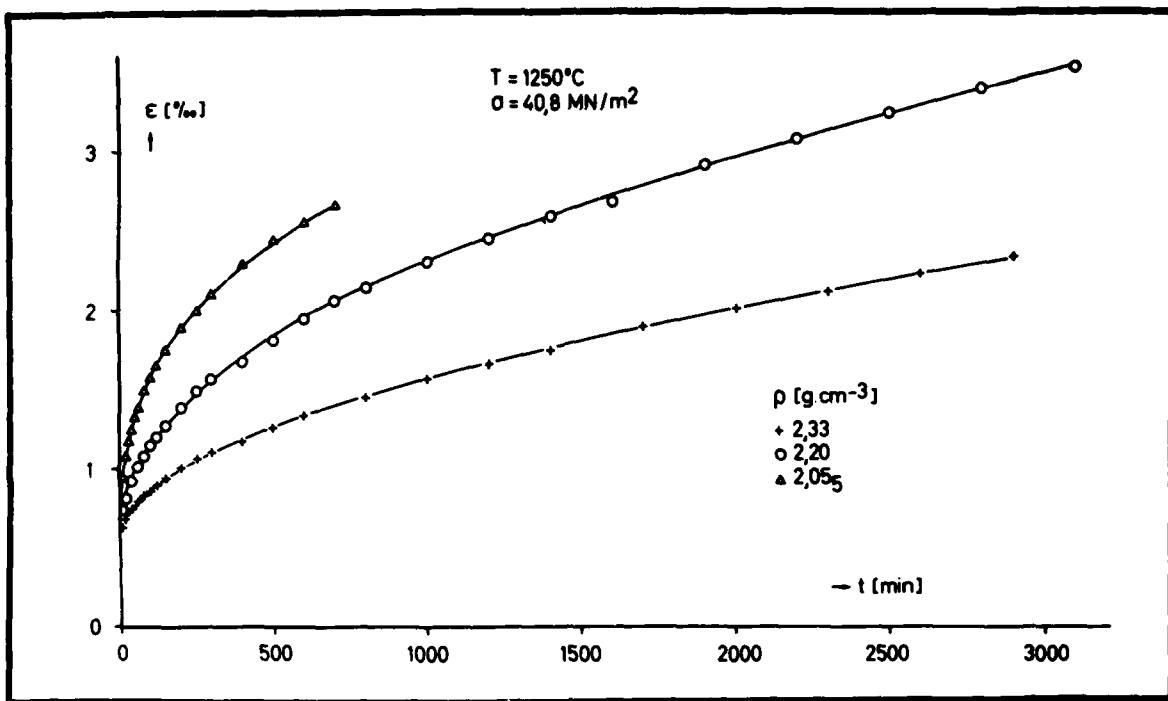
Fig. 11 : Creep dependence on density of RBSN /7/
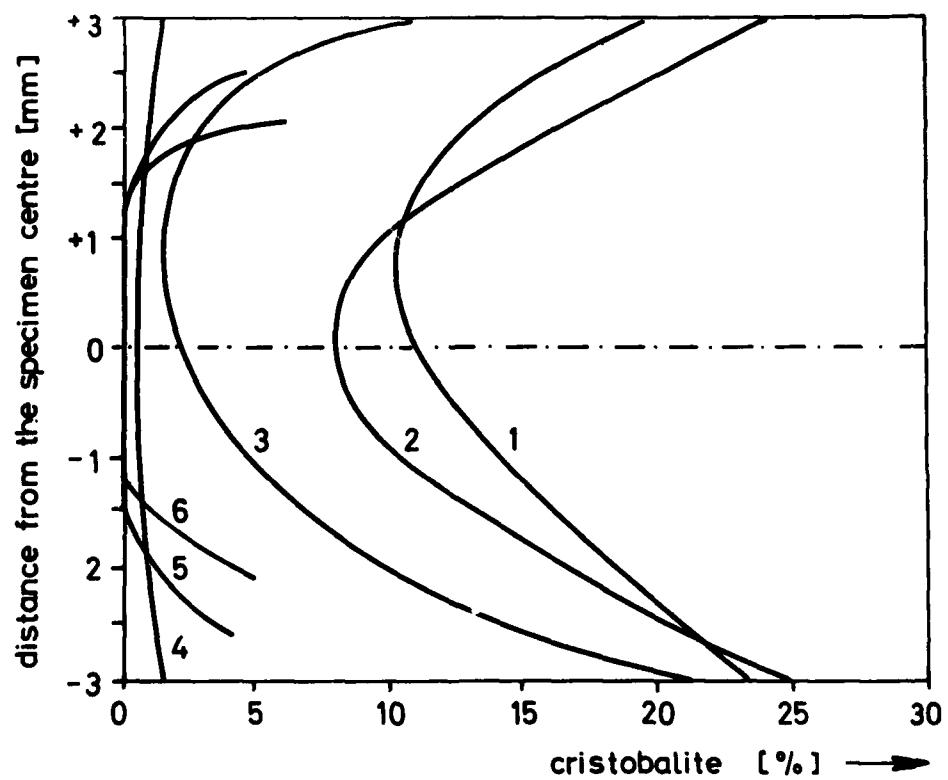
Fig. 12 : Profiles of cristobalite in RBSN-samples after creep experiment /50/
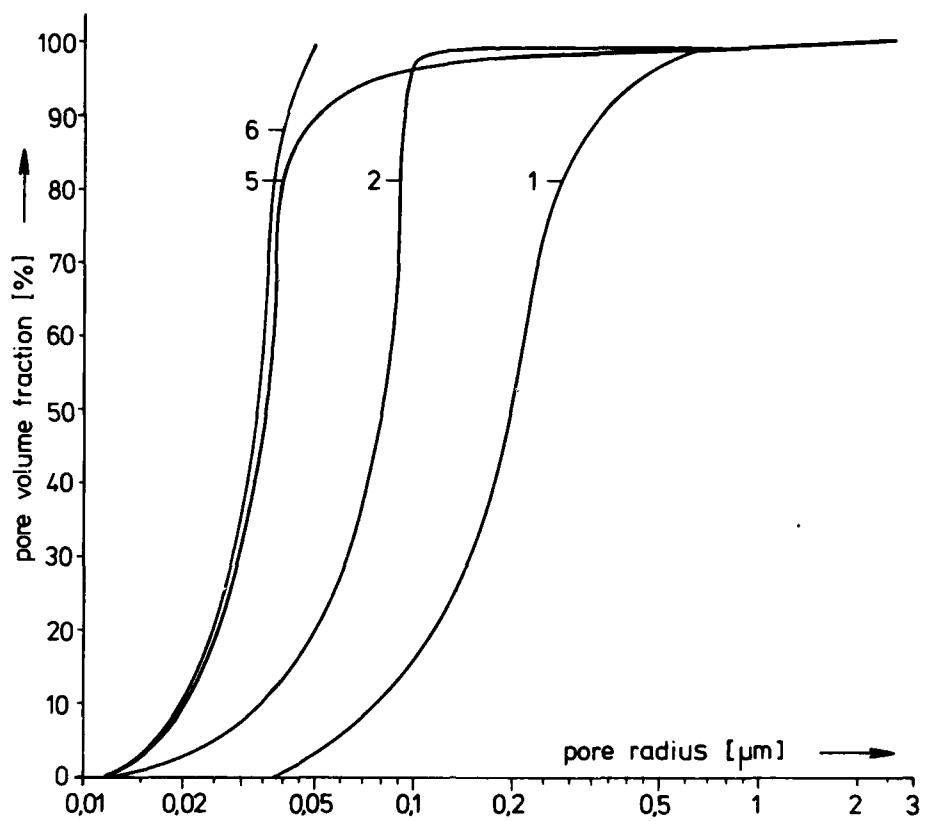
Fig. 13 : Pore size distributions in different RBSN qualities   /50/
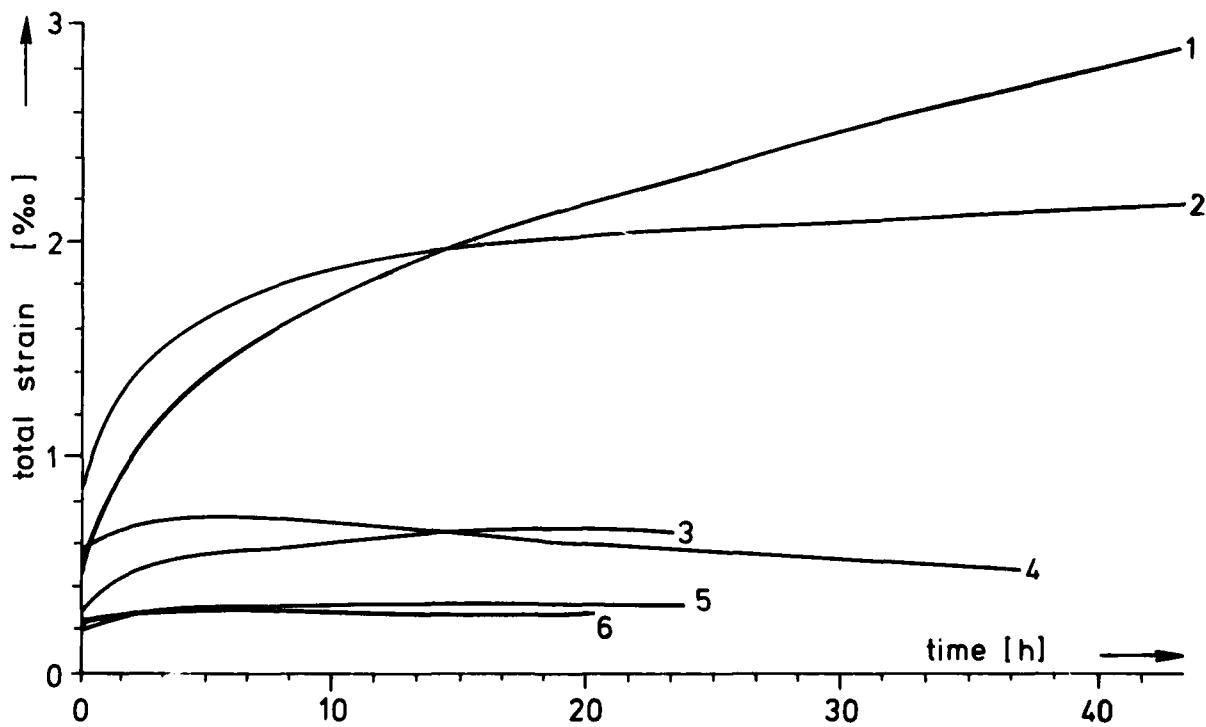
Fig. 14 : Creep curves of different RBSN qualities   /50/
(1300°C, sample 4 1350°C, 40 MN/m² in air)

specimen	characterization	density/g/cm3/	r_{50}/µm/ [×]
1	Annawerk, 98/1	2.18	0.2
2	Annawerk, 98/2	2.14	0.08
3	Annawerk, 98/2 SiO_2beschichtet	2.12	0.08
4	Annawerk, 98/2 SiC beschichtet	2.13	0.08
5	Annawerk, Ar 1200	2.56	0.035
6	Norton, NC-350	2.45	0.034

Table 2 : Characterization of RBSN samples with respect to fig. 12-14
×) 50% of the pore volume is found below the r_{50} value

exp.cond. and results ╲ Authors	Coble et al. /57,58/	Marshall and Jones /59/
material	SiC,polycryst. hot pressed >99%T.D. av.grain size 26µm Al:1,65% Fe:0,97% W:0,20% Si,0 not determined	SiC, polycryst. react. sintered,grain size ∿10µm, ∿8% porosity, filled with Si (5-10vol-%),Al: 0,025%,Fe: 0,045%, Ti 0,020%, 0 not determined
test machine and procedure	Instron, 4-point-bending constant crosshead velocity $\dot{\omega}$=1,27·10^{-4}-1,27·10^{-3}mm/min plot: load vs.crosshead displacement	Creep machine, 4-point-bending, constant load apply, plot:deflection vs. time
test conditions	$1900°-2200°C$ in Argon up to 20,7 MN/m^2	$1000-1300°C$ in air 20,7 MN/m^2 to 49,6MN/$m^2$1000h
principal result	steady state creep viscous deformation via grain boundary diffusion D_b.W=7·10^{-8} exp (Q/RT) Q_b∿ 306 kJ/mole example:2000°C 1h 100MN/m^2 outer fiber strain:0,5% $\dot{\varepsilon}$=5·10^{-3}/h	transition creep ε_t=At^m m = 0.2 - 0.5 A∿σ^n exp (-Q/RT) n=1(1000°C)Q∿230 kJ/mole n=2(1100-1200°C) example: 1200°C,1h 30,3MN/m^2 outer fiber strain:0.05%

Table 3 : Comparison of creep experiments on SiC under very different conditions
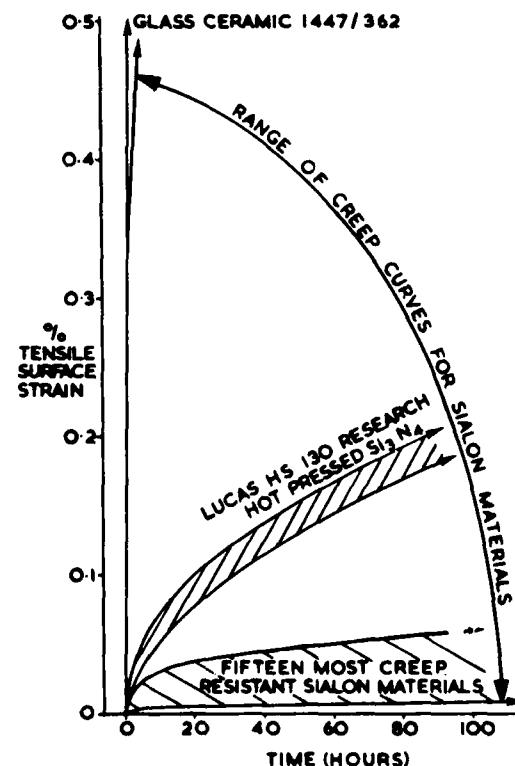
Fig. 15 : Creep of research sialon materials (1227°C, 77 MN/m^2)/44/
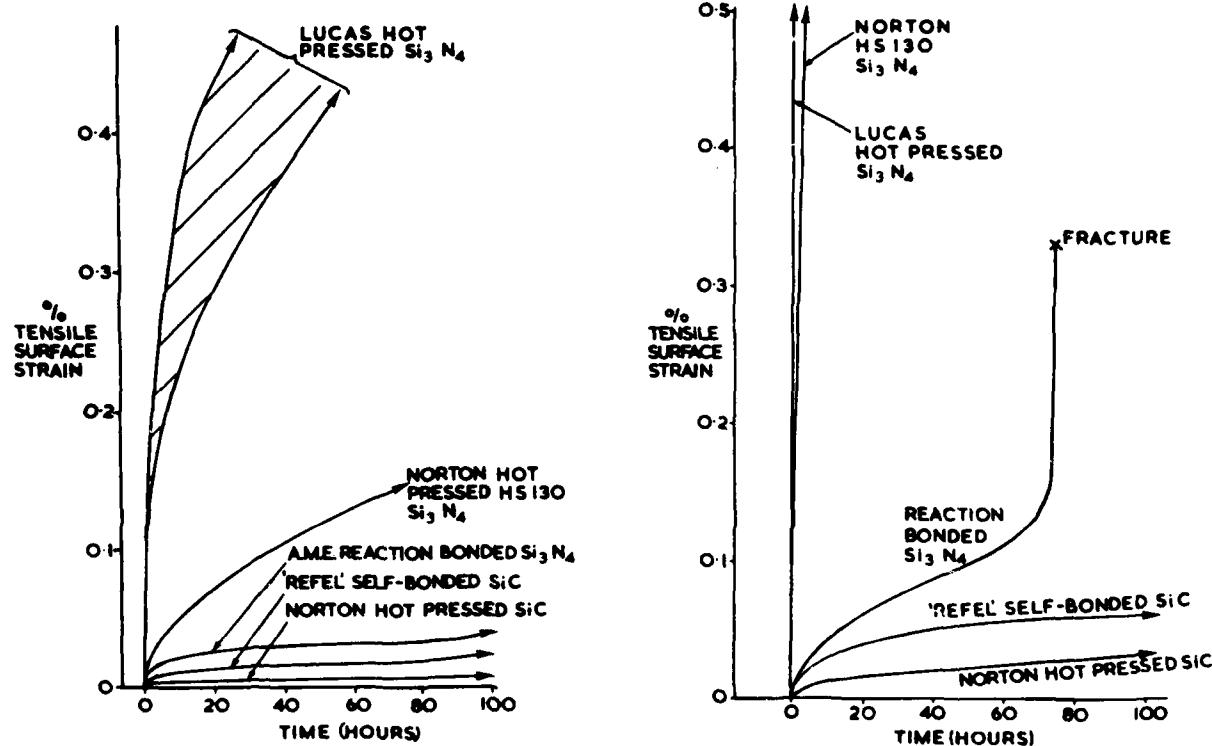
Fig. 16:Creep of commercially available SiC, compared with Si₃N₄ qualities /44/ (1227°C, 77MN/m²)

Fig. 17: Creep of commercially available SiC compared with Si₃N₄ qualities /44/ (1370°C, 77MN/m²)
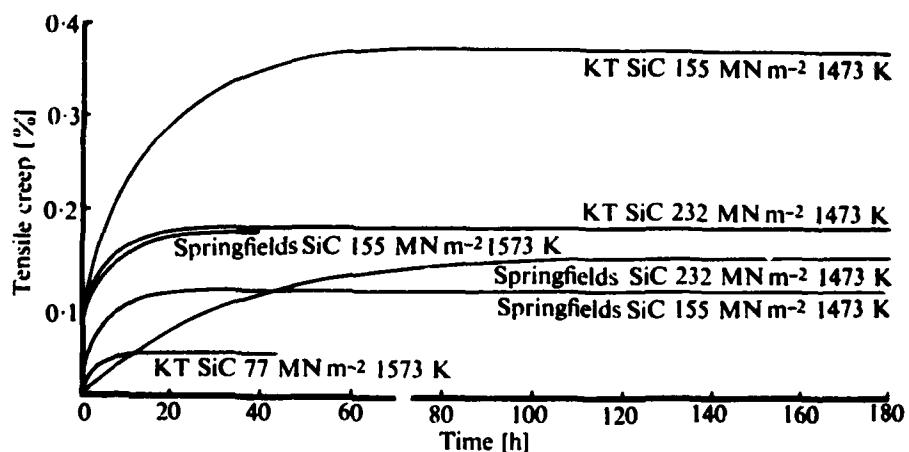

Fig. 18: Typical bend-creep behaviour of reaction-sintered silicon carbide /43/

FRACTURE MECHANICS OF HIGH TEMPERATURE CERAMICS

by

P.M. Braiden
Department of Engineering Science
University of Durham
Durham DH1 3LE
U.K.

SUMMARY

This paper discusses the general concepts of fracture mechanics as applied to ceramics. The experimental techniques necessary for accurate measurement of fracture mechanics parameters are described. Some approaches to the characterisation of the fracture properties of some engineering ceramics are discussed with particular attention to slow strain rate tests.

1.   INTRODUCTION

In recent years considerable attention has been focussed on ceramic materials for aerospace and gas turbine applications. These potential uses have led to a broader understanding of the fracture of ceramic materials which have always been of interest to the materials scientist studying fracture and flow.

Ceramics have a number of outstanding properties, including high hardness and stiffness (at values which are the highest for all known materials), chemical inertness, low thermal and electrical conductivities and high temperature stability. They are also very brittle, which in an engineering sense means that they break with no warning and no prior plastic deformation. In a materials science sense this brittleness means that they have very low toughness values. It is thus particularly important for the successful structural use of ceramics that the fracture mechanics parameters are well defined.

The somewhat intractable mechanical properties of ceramics together with the benefits which would result if they should find effective use have lead to a considerable amount of research in these materials, and a number of excellent reviews have been published (1-5).

2.   CONCEPTS OF FRACTURE MECHANICS

If the tensile strength of a material is calculated simply on the basis of the force required to seperate rows of adjacent atoms a value of about $E/10$ where E is the elastic modulus is obtained (6). However, measured strengths of bulk materials are between $E/10^2$ and $E/10^3$. This discrepancy is due to the presence of cracks and flaws which are present in all materials. These flaws produce stress concentrations when the body is loaded. The commencement of fracture can be simply considered as the stress concentration at the tip of a critical flaw reaching the theoretical strength. An alternative approach is to consider the energy balance in a cracked body. The crack will grow only when the strain energy release rate per unit increase in crack area is equal to or greater than the energy contained in the new surface created. Both of these concepts lead to similar expressions for the fracture stress σ_f in terms of the Young's Modulus, E, the thermodynamic surface energy of the material γ_o, and the crack length of 2c. However which of the concepts forms the necessary and sufficient condition for fracture remains unclear.

The above ideas were first proposed by Griffith, (7,8) who verified them by experiments on glass specimens, and hence obtained the classical "Griffith fracture" expression.

$$\sigma_f = \left[\frac{2E\gamma_o}{\pi C} \right]^{\frac{1}{2}} \tag{1}$$

In experimental verifications of this expression an effective surface energy for the initiation of fracture γ_i replaces γ_e, C is identified as the length of some critical flaw, and a geometric factor Y is introduced.

In recent years an alternative approach has been developed through fracture mechanics. This considers fracture as three modes of crack surface displacements, (fig. 1), and the stresses at the tips of any given crack may be found by stress analysis, and expressed as an algebraic equation. The equations may be rearranged to employ three parameters K_I, K_{II}, K_{III}, where the subscript refers to the appropriate displacement mode. These parameters are the "stress intensity factors", and they control the intensity but not the distribution of the stress field, and reflect the redistribution of stress in a cracked body due to the crack. Solutions have been obtained giving K_I, K_{II}, K_{III}, for cracks in a variety of locations within loaded bodies,(9)(for example an edge crack in a beam subjected to bending loads), and this has enabled a great   number of experiments to be performed with a variety of specimen geometries. Thus critical values of the stress intensity factors for example, K_{IC}, have been defined for various materials and testing conditions, and these may be regarded as material properties.

The fracture mechanics approach is related to the classical Griffith work by defining the K_I stress intensity factor as

$$K_I = Y.\sigma_I . C^{\frac{1}{2}} = (2EY_i)^{\frac{1}{2}} \tag{2}$$

In general, the Griffith equation has been used in the materials science approach whilst the fracture mechanics expressions are more valuable for engineering assessments. In materials science investigations the object is usually to find a value for Y_i and then to relate this to the crack length C through micro-structural considerations. In the engineering approach, which appears to have been employed only rarely until very recently, the object is to find a value for K_{IC} so that this may be used in design or materials development.

An alternative approach using fracture mechanics is the use of the strain energy release rate G. Thus G_{IC}, G_{IIC}, G_{IIIC} may be defined similarly to K_{IC}, K_{IIC}, K_{IIIC} and represent the critical strain energy release rates for cracks under modes I, II and III respectively. G_{IC} and K_{IC} are related according to

$$G_{IC} = \frac{(1 - \nu^2) K_{IC}^2}{E} \tag{3}$$

3. FRACTURE MECHANICS AS APPLIED TO CERAMICS

In fracture mechanics experiments on ductile materials such as metals a number of precautions are necessary. Most of these precautions are required because ductility implies that plastic flow occurs at the tip of any crack and the rationale of fracture mechanics was developed from linear elasticity. It follows therefore that in materials where only very limited crack tip plasticity might be expected, such as ceramics, major modifications of the original approach are not required.

In general ceramic materials exhibit no deviation from linear elasticity and there is no pop-in effect preceding crack propagation. Due to the limited plastic flow at the crack tip there is no crack opening displacement without some crack growth, and the load at the commencement of crack propagation may be used to calculte K_I.

In making plane strain fracture toughness measurements on metals a thickness constraint must be satisfied(10), so that true plane strain conditions are obtained at the centre of the crack plane. This condition may be expressed as

$$t > 2.5 \left[\frac{K_{IC}}{\sigma_{ys}} \right]^2 \tag{4}$$

where t is the thickness, and σ_{ys} the yield strength of the material. For ceramic materials this thickness criterion is almost always satisfied, which is once again a function of the limited plastic flow at the crack tip.

The difficulties associated with making reliable fracture mechanics measurements on ceramics are due to the need to produce a sharp pre-crack in the test piece, and the fact that results are often required at temperatures which are in the useful operating range of ceramics, say above 1200°C.

3.1 Methods of pre-cracking

For some ceramics reproducible results have been obtained by testing a specimen containing a slot machined with a fine diamond slitting wheel (11). In this case the many small cracks produced at the root of the notch appear to behave in the same way as a single large flaw. However to ensure reliability in the results it is usually necessary to attempt to produce a single large crack.

There are four basic methods used to produce sharp cracks in fracture toughness specimens. These are

i) cyclic load mechanical fatigue

ii) by mechanical loading of a notched specimen

iii) by thermal loading of a notched specimen

iv) by a method producing slow crack growth and permitting crack arrest

In metallic specimens sharp cracks are most commonly produced by cyclic mechanical fatigue using a sawn notch as a crack initiator. Most ceramics are not susceptible to fatigue crack growth and this technique is therefore not useful.

Sharp cracks may be produced at the root of a sawn notch in certain types of specimen by mechanical loading. For example a wedge made from a hard friable material such as tungsten carbide may be driven into the notch causing the crack to "jump" in the specimen(3,11). Crack arrest can be facilitated in this method by applying a compressive stress just ahead of the crack by means of a mechanical clamp. Care should be taken in applying the transverse compressive load as the altered stress field may cause the crack to curve in its path. Alternatively the crack opening displacment and the load due to the wedge action may be monitored and hence some degree of control may be exercised over the crack propagation.

For the particular case of ceramics it may be possible to produce a fine crack by means of thermal shock. and some experiments have been reported in which this method was used(12,13). In one of these tests a pre-notched specimen was heated in the notch by means of a hydrogen flame. The flame was then withdrawn and some water droplets were introduced into the notch. It is difficult to control the amount of cracking in this technique and doubts remain as to its validity because of the unknown magnitude of the residual stresses which develop during cooling.

Slow crack growth in ceramics has been the subject of considerable study in recent years(5), and the methods used to obtain slow crack growth, (usually employing constant K specimens in a corrosive atmosphere), may be used to pre-crack specimens for evaluation of K_{IC}. The advantage of employing constant K specimens in this procedure is that a constant displacment rate may be used until the load vs time plot is constant, which signals the formation of a suitable pre-crack. The load can then be used to find the crack length, which is particularly valuable for porous materials or those where dye penetrants cannot be used.

3.2 Test techniques

The particular test specimen chosen depends on material factors, such as the porosity, the test temperature, whether data is required at a slow or rapid strain rates and the machining and pre-cracking facilities available.

Porosity is a factor because of the difficulty of identifying a pre-crack in porous materials using dye penetrants. If a porous material is to be tested therefore it is usually better to choose a constant K specimen so that the pre-crack may be formed and its length found using the compliance method (see below). Tests at high temperature create difficulties in that metallic load points cannot be used at the temperatures of interest for ceramics. The uncertain tensile strength of ceramics themselves means that even if ceramic load points are employed they are best used under conditions of compressive stress, which eliminates certain specimen geometries.

These and other considerations effectively eliminate many of the test techniques which have been developed for metals. For example single edge cracked tension specimens and edge cracked plate specimens may not be used because of the difficulties of producing axial loading, and avoiding spurious bending effects.

The most useful specimens for tests with ceramic materials are:

  i)   Edge cracked three or four point bend beams

  ii)   The double cantilever beam

  iii) The tapered cantilever beam

  iv)   The constant moment specimen

  v)   The double torsion specimen

The advantages, disadvantages and best applications of these configurations are discussed below.

3.2.1 Edge cracked three or four point bend specimens

This is a very convenient specimen which is simple to fabricate and test. One disadvantage is that it is difficult to pre-crack, although some success has been reported using the thermal shock method (12,13). In general bend specimens are cut from larger blocks of material after some pre-cracking procedure (e.g. by wedge action) has been performed. This specimen geometry is limited to experiments where it is not necessary to observe the crack growth visually, as the crack obviously cannot be contained within the specimen for sufficient time to afford successful observations. It is suitable for high and low strain rate experiments and for use at high temperatures. A typical K calibration for a single edge cracked beam specimen is given in fig. 2. Calibrations for other dimensions may be found in the literature(10).

3.2.2. The double cantilever beam

This specimen geometry which was first used by Gilman,(14) is illustrated in fig. 3. The stress intensity factor K, and the displacment of the loading points δ, given in the figure are due to Weiderhorn, (15) who developed Gilman's original method. Double cantilever beam specimens are relatively easy to pre-crack, using a wedge driven into the specimen. They have found greatest applications in slow crack growth experiments where the propagation of the crack front under constant load may be followed using a travelling microscope. Unfortunately the stress intensity factor K, depends on the crack length (fig. 3) and for accurate results therefore the crack increments measured for each load application must be much smaller than the crack length. Crack length increments of 10% of the crack length are usually employed and lead to acceptably low errors. Because of the need for direct visual observation of the crack propagation these specimens are not suited to porous materials, measurements at high temperatures, or hostile environments.

3.2.3. The tapered cantilever beam

This configuration is illustrated in fig. 4. The great advantage of this specimen is that the stress intensity factor is independent of the crack length. This is known in fracture mechanics as a "constant K" specimen, and this enables a compliance technique (see below) to be used which means that visual observation of the crack is not required. This is of great value in pre-cracking and slow crack growth experiments and when testing porous materials, since the progress of the crack front can be monitored by simply recording the applied load. The disadvantage of the tapered cantilever beam is that the load is applied in a tension mode which makes it unsuitable for high temperature tests.

3.2.4 The constant moment specimen

This is illustrated in fig. 5, which shows that this is a modification of the double cantilever beam specimen (16). However, it has a major advantage over that system in that it is a constant K specimen. Unfortunately the method of load application, through relatively long beams, does not lend itself to high temperature applications.

3.2.5. The double torsion specimen

This test uses the specimen illustrated in fig. 6 which is simple to fabricate, the only difficulty being the need to introduce a control notch along the length of the specimen to ensure that the crack does not deviate from the centre.

The specimen gives a constant K being independent of crack length, and is thus ideally suited to measurements in porous materials and also to measurements at high temperatures since all of the loading points are in compression. The long crack lengths attainable are particularly useful for slow crack growth tests. Alternatively a number of values for K may be obtained from one specimen.

The method was devised by Outwater (17) who used a travelling microscope to measure the rate of crack growth under a constant applied load. However the method was improved and extended by Evans (18,19) who showed that at a constant displacement (or constant displacement rate) the crack growth may be obtained directly from the load P or the load relaxation rate $dP/_{dt}$. This is the basis of the compliance technique, and it is this development which makes the double torsion test so useful. Two approaches are available, the constant displacement method or the constant displacement-rate method as follows.

It may be shown by experiment that the displacement of the loading points y, is linearly related to the crack length a and the applied load P, by the compliance relationship

$$y = P(Ba + c) \qquad (5)$$

Differentiating with respect to time we obtain the displacement rate $dy/_{dt}$

$$\frac{dy}{dt} = \frac{dP}{dt}(Ba + c) + PB\frac{da}{dt} \qquad (6)$$

Note that $\frac{da}{dt}$ is the crack velocity, which at constant displacement ($\frac{dy}{dt} = 0$) is given by

$$\frac{da}{dy} = \frac{-(Ba + c)\frac{dp}{dt}}{BP} \qquad (7)$$

At constant displacement (y = constant, equation 5) for a specimen with an initial crack length a and load P, and a final crack length a_f, load P_f,

$$P(Ba + c) = P_f(Ba_f + c) \qquad (8)$$

Thus $$(Ba + c) = \frac{P_f(Ba_f + c)}{P} \qquad (9)$$

and substituting into equation 7 we obtain

$$\frac{da}{dt} = -\frac{P_f}{P^2B}(Ba_f + C)\frac{dP}{dt} \qquad (10)$$

For a sufficiently large initial crack length a_i, $c \ll B$, and thus equation (10) simplifies to

$$\frac{da}{dt} = -\frac{P_f}{P^2}a_f\frac{dP}{dt} \qquad (11)$$

The crack velocity can thus be found if the initial and final loads, the load relaxation with time, and the final crack length can be found. In performing the experiment the specimen is loaded rapidly so that no significant crack growth occurs during load application, and the displacement is fixed. The load decay is followed on a pen recorder. After a suitable time the load is removed and the final crack length measured.

An alternative approach is to employ a constant displacement rate. When the change in specimen compliance due to crack growth is equal to the displacement rate of the load points a constant load is obtained. The load/time graph is illustrated in Fig. 7. Thus in equation (6), $dP/dt = 0$, and we obtain

$$\frac{dy}{dt} = PB \frac{da}{dt} \tag{12}$$

In this method the crack velocity da/dt is obtained by measuring the load P and the displacement rate of the load points dy/dt. The constant B has been evaluated analytically (19) as

$$B = \frac{3W_m^2 a}{Wt^3 G} \tag{13}$$

where G is the shear modulus of the material.

One useful application of the constant load approach is in the pre-cracking of constant K specimens. To form the pre-crack a low constant displacement rate is applied and the load vs time relationship is obtained from the recorder on the test machine. This is illustrated in Fig. 7. When the load is constant a suitable sharp crack has formed, and the load may be used to monitor the crack length if necessary, using equation (11). Once an effective pre-crack has been formed K_{IC} may be determined by rapidly loading the specimen to failure noting the load P_{IC}, when K_{IC} is obtained through

$$K_{IC} = P_{IC} W_m \left[\frac{3(1 + \nu)}{Wt^3 t_n} \right]^{\frac{1}{2}}$$

where ν is Poisson's ratio.

3.3 The work of fracture

An additional method which has been developed specifically from the study of the fracture of ceramics is the work of fracture test. In this test a notched beam is loaded in three point bending, and depending on the notch depth either a catastrophic, semi-controlled or a controlled fracture is obtained, as illustrated in Fig. 8. The object behind the test is to obtain a controlled fracture so that γ_f, which is defined as the energy required to generate unit area of fracture surface, may be equated with γ_i, the effective surface energy for the initiation of fracture. The difficulty with this technique is that there is always additional energy (for example in deformation at the loading points) associated with the specimen, and not all of the energy supplied goes into the fracture face. However, some successful applications have been reported, and in principle the test is valid and useful, but the methods noted above are to be preferred if reliable design data is required.

4. COMPARISON OF TECHNIQUES

For any materials test to be acceptable it must be capable of giving accurate reproducible results. Moreover, the results obtained on the same material from different test techniques must agree within the limits of experimental error. Immediately there arises a difficulty with ceramics because the fracture energy values obtained depend on the microstructure. The measured fracture energy depends on the grain size, the porosity, the purity, and, for some materials, the specimen and the method of preparation.

4.1 Tests at slow strain rates

The most usual form of test is that performed at slow strain rates giving values of γ_i or K_{IC} appropriate to general engineering usage. A wide variety of these tests have been performed on ceramics with confusing results from the point of engineering applications. Comparable results have been found between some of the methods noted above when the tests have been performed on the same material under the same conditions. Meredith and Pratt (20) measured K_{IC} for a 95% commercially pure alumina using single edge notched beam, compact tension and double cantilever beam techniques and found that the results agreed within 5%. Weiderhorn et al (21) found closely similar values of K_{IC} for a range of glass compositions, using the double cantilever and the single edge cracked three point bend method. However much more data is required before reliable conclusions can be drawn regarding the reliability of the results obtained.

The first difficulty facing the engineer who requires reliable K_{IC} data is the choice between precracked or machine notched specimens. For example, Davidge and Tappin (11) obtained similar results from machine notches and from sharp cracks formed by a wedge action when testing single edge notched beams of alumina. They concluded that the machining action introduced small microscopic cracks at the root of the notch which were sufficient to provide equivalent atomically sharp cracks. Meredith and Pratt (20) were unable to reproduce this effect with their alumina, and had to pre-crack all of their specimens.

In silicon nitride Evans and Davidge (22) found that the stress to extend a machined notch was about twice that to extend a sharp crack, using single edge notched three point bend specimens. However, similar values for K_{IC} (about 4.5 to 5.0 MN m$^{-3/2}$) for silicon nitride at room temperature have been obtained by Henshall et al, (23), Lange (24) and Evans and Weiderhorn (25). This is interesting in that Henshall used single edge notched beams with no pre-cracking whilst Lange used mechanically pre-cracked double cantilever specimens and Evans the double torsion method. The results of these investigations are summarised in Table 1 and show decreasing agreement at higher temperatures, although whether this is due to the absence or otherwise of pre-cracking or other experimental differences is not clear. Working with refel silicon carbide, Henshall et al (13) found no significant difference in the value of K_{IC} (about 4.4 $\pm$0.2 MN m$^{-3/2}$) obtained with thermally pre-cracked samples or from specimens with machined

notches in four point bend tests. With the same material in three point bend tests McLaren et al (26) found that the results obtained from specimens containing mechanically formed pre-cracks were consistently below those obtained from samples with machined notches. It may be that the thermal pre-cracking technique used by Henshall was not successful in producing true atomically sharp crack fronts. Recent work on both hot pressed and sintered silicon carbide (27) has shown that similar results (room temperature K_{IC} from about 3.8 to 4.2 MN m$^{-3/2}$) may be obtained using pre-cracked double torsion and double cantilever beam specimens. The results of these investigations on silicon carbide are summarised in Table 2.

The greatest difficulty in the choice of test method for reliable K_{IC} values occurs when relationships between K_{IC} and microstructural features are required. The relationship between microstructure and K_{IC} in ceramics is complex and depends on a number of factors including grain size, porosity and the distribution of impurities which may be associated with the type of fracture obtained. In addition pressing and orientation effects may also be present. When the single edge notched beam test method is chosen the notch width and the notch tip radius can also influence the results and analyses of this test (28, 12) have shown that K_{IC} is proportional to the square root of the notch radius. Simpson (29) has compared the double cantilever beam (DCB) containing a wedge loaded pre-crack, with saw notched bend specimens (SENB) using samples of alumina, silicon carbide and graphite. For a sharp crack both test techniques should give the same answer for K_{IC}. However in every case the SENB results were greater than the DCB values. The difference was relatively small, (some 15%) for the alumina used but was much more significant for silicon carbide and graphite. Furthermore the SENB results were strongly dependent on notch geometry, both notch width and depth influencing the results. These tests were all performed on uniformly fine grained materials so that effects of grain size were eliminated as far as possible.

A number of workers have studied the relationship between K_{IC} (or fracture surface energy) and grain size with confusing results (20, 31, 32, 33). In some cases the fracture energy was found to increase with increasing grain size (31) whilst in others a decrease was obtained. The disturbing feature of these results is that there appears to be a correlation between test technique, grain size, and mode of fracture. However, in general for fine grained materials SENB and DCB methods are in agreement, whilst for larger grain sizes the results differ. It appears that the DCB method is more sensitive to grain size than the SENB technique and Simpson (33) has suggested that this may be due to the stress state at the crack tip in a DCB specimen. In addition it is difficult to make positive recommendations on the basis of published data because the mode of fracture often changes from transgranular to intergranular as grain size is varied. Since impurities in ceramics are usually situated at the grain boundaries comparisons between materials of different purity is impossible unless the fracture mode is noted. Further work is required before reliable inferences can be drawn.

4.2 Tests at high strain rates

High strain rate tests are of importance in ceramics because of their potential applications as stators and rotors in gas turbines. In such an application the component could be subjected to high speed low mass particle impact. This has been studied by Evans (34) who found that a critical value of particle momentum must be exceeded before strength loss can occur.

The more familiar techniques for studying fracture under impact conditions such as Charpy and Izod tests have been applied to ceramics (12, 35), but as expected in materials with limited crack tip plasticity the values obtained for the dynamic stress intensity factor K_{ID} are very similar to K_{IC}.

4.3 Slow crack growth measurements

It is not intended in this paper to discuss the results of slow crack growth experiments since that subject, and the development of crack velocity/stress intensity factor diagrams into a design tool for ceramic systems formed the major part of a recent AGARD manuscript (36).

For crack growth rate measurements, specimens which permit a long crack travel are clearly to be preferred and thus the DCB and DT specimens are used. For high temperature measurements the DT specimen is better since the compliance method may be used and thus the crack length obtained without direct visual observation of the specimen. These methods have been widely used (1, 5, 18, 21, 25, 27) and the long term influence of corrosive environments on ceramic materials is now understood in terms of lifetime predictions for ceramic components (36).

5. CONCLUSIONS

In this paper, the concepts of fracture mechanics as applied to ceramic materials have been discussed and the techniques for making useful measurements have been described. Some approaches to the characterisation of the fracture behaviour of these materials and the results obtained have been discussed in detail for slow strain rate tests. It is concluded that further work is required to ensure that the techniques are reliable and to evaluate the effects of microstructural features in ceramics.

Table 1 : Comparison of results obtained on HS 130 silicon nitride

K_{IC} value MN $m^{-3}/2$	Temperature $^\circ C$	Method	Reference
4.5	RT	Single edge notched beam (SENB) no pre-cracking	23
5.1	RT	Double cantilever beam (DCB)	24
4.8	RT	Double torsion (DT)	25
6.3	1300	SENB	23
5.0	1300	DT	25
10.3	1600	SENB	23
12.0	1600	DT	25

Table 2 : Comparison of results obtained by various methods on silicon carbide compositions

Material	K_{IC} MN $m^{-3}/2$	Temperature $^\circ C$	Method	Reference
Refel silicon carbide	4.4 ± 0.2	RT	Single edge notched beam (SENB) four point bend with and without pre-cracking	13
Refel silicon carbide	4.8	RT	SENB three point load no pre-cracking	26
	5.7	1000		
	8.1	1400		
Hot pressed silicon carbide	3.8	RT	Double torsion DT	27
	4.2	RT	Double cantilever beam DCB	27
	3.8	1000	DT	27
	2.8	1400	DT	27
Sintered silicon carbide	3.0	RT	DT	27
	3.1	1000	DT	27
	3.2	1400	DT	27

REFERENCES

1. S.M. Wiederhorn, Fracture of ceramics, in Mechanical and Thermal Properties of Ceramics, NBS Special Publication No. 303, 1969, p 217

2. J.B. Wachtman, Mechanical properties of ceramics : an introductory survey, American Ceram. Bull. Vol 46, No 3, 1967, p 756

3. R.W. Davidge and A.G. Evans, The strength of ceramics, Mater. Sci. Eng., Vol 6, 1970, p 281

4. A.G. Evans, Fracture mechanics determinations, in Fracture mechanics of ceramics, edited by R.C. Bradt, D.P.H. Hasselman, and F.F. Lange, Plenum Press, 1973, p 17

5. S.M. Wiederhorn, Subcritical crack growth in ceramics, in Fracture mechanics of ceramics, edited by R.C. Bradt, D.P.H. Hasselman, and F.F. Lange, Plenum Press, 1973, p 613

6. A. Kelly, Strong solids, Clarendon Press, Oxford, 1966

7. A.A. Griffith, The phenomenon of flow and rupture in solids, Phil. Trans. Royal Soc. London Series A, Vol 221, 1920, p 163

34

8. A.A. Griffith, The theory of rupture, Proc. First Internat. Congr. Appl. Mech., Delft, 1924, p 55

9. P.C. Paris and G.C. Sih, Stress analysis of cracks, in Fracture Toughness testing and its applications, A.S.T.M., S.T.P. No 381, 1965, p 30

10. W.F. Brown and J.E. Srawley, Plane strain crack toughness testing of high strength metallic materials, ASTM STP No 410, 1966

11. R.W. Davidge and G. Tappin, The effects of temperature and environment on the strength of two polycrystalline aluminas, Proc. Brit. Ceram. Soc. 15, 1970, p 47

12. R. Bertolotti, Fracture toughness of polycrystalline alumina, J. Amer. Ceram. Soc. 56(2), 1973, p 107

13. J.L. Henshall, D.J. Rowcliffe, J.W. Edington, Fracture parameters in refel silicon carbide, J. Mat. Sci. 9, 1974, p 1559

14. J.J. Gilman, The direct measurement of the surface energies of crystals, J. of Applied Physics 31, 1960, p 2208

15. S.M. Wiederhorn, A critical analysis of the theory of the double cantilever method of measuring fracture surface energies, J. Applied Physics 39, 1968, p 1569

16. S.W. Freiman, D.R. Mulville, P.W. Mast, Crack propagation studies in brittle materials, J. Mat. Sci. 8, 1973, p 1527

17. J.O. Outwater and D.J. Jerry, On the fracture energy of glass, Interim report, contract NONR-3219 (ONX) University of Vermont, 1966

18. A.G. Evans, A simple method for evaluating the time-dependent failure characteristics of brittle materials – and its application to polycrystalline alumina, J. Mat. Sci. 7, 1972, p 1137

19. D.P. Williams and A.G. Evans, A simple method for studying slow crack growth, J. of Testing and Evaluation, 1(4), 1973, p 264

20. H. Meredith and P.L. Pratt, The observed fracture stress and measured values of γ_{IC} in commercial polycrystalline aluminas, Special Ceramics No 6, B.C.R.A. publication, 1975, p 107

21. S.M. Wiederhorn, A.G. Evans and D.E. Roberts, A fracture mechanics study of the skylab windows, in Fracture Mechanics of Ceramics, Plenum Press, 1973, p 829

22. A.G. Evans and R.W. Davidge, The strength and oxidation of reaction-sintered silicon nitride, J. of Mat. Sci. 5, 1970, p 314

23. J.L. Henshall, D.J. Rowcliffe and J.W. Eddington, The fracture toughness and delayed fracture of hot-pressed silicon nitride, Special Ceramics No 6, B.C.R.A. publication, 1975, p 185

24. F.F. Lange, Relation between strength, fracture energy, and microstructure of hot pressed silicon nitride, J. Amer. Ceram. Soc. 56, No 10, 1973, p 578

25. A.G. Evans and S.M. Wiederhorn, Crack propagation and failure prediction in silicon nitride at elevated temperatures, J. Mat. Sci. 9, 1974, p 270

26. J.R. McLaren, G. Tappin and R.W. Davidge, The relationship between temperature and environment texture and strength of self-bonded silicon carbide, Proc. British Ceram. Soc. 20, 1972, p 259

27. A.G. Evans and F.F. Lange, Crack propagation and fracture in silicon carbide, J. Mat. Sci. 10, 1975, p 1659

28. T.R. Wilshaw, C.A. Rau, and A.S. Tetelman, General model to predict the elastic-plastic stress distribution and fracture strength of notched bars in plane strain bending, Eng. Fract. Mech. 1, 1968, p 191

29. L.A. Simpson, Use of the notched beam test for the evaluation of the fracture energies of ceramics, J. Amer. Ceram. Soc. 57, 1974, p 151

30. R.W. Davidge, Effects of microstructure on the mechanical properties of ceramics, in Fracture Mechanics of Ceramics, Plenum Press, 1972, p 447

31. P.L. Gutshall and G.E. Gross, Observations and mechanisms of fracture in polycrystalline alumina, Eng. Fracture Mech. 1, 1969, p 463

32. A.G. Evans and G. Tappin, Effects of microstructure on the stress to propagate inherent flaws, Proc. British Ceram. Soc. 20, 1972, p 275

33. L.A. Simpson, Microstructural considerations for the applications of fracture mechanics determinations, in Fracture Mechanics of Ceramics, Plenum Press, 1973, p 567

34. A.G. Evans, Strength degradation due to projectile impacts, J. Amer. Ceram. Soc. 56, 1973, p 405

35. H. Abe and R.C. Bradt, Instrumented charpy impact testing of silicon carbides, Proc. Conf. Dynamic Fracture Toughness, The Welding Inst. London 1976, paper 3

36. R.W. Davidge and J. Massmann, Mechanical property testing of high temperature materials, AGARD
report 634
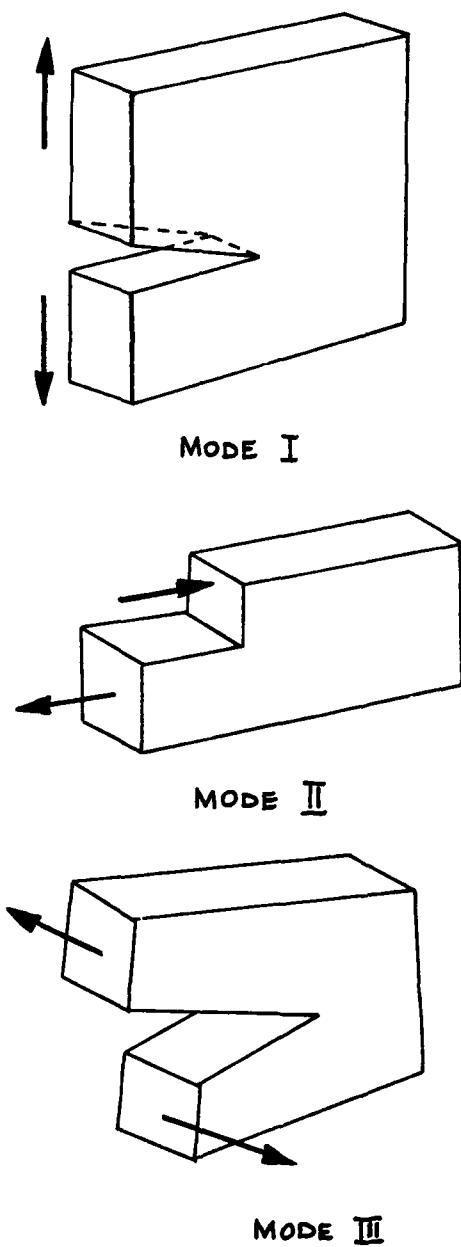

Fig.1   Three modes for crack opening displacement
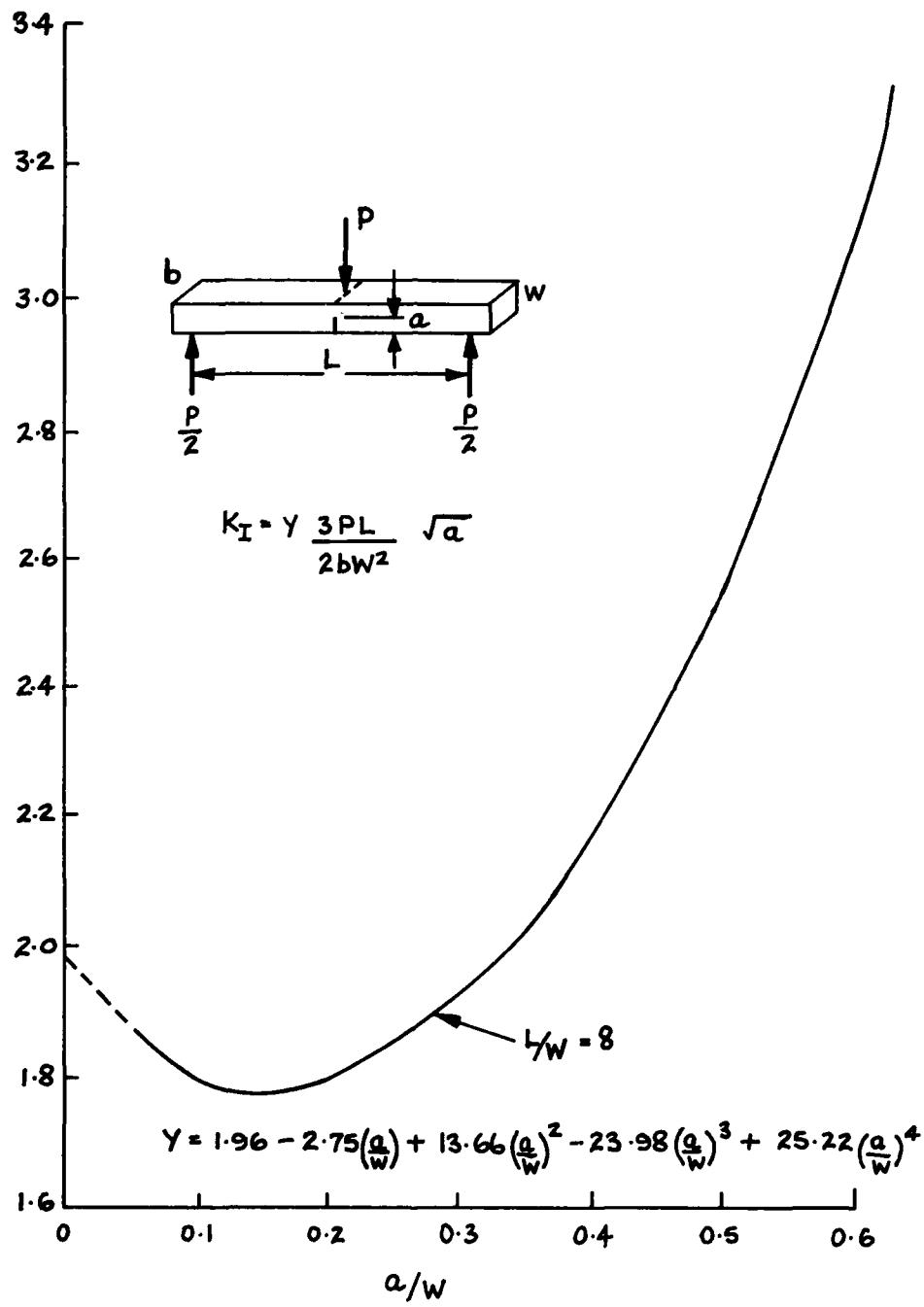
Fig.2 K_I calibration and geometry of SENB 3 point bend specimen

$$K_I = 3.45 \frac{Pa}{bt^{3/2}} \left[1 + 0.7 \left(\frac{t}{a}\right)\right]$$
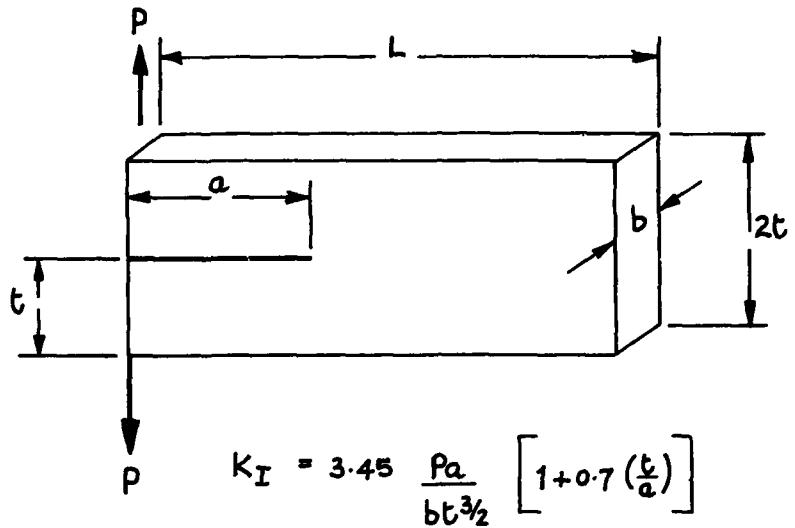
$$\delta = \frac{4Pa^3}{EWt^3} + 7.92 \frac{Pa^2}{EWt^2} + 2.65 \frac{Pa}{GWt}$$

Fig.3   Double cantilever beam (DCB) specimen
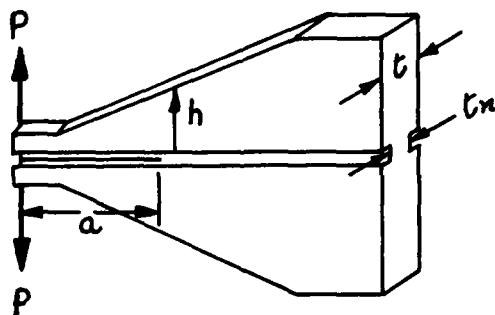
$$K_I = 2P \left(\frac{m}{t t_n}\right) \qquad M = \frac{1}{t} + \frac{3a^2}{h^3}$$

Fig.4   The tapered double cantilever beam (TCB) specimen

38

P   P

$$K_I = \frac{MOMENT}{\sqrt{It}}$$

I IS INERTIA OF ONE ARM.
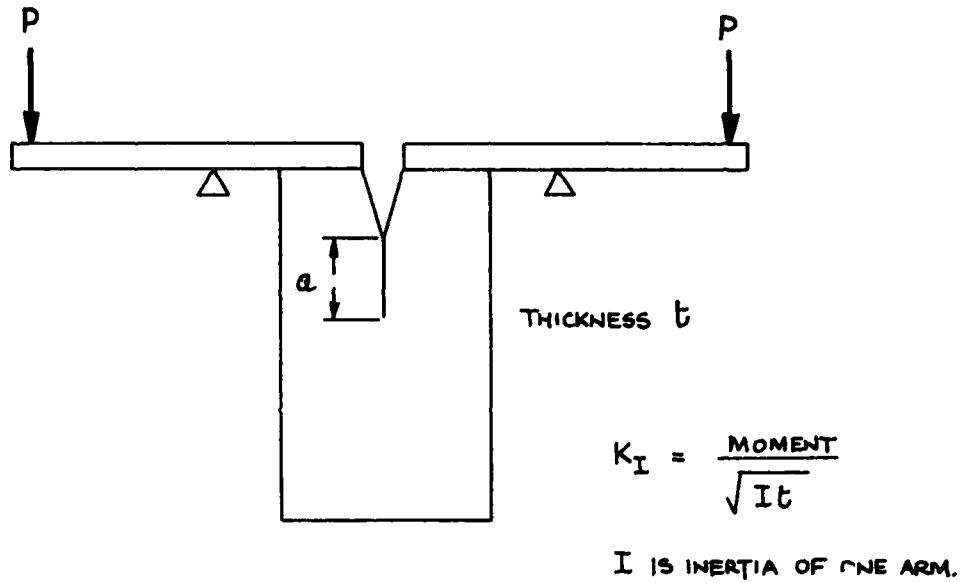
Fig.5   The constant moment specimen

$$K_I = PW_m \left[\frac{3(1+\nu)}{Wt^3 t_n} \right]^{\frac{1}{2}}$$
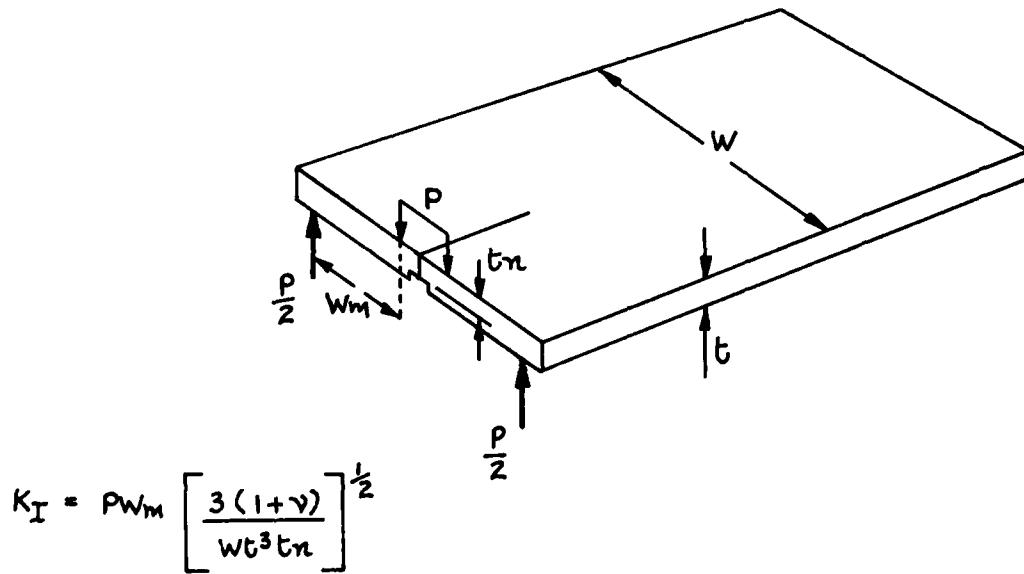
Fig.6   Double torsion (DT) specimen
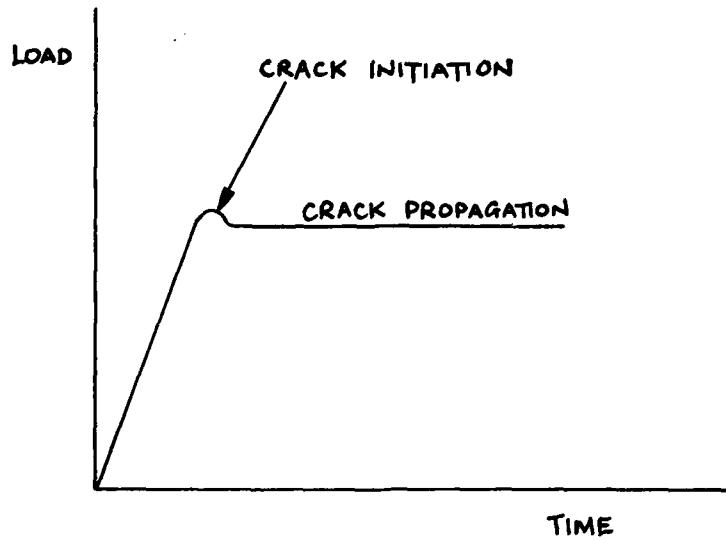
Fig.7 Constant displacement rate load/time graph used in pre-cracking constant K specimens
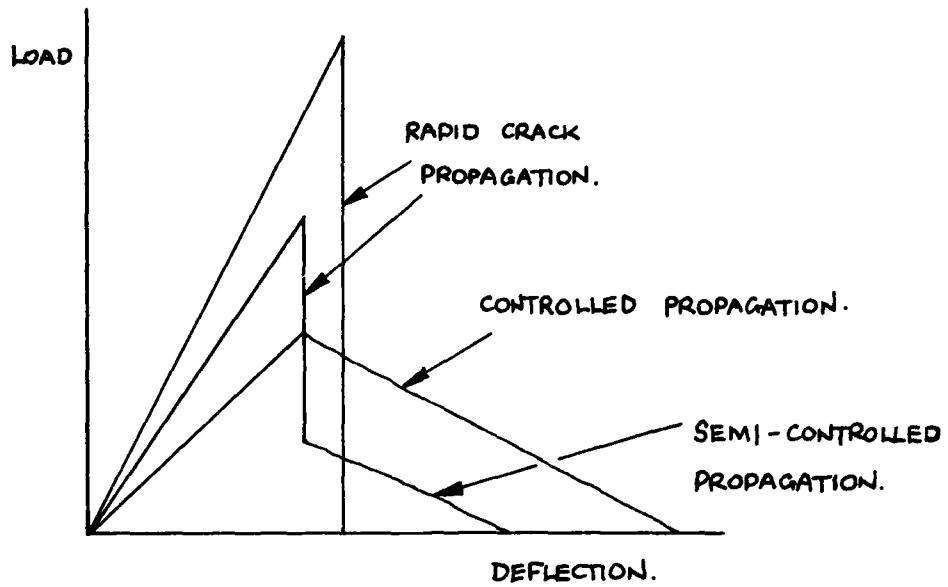
Fig.8 Load/deflection curves in work of fracture method

NEW DESIGN TECHNIQUES FOR BRITTLE MATERIALS

S. M. Wiederhorn and N. J. Tighe
Institute for Materials Research
National Bureau of Standards
Washington, DC   20234

A. G. Evans
Science Center
Rockwell International
Thousand Oaks, CA   91360

Abstract

Methods of design for improving the reliability of ceramics
in structural applications are described. Based on the science of
fracture mechanics, these methods provide a rational basis for
estimating the lifetime of structural components that are subjected
to applied loads. Data obtained by standard strength or fracture
mechanics techniques are used to develop design diagrams from
which component performance is evaluated. Three types of diagrams
are described, depending on whether the critical flaw size in a
component is estimated by nondestructive evaluation, proof testing,
or statistical evaluation. The validity of the theory has been
tested experimentally, and, on the whole, agreement between
theory and experiment is satisfactory. However, additional
experimentation is suggested to fully evaluate the limits of the
theory.

1.   Introduction

The anticipated use of ceramic materials in aerospace applications represent a new
challenge for engineers and scientists: the challenge of designing structural components
with brittle materials. Because ceramics are brittle, their strength is not a well-
defined quantity, but may vary widely for any given material. Thus, for glass that is
normally used in structural applications, the strength of a given test specimen may
vary by as much as 20% from the mean measured strength. This dispersion in strength
often becomes greater as the mean strength is increased, a behavior that is particularly
apparent for freshly drawn glass fibers. To complicate the situation even more, ceramic
materials exhibit a time delay to failure, so that the strength is actually a function
of time. Thus, a ceramic component will typically support an applied load for a period
of time and then fail abruptly, days, weeks, or even months after the first application
of load. The net result of this dispersion of strength and time delay to failure is to
severely reduce the allowable design stresses in ceramic components. This reduction in
allowable stresses results in the production of bulky components that are not consistent
with the need in aerospace applications for low weight. Thus, it is hoped that new
design techniques will not only increase the reliability of structural ceramics, but
also result in a net reduction in size and weight of structural components.

To understand the design techniques suggested in this paper, it is perhaps best to
discuss briefly the basic cause for dispersion of strength and delayed failure. These
phenomena result from the fact that ceramic materials are brittle: failure occurs
without perceptible plastic flow. As a consequence of this brittle behavior, ceramics
are extremely sensitive to sources of stress concentration, such as material defects
(flaws, cracks, or notches), or contact loads. In these situations, the plastic flow
that normally relieves localized stress concentrations in metals or plastics is absent
in ceramic materials. Therefore, the only way to relieve localized stresses in ceramics
is by fracture.

Surface cracks or flaws are a particularly severe form of stress concentration.
When loads are applied to ceramic materials that contain these defects, the stresses in
the vicinity of the defects often exceed the inherent strength of the ceramic component
at relatively low applied loads and, as a consequence, fracture occurs. Since the size
of these defects may vary widely, strength also varies widely, thus accounting for the
large dispersion in the strength of ceramic materials. Surface defects also account
for delayed failure because they are known to propagate as cracks under modest loads.
When the cracks reach a critical size, abrupt failure occurs. The time delay to
failure is the time necessary for these cracks to grow from a subcritical to a critical
size. Techniques that have been developed to improve the mechanical reliability of
ceramic components are all based on an improved understanding of how crack growth
affects strength. By characterizing the size and growth rate of cracks in ceramic
materials, it has proven possible to develop new techniques of improving the reliability
of ceramic components in structural applications.

This paper presents a review of design techniques that can be applied to ceramic
materials. In order to develop the subject in a logical sequence, a historical pro-
gression is followed. First, a brief discussion is presented of the basic phenomenon:
the occurrence of delayed failure, and the dependence of strength on the rate of loading.

42

Then a description is given of the use of fracture mechanics as a means of representing the time dependence of strength. Using fracture mechanics as a framework, it is shown how techniques of strength measurement, nondestructive analysis, and crack growth characterization can be used to improve structural reliability. Finally, laboratory procedures which are being employed to check the basic theory are described and results from laboratory measurements are presented.

2. Delayed Failure of Ceramic Materials

Delayed failure was first observed in glass by Grenet [1], who described the essential features of the phenomenon. When glass was subjected to a constant load, he found that the strength depended on the duration of the load: high strengths were recorded for short-term load durations while low strengths were recorded for long-term load durations. Grenet also found that when glass was loaded to failure at a constant rate of loading, the strength depended on the loading rate: the strength increased as the loading rate was increased. Other investigators have subsequently confirmed these observations on glass [2], and still others have shown them to be applicable for a wide range of ceramic materials [3]. Most often, delayed failure resulted from a stress enhanced chemical reaction between the test material and the environment. But, examples can also be noted where delayed failure occurred without the presence of a hostile environment.

Diagrams of the phenomenon of delayed failure are given in figure 1. Figure 1a shows the behavior that occurs when a ceramic test specimen or component is subjected to a static load. The failure time is found to increase as the applied load is decreased.
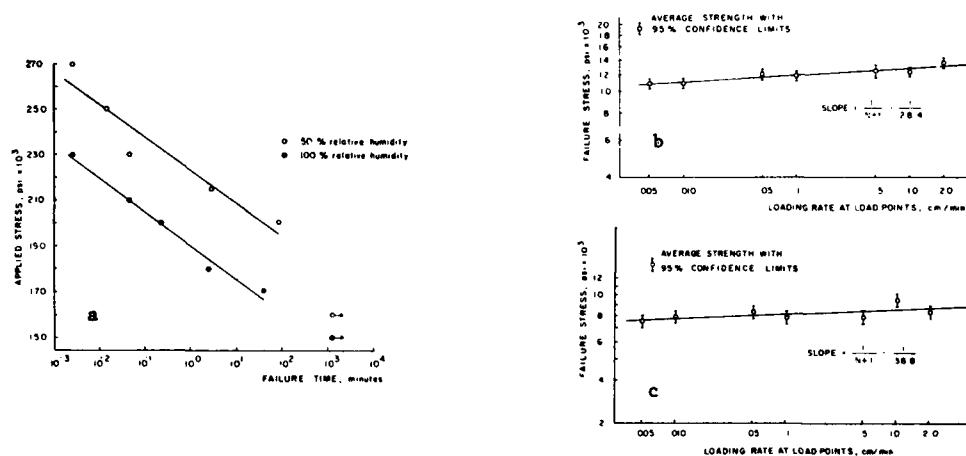

Figure 1. Illustrations of delayed failure in glass: (a) static loading, soda-lime-silicate glass. Loading rate experiments: (b) borosilicate glass, (c) fused silica [26].

At sufficiently low loads, however, a fatigue limit is often observed. This limit is the load below which failure will not occur regardless of the load duration. It should be noted from figure 1a that the load duration is a very strong function of the applied load, so that small changes in applied load result in large changes in load duration. Depending on the material being tested, a 50 percent change in load can result in a change of load duration of 4 to 10 orders of magnitude. As a consequence of this dependence of load duration on load, several types of equations have been used to represent these curves. These include power functions and exponential equations of various types. Because of its simplicity for analytical analysis, the power function representation is particularly appropriate for describing failure phenomena. Experimental data of the sort represented by figure 1a usually exhibits a large amount of scatter in the load duration: two orders of magnitude are not uncommon. This scatter in the data leads to a relatively large uncertainty in the data fit.

Figures 1b and 1c give a representation of the delayed failure process obtained from loading rate experiments. Here, we observe that as the loading rate is increased, the strength of the test components also increases. Though not usually observed, a static fatigue limit should also appear in this type of plot at extremely low rates of loading. The static fatigue limit on this type of plot is the strength below which there is no effect of loading rate upon strength. For the type of plot given in figures 1b and 1c, the scatter in the measured strengths is usually considerably less than that obtained for the load duration in figure 1a, so that a straight line can be fitted with greater confidence to the linear portion of the data. However, if the constant loading rate data were converted into load duration data, the uncertainty in the measured strength would reflect an equally large uncertainty in the calculated load duration.

It should also be noted from figures 1b and 1c, that the loading rate is a very strong function of the strength: the rate of loading changes over many orders of magnitude for small variations of strength. As with the time-to-failure data, the strong dependence of strength on loading rate means that the data can be expressed equally well by several different functional relationships between strength and loading rate.

The representations of delayed failure data shown in figures 1a, 1b, and 1c can be described analytically by the following two equations

$$t = A\sigma^{-n} \tag{1}$$

$$\sigma = B\dot{\sigma}^{1/(n+1)} \tag{2}$$

where t is the time-to-failure, σ is the strength or applied stress, and $\dot{\sigma}$ is the stressing rate. A, B, and n are experimental constants determined by a least-squares fit of the experimental data. As mentioned above, a logarithmic representation of the data is most useful because it simplifies analytical treatments of the data. The exponent of the loading rate in eq. (2) can be justified by theoretical treatments of the loading rate data [4,5]. Laboratory studies show that for a given environment and test material, n is a constant of the material that is independent of the surface treatment of the test specimens or the test specimen history. By contrast, the constants A and B depend on the specimen history and on the surface condition of the specimen. But for this fact, eqs. (1) and (2) could be used directly to obtain predictions of either failure-time, or failure strength. Therefore, one of the goals of developing new test techniques is to determine how these constants vary as a function of specimen history. The key to determining the dependence of the constants A and B on specimen history and surface condition was obtained through the use of fracture mechanics.

3. Fracture Mechanics Representation of Delayed Failure

3.1 Fracture Mechanics Framework

Fracture mechanics relates applied loads to the localized stresses or displacements in the vicinity of crack tips. Since these local displacements cause fracture, fracture mechanics affords a basic description of the fracture process. The fracture mechanics approach characterizes the stress, σ_{ij}, or displacement, u_{ij}, in the vicinity of the crack tip in terms of a parameter known as the stress intensity factor, K_I [6]:

$$\sigma_{ij} = K_I f_{ij}(\theta)/\sqrt{r} \tag{3a}$$

$$u_{ij} = K_I \sqrt{r} g_{ij}(\theta)/E \tag{3b}$$

where θ and r are respectively the angle and distance of a point from the crack tip (figure 2) and E is Young's modulus. For opening mode failure (where the applied
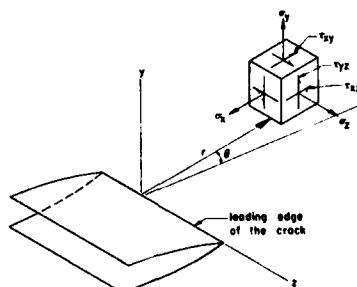

Figure 2. Coordinate relationship near a crack tip [6].

stresses are perpendicular to the crack plane) the radial and angular dependence of the stress fields are the same for all cracks regardless of shape or size. Therefore, the stress intensity factor gives the level of stress at the crack tip; by increasing the stress intensity factor, the stresses are increased. Because of the importance of the stress intensity factor with regard to the level of stress at the crack tip, it is this parameter that is used to characterize the motion of cracks when they are subjected to applied loads.

In practice, it is found that the crack velocity, v, in ceramic materials can be uniquely described by the stress intensity factor [3]. While the relationship between the two may be fairly complicated because of environmental considerations, it has been found experimentally that at low velocities, the following empirical relationship applies for most situations (fig. 3):

$$v = v_0 (K_I/K_o)^n. \tag{4}$$

v_0 and n are experimental constants determined by a fit of the crack propagation data, while K_o is an arbitrary constant used to normalize K_I. For a given environment and
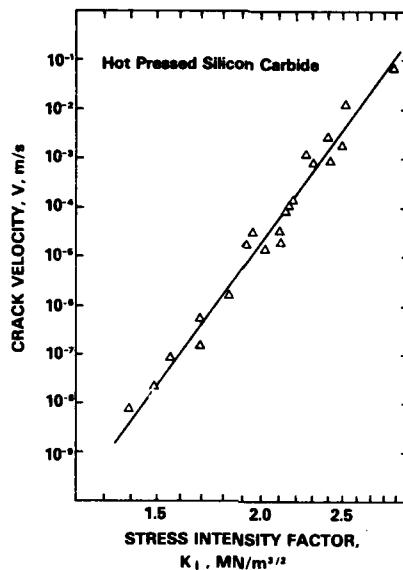

Figure 3. Crack velocity as a function of applied stress intensity factor. Hot pressed silicon carbide tested in air at 1400 °C [22].

material, v_0 and n may be considered material constants.* At low temperatures, the crack growth described by eq. (4) usually results from a chemical or physical interaction between components of the environment and the stress material at the crack tip [7]. While at high temperatures, crack growth is often caused by creep or diffusion at the crack tip [7]. These processes effectively weaken the material and permit crack growth to occur at crack tip stresses that are less than the inherent strength of the material in the absence of these processes. However, if the stress intensity factor is raised to a sufficiently high level, then the inherent strength of the material is exceeded at the crack tip and rapid crack growth occurs. The condition for rapid crack growth can be defined by a critical value of the stress intensity factor, K_{IC}. As with n and v_0, the critical stress intensity factor is also found to be a material constant.

Experimental techniques that are based on fracture mechanics can be used to obtain accurate measurements of v_0, n, and K_{IC} [8]. These techniques use large specimens that contain macroscopic size cracks so that accurate measurements of crack size can be made as a function of applied load. Elastic solutions of the specimen geometry can then be used to determine the stress intensity factor. The crack velocity is determined either by direct measurement or by a variety of indirect techniques. Because eqs. (1) and (2) can be derived from eq. (4), see below, it is usually considered that the parameters v_0, n, and K_{IC} determined in this way are directly applicable to the small cracks contained in ceramic components. Although several quantitative exceptions to this equivalence have been reported [9], the applicability of n, v_0, and K_{IC} to small cracks is supported by experimentation on a variety of materials [3]. Herein, this equivalence is assumed; but exceptions, when they occur, are discussed and rationalized.

For the small cracks typically encountered in ceramic components, the following equation relates the stress intensity factor to the applied stress, σ, and the crack length, a:

$$K_I = \sigma Y \sqrt{a} \tag{4}$$

where Y is a constant that depends on the crack geometry. For a simple penny-shaped crack in a uniform tensile stress field $Y = 2/\sqrt{\pi}$. If we assume that delayed failure is

---

* v_0 and n are also a function of microstructure, so in the characterization, of a material in terms of crack growth parameters, both chemical composition and micro-structure must be held constant.

due entirely to subcritical crack growth and that failure is instantaneous once the applied stress intensity factor reaches a critical value, the following equation for the time to failure under a constant applied stress can be derived from eqs. (4) and (5):

$$t = [2K_o^n(K_{IC}/\sigma_{IC})^{2-n}/v_oY^2(n-2)]\sigma^{-n} \tag{6}$$

where σ_{IC} is the strength of the component in an inert environment (i.e., subcritical crack growth does not precede abrupt failure). The inert strength σ_{IC} is not a material constant, but depends on the size distribution of critical flaws contained in the specimen through the relation;

$$\sigma_{IC} = K_{IC}/Y\sqrt{a} \ . \tag{7}$$

As such, it depends on surface condition and specimen history.

An equation for the strength as a function of loading rate has been obtained by Evans [5] using assumptions similar to those employed in the derivation of eq. (6)

$$\sigma = [2K_o^n(n+1)(K_{IC}/\sigma_{IC})^{2-n}/v_oY^2(n-2)]^{1/(n+1)} \ \dot\sigma^{1/(n+1)} \tag{8}$$

Two points should be noted about eqs. (6) and (8). First, as indicated above, they are in the same form as eqs. (1) and (2) and can therefore be used to describe the phenomenon of delayed failure. Second, the constants of these two equations are determined by the fracture mechanics parameters n, v_o, and K_{IC} and by the inert strength, σ_{IC} (or equivalently, the pre-existing flaw size distribution). The fracture mechanics parameters are easily evaluated by techniques that have been developed for this purpose. By contrast, the pre-existing flaw sizes are not so easily evaluated because the flaws are small (< 0.1 mm). Nevertheless, several techniques have been developed to estimate the flaw sizes.

3.2 Flaw Size Estimation Techniques

The pre-existing flaw size distribution in ceramic components can be determined in one of three ways: by direct measurement, by proof testing, and by statistical treatments of strength data. The direct measurement technique is commonly employed with metallic systems because the critical flaw sizes are generally quite large (>1 mm) and subcritical flaws can often be detected using techniques such as radiography, dye-penetrants, or ultrasonics. However, the direct detection of the much smaller (< 0.1 mm) subcritical flaws in ceramic materials requires the development of evaluation techniques with a greatly superior resolution than that attainable with present systems.

Probably the most promising technique for the detection of small flaws is ultrasonics [11,12]. With this technique, sound waves are sent through the material in an attempt to obtain detectable reflections from the critical flaws. For the critical cracks expected in structural ceramic materials, 10 to 100 μm, detectable scattering that contains sufficient information to enable flaw size and type to be deduced from the return signal requires that frequencies up to 400 MHz be used. The transducers and circuitry for generating and detecting this range of frequencies have recently been developed [12]. However, high frequency detection devices can be used only if the specimen does not cause excessive attenuation of the ultrasonic waves. In this regard, it has been shown that fine grained (or amorphous) nonporous ceramics (such as glass, hot-pressed silicon nitride, and hot-pressed silicon carbide) exhibit an acceptable attenuation up to 400 MHz, whereas coarse grained ($\gtrsim$ 20 μm) or porous ceramics are excessively attenuating at frequencies greater than $\sim$ 50 MHz. The ultrasonic technique may thus be usable only for the former class of materials.

Direct detection techniques require that the flaw type as well as the flaw size be determined because all flaws of a given size are not equally deleterious. For example, surface cracks that result from machining, large pores, and certain large inclusions can be a major source of premature failure; whereas many other inclusions are relatively innocuous. In order to obtain information about the size and type of the defect from the scattered ultrasonic signal, ultrasonic spectroscopy or imaging techniques can be used. The former appear to have the more immediate applications to ceramic systems, and requires that the return signal be frequency analyzed (using a fast Fourier transform for example) and possibly that the scattering be evaluated at several scattering angles. Instrumentation for this purpose is presently being assembled, using principles that have been sucessfully utilized for defect evaluation on metal systems at lower frequencies. Finally, since the scattering from defects with a similar acoustic impedence to the host material (e.g., certain inclusions, large grains) will be minimal, signal averaging instrumentation might be required to detect such defects. It is, of course, premature to define the role of ultrasonics in the overall flaw determination scheme, but the available high frequency results are encouraging and suggest that the technique will find applicaton on ceramic materials.

A second technique for establishing the critical flaw size in structural components is proof testing [10,13]. In proof testing, a load larger than expected in service is applied to the structural component. This load causes the fracture of specimens that contain flaws greater than a given size. Once the proof test has been applied to the specimens, one can assume that all weak components containing large flaws have been eliminated. The load applied during proof test establishes the minimum inert strength of the component. Thus, by substituting proof test stress, σ_p, into eqs. (6) or (8),

one obtains either a minimum expected failure time as a function of load duration, or a minimum strength as a function of rate of loading. The proof test technique does not have the problem of distinguishing between different types of flaws. However, proof testing has the distinct disadvantage that it can be applied only to ceramic components with relatively simple test geometries. The reason for this difficulty is that the stresses within the component during service must be exactly duplicated during the proof test to obtain valid results. Furthermore, the proof test has to be conducted in a relatively inert environment so that crack growth during the proof test loading does not become a serious problem. For some ceramic components, such as Si_3N_4, environmental considerations are not crucial because crack growth does not occur in air at room temperature. However for others, such as glass, air (which contains water vapor) must be avoided in order to obtain valid results.

The third technique for establishing the inert strength is based on statistical considerations [10,14]. The strength of a set of test specimens is measured in an inert environment. By ordering the strength data, the probability of failure, P, for each strength value is calculated from the following equation:

$$P = r/(R+1) \qquad (9)$$

where r is an integer which designates the position of the strength measurement in the ordered sequence (for the weakest component r = 1; for the second weakest r = 2; and so on), while R is the total number of strength measurements.

It is often observed that the inert strength is related to the failure probability by the following equation [15]:*

$$\sigma_{IC} = \sigma_0 [\ln(1-P)^{-1}]^{1/m} \qquad (10)$$

Equation (10) is obtained from Weibull statistics; m and σ_0 are empirical constants determined by fitting the strength data to the estimated probability for failure. By substituting the inert strength value from eq. (10) into eqs. (6) or (8), the time-to-failure or the strength can be expressed in terms of the failure probability. The use of statistics to describe the inert strength has some advantages over proof testing and nondestructive evaluation, because the constants that are used in the statistical equations can, in principle, be obtained on specimens that are much smaller and less expensive than the ceramic components. Once the constants of eq. (10) have been evaluated on laboratory specimens, they can be used to determine the strength distribution of larger components since statistical analyses provide us with scaling laws which indicate how the relationship between strength and probability changes with specimen size. In practice, the scaling laws are not always reliable because the flaw population may not be invariant; therefore, tests of strength should be performed on the actual components when possible. Even in conducting such tests, difficulties can be encountered because of the dependence of the flaw population on manufacturing parameters such as surface finish, chemical composition and microstructure. Despite these uncertainties, a statistical approach is often the only one that can be used when flaws are too small to be measured by nondestructive evaluation techniques and when proof testing is not feasible.

4. Strength Techniques As A Means for Assuring Reliability

Now that the fracture mechanics framework has been discussed, it will be shown how strength techniques can be used to assure the reliability of ceramic components. This approach to assuring reliability was first used by Davidge, et al. [14], who applied it to the statistical method of failure prediction, and then by Ritter and Meisel [9], who applied it to proof testing. Comparing eq. (1) with eq. (6), and eq. (2) with eq. (8), we see that the constants A and B can be determined entirely in terms of fracture mechanics parameters, and the inert strength, σ_{IC}. Since the inert strength is the only parameter in eqs. (6) and (8) that is not a material constant, it is this strength that determines how the constants A and B will transform.

Now, let us consider a set of ceramic components and a set of laboratory test specimens on which the delayed failure characteristics of the material are to be determined. The ceramic components are assumed to be characterized by the constant A_1 and by an inert strength, σ_{IC1}; while the laboratory test specimens are characterized by the constant A_2 and the inert strength, σ_{IC2}. The relationship between A_1 and A_2 is given by the following equation:

$$A_1 = A_2(\sigma_{IC1}/\sigma_{IC2})^{n-2} \qquad (11)$$

The relationship between B_1 for the ceramic components and B_2 for the laboratory test specimens is given by a similar equation:

$$B_1 = B_2(\sigma_{IC1}/\sigma_{IC2})^{(n-2)/(n+1)} \qquad (12)$$

---

*While the Weibull function (eq. (10)) is a convenient empirical respresentation of strength data, it is not a necessary part of the above analysis since the distribution function can be derived directly from the strength data [16].

The above equations may be used to rewrite eqs. (1) and (2) in a more general form:

$$t = A(\sigma_{IC1}/\sigma_{IC})^{n-2} \sigma^{-n} \tag{13}$$

$$\sigma = B(\sigma_{IC1}/\sigma_{IC})^{(n-2)/(n+1)} \dot{\sigma}^{1/(n+1)} \tag{14}$$

where the subscript 2 has been dropped from both equations. We emphasize that in these equations, σ_{IC} is the inert strength of laboratory specimens used to characterize the delayed failure of the material, while σ_{IC1} is the inert strength of the component, which must be estimated by one of the three techniques discussed in Section 3.2 (i.e., nondestructive evaluation, proof testing, or statistics).

Laboratory studies of the time-to-failure under a constant load are used to evaluate A, while strength measurements as a function of loading rate are used to evaluate B. The value of n can be estimated by either technique. If the proof test method is used to determine σ_{IC1} ($\sigma_{IC1} = \sigma_p$) then the equations obtained are identical to the ones suggested by Ritter and Meisel [9]. If the statistical method is used to determine σ_{IC1} ($\sigma_{IC1} = \sigma_o[\ln(1-P)^{-1}]^{1/m}$), then the equations obtained are identical to the ones first suggested by Davidge, et al [14].

Before turning from the subject of strength techniques, it is worth noting that the constants A and B are related:

$$B^{n+1} = A(n+1) \tag{15}$$

This means that the two constants can be freely interchanged in eqs. (13) and (14). Thus, by substituting eq. (15) into eq. (13) constant loading rate experiments can be used to evaluate the lifetime of components that are subjected to static loads. Conversely, constants obtained from static load experiments can be used to evaluate strength under constant loading rate conditions.

5. Design Diagrams

Equations (6) and (13), which were discussed in the last section, can be used to develop engineering design diagrams. As mentioned earlier, the constants of eqs. (6) and (13) may be obtained either by fracture mechanics techniques or by strength techniques. The inert strength is obtained by the three techniques discussed in Section 3.2, proof testing, statistics, or nondestructive evaluation. Each of these techniques of estimating σ_{IC} results in a specific design diagram that can be used to relate time to failure to applied load [10,14,17]. These diagrams will be discussed in this section.

Three types of design diagrams are shown in figures 4 through 6. Although these were obtained from crack propagation data, the same types of diagrams can be derived from strength measurement techniques. Thus, the diagrams generally represent the techniques discussed in this paper. Plotted on the diagrams is the failure time as a function of the service stress.
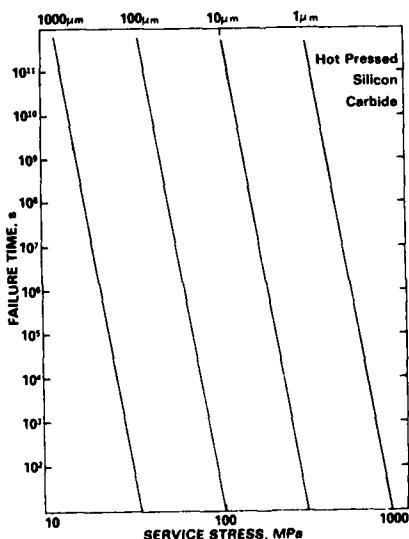

Figure 4. Design diagram based on direct flaw size measurement, silicon carbide [17].
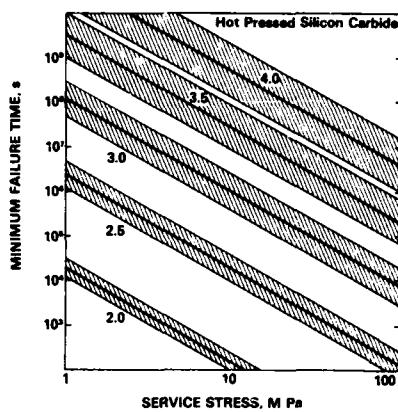
Figure 5. Design diagram based on proof testing, silicon carbide [17].
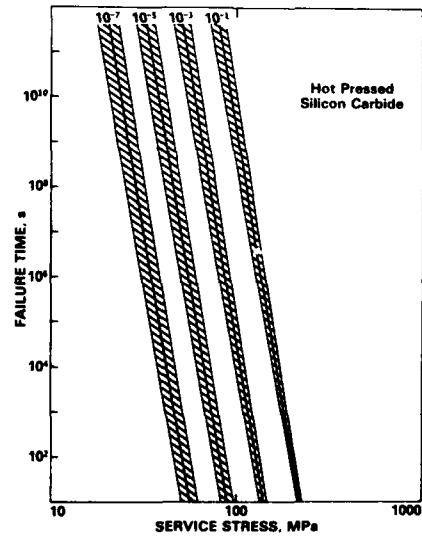

Figure 6. Design diagram based on statistical techniques, silicon carbide [17].

The error bands included on the proof test and statistical diagrams (figs. 5 and 6) are 90 percent confidence limits for the position of the central line [17]. The uncertainty in the position of these lines reflects the experimental scatter in the data that were used to calculate these diagrams. Though not included in figure 4, similar error bands are expected for the design diagram that is based on direct flaw size measurement. The error bands for figure 4 will depend on the accuracy of the flaw detection scheme. Since this accuracy is currently unknown (because the techniques of detection are just now being developed), error bands were not included in figure 4.

The design diagrams that are based on direct flaw size measurement are shown in figure 4. They contain a series of lines that relate the time-to-failure to the design stress. Each line has a slope of -n, and each represents a given flaw size, as marked on the diagram. As might be expected, the lines move to higher design stresses as the flaw size is decreased. The diagram gives the maximum flaw size that can be tolerated by a design and so sets the minimum limits needed for flaw detection by nondestructive techniques. Alternatively, if the flaw size is controlled by the microstructure of the material, then the diagram gives a relationship between failure time and service stress that should not be exceeded for safe design practice.

The design diagram based on proof testing (fig. 5) can be used to determine the proof test load needed to meet specific design criteria. The diagram has a series of lines on it, each surrounded by an uncertainty band. These lines relate the minimum time-to-failure to the service stress for specific values of the proof test ratio (the ratio of the proof test load to the design load). We see that as the proof test ratio increases, the position of the lines moves towards higher failure times and higher service stresses. In general, the higher the proof test ratio, the greater is the time that can be assured for component survival. This diagram is used to establish proof test loads for specific engineering conditions. If the engineer knows the minimum lifetime required for a given application, and the service stress that would have to be supported, then a proof test load can be selected from this diagram. The proof test technique is being seriously considered for use in the design of optical fibers for communication purposes. In this application, it is anticipated that the optical fibers one kilometer in length will be proof tested during the manufacturing process so as to break the fibers that are below a certain standard strength.

The design diagram based on statistical techniques (fig. 6) is similar in appearance to the one based on direct flaw size measurement. Each of the lines that relate failure time to service stress represents a given probability of failure. This diagram is essentially the same as the one suggested earlier by Davidge, et al [14]. For a given failure time, the service stress decreases as the failure probability decreases, as would be expected. The diagram can be used by engineers in a number of ways. If the probability of failure is known (i.e., the engineer is willing to accept a certain percentage of in-service failures), then either the failure time or the service stress can be selected if the other one is known. Alternatively, if the failure time and the service stress are known, then the chance of failure during service can be estimated.

In practice, the three types of diagrams should be used concurrently. The first step in design is to examine the statistical diagram and to determine if the material can meet engineering criteria without further testing. If the chance of failure is greater than can be accepted, then the possibility of proof testing should be investigated. It is worth noting that the number of failures during the proof test will be identical to that obtained from the probability diagram. If proof testing cannot be used for reasons of component geometry, then the flaw detection scheme should be investigated, in which case one must analyze the system to be used for flaw detection to determine whether it can detect flaws of sufficiently small size to satisfy the design criterion. Confidence requirements are taken into account by using the lower confidence limit as the basis for the above decisions [17].

An example of how proof testing has been used in combination with the statistical technique is shown in figure 7. The data in this figure was obtained by crack propagation techniques on a glass that was intended for use in the space shuttle vehicle [18,19].
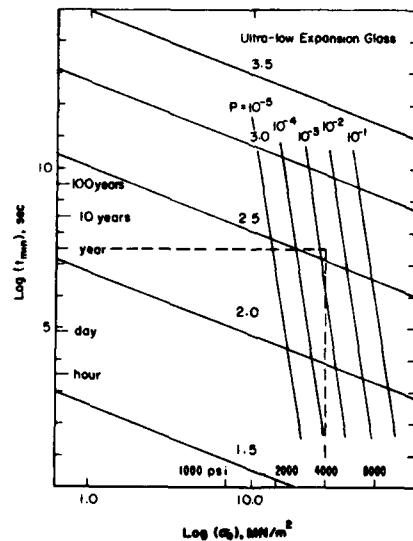

Figure 7. Illustration of the use of design diagrams for spacecraft windows [19].

Superimposed on the failure diagram are the lines derived from proof testing and lines derived from the statistical approach to design. In establishing the engineering requirements, it was known that the space shuttle windows would have to support a stress of approximately 30 MPa (4000 psi), and that under the most extreme conditions, this load would have to be supported for a period of one year. The two conditions defined a point on the plot from which it was determined that if the vehicle were sent up without proof testing, the chance of failure would be 1 in 500. The chance of failure was considered to be too high and it was decided that proof testing would be required. From the diagram, it can be seen that the proof test level of approximately 2.6 to 1 would be required for this application. Thus, a proof test load of 80 MPa

(11,000 psi) was required for a service load of 30 MPa (4,000 psi). During the proof test, it was expected that one out of 500 windows would fail. While the ultra-low expansion glass shown in figure 7 was never actually used, a similar procedure was followed with the silica glass that was eventually adopted for use in the space shuttle vehicle. This ratio was decided upon after examining data similar to that shown in figure 7.

6. Experimental Confirmation of Design Procedures

Up to this point, a theoretical basis for design techniques has been outlined and methods of developing design diagrams have been discussed. In this section, we review the available experimental data to see how they compare with the theory. Unfortunately, the data are not as plentiful as would be desired for a general confirmation of the theory and more work is clearly needed for this purpose.

Two approaches have been used to test the theory discussed in this paper. In one, the consistency of crack propagation data with strength data was checked by using the crack propagation data to calculate curves expected from the strength data (or vice versa). The second approach that has been used tests the predictions of the theory directly by measurements of strength distributions or failure times after proof testing.

The first approach was used by Wiederhorn, et al. [18], Evans and Johnson [20], Ritter and LaPorte [21], and Evans and Lange [22] to check the consistency of crack propagation data and strength data. Examples of their findings are found in figures 8, 9, and 10. In figures 8 and 9, the strength as a function of loading rate is presented for two glasses: an ultra-low expansion glass and a soda-lime-silicate glass. The data on these figures were collected by strength measurement techniques. For the ultra-low expansion glass, the dashed line in figure 8 represents the curve predicted from crack velocity data, while the solid line represents a least squares fit of the strength data. It is observed that the dashed line falls within the 95% confidence bars of the strength data. Thus, the crack propagation data compares favorably with the strength data. For the soda-lime-silicate glass, the data points in figure 9 represent specimen strength at 10, 50, and 90 percent failure probabilities, while the curves represent the strengths predicted from crack propagation data. Again we observe that the predicted and measured strengths agree quite well.
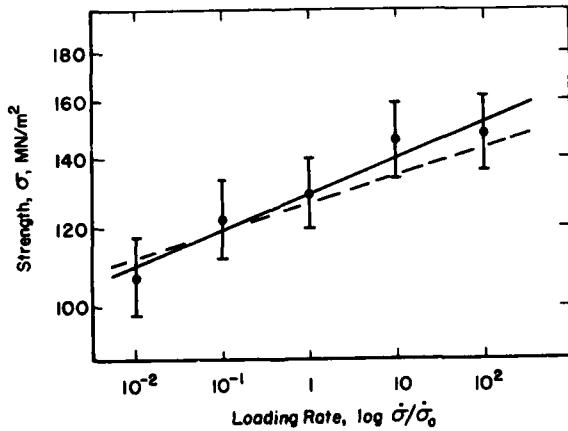

Figure 8. Strength as a function of loading rate, ultra-low expansion glass. Bars represent 95% confidence limits of data. Solid line is least squares fit of strength data. Dashed line was calculated from crack velocity data [18].
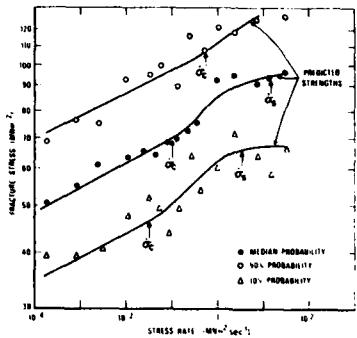
Figure 9. Strength as a function of loading rate, soda-lime-silicate glass. The solid lines represent curves calculated from crack propagation data [20].

Ritter and LaPorte have compared values of n obtained both by crack velocity and by strength techniques. Table 1 gives a summary of their results for a soda-lime-silicate glass and a chemical borosilicate glass. It is observed that n values obtained by crack velocity data are consistent with those obtained by strength measurement techniques for tests conducted in basic and neutral environments. However, for tests conducted in acidic environments, a serious inconsistency is found for the borosilicate glass. The agreement for data obtained on the soda-lime-silicate glass is also not as good in acidic environments as in the other environments.

Table 1. Comparison of strength and crack velocity data (abraded glass) [19]

Glass	Environment	n	
		Crack velocity	Strength
Soda-lime-silica	6N NaOH	19.4	19.5
	H_2O	16.6	13.0
	6N HCl	32.0	25.1
Borosilicate	6N NaOH	22.7	22.6
	H_2O	34.1	35.1
	6N HCl	57.1	26.9

Evans and Lange [22] have checked the consistency of strength and crack propagation data for hot-pressed silicon carbide (fig. 10). They show that the strength data obtained by flexural tests (solid lines in figure 10) are consistent with curves obtained from crack velocity predictions (dashed lines in figure 10).

The above sets of data are representative of those available in the literature. In most cases, a good comparison is obtained between crack growth data and strength data. However, some differences are found. These differences undoubtedly reflect the fact that small cracks contained in solid materials do not always behave in the same way as large ones contained in fracture mechanics specimens. The reasons for these discrepancies in results includes differences in crack tip compositions and local microstructure for the two types of test specimens. Thus, while a general consistency is found between crack growth data and strength data, differences that have been observed suggest that strength data should be used as a primary source of failure diagrams, except in circumstances where tests have been conducted to show that the two types of data are consistent.

52
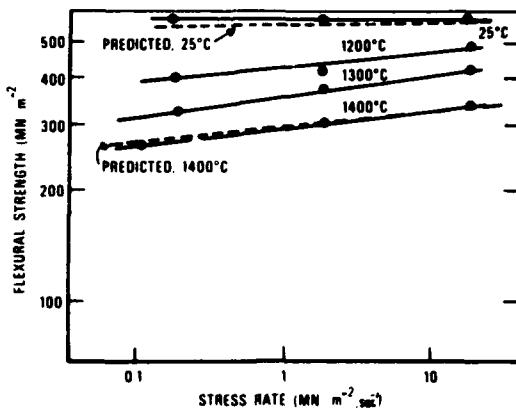
Figure 10. Strength as a function of loading rate, hot pressed silicon carbide.
Dashed lines calculated from crack propagation data at temperatures of 25 °C
and 1400 °C [22].

The second approach that has been used to check the basic theory is more direct
than that just discussed. Instead of checking the relationships between crack growth
rate and strength, the predictions of the theory are checked directly. Evans and
Wiederhorn [10], for example, checked the predictions of proof testing on soda-lime-
silicate glass by measuring the time-to-failure after proof test (figure 11). Several
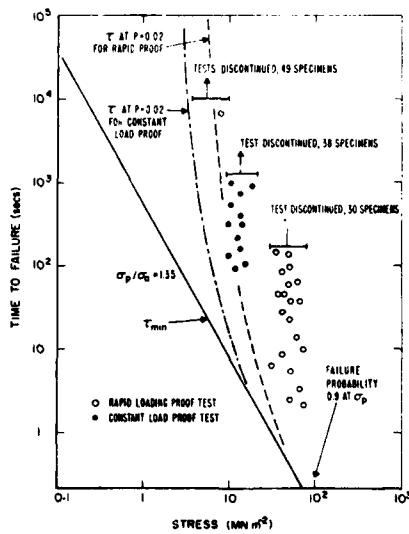

Figure 11. Measurements of time-to-failure after proof testing [10].

different proof test procedures were followed in their study. In no case did failure
occur in a time shorter than that predicted by the theory. The same data could also
be checked with the probability method of predicting failure time. As is noted in
figure 11 (dashed lines), failure occurred at a time greater than that predicted from
probability considerations. Ritter and Meisel [9] followed a procedure similar to
that used by Evans and Wiederhorn to show that the predicted times-to-failure were
always less than those actually measured experimentally. These studies suggest that
the theory discussed in this paper provides a conservative estimate of the failure
time in service. By contrast, Ritter has shown that predictions of failure times
based on the direct use of delayed failure curves without a fracture mechanics framework
can lead to erroneous results. In one case, he found that the experimental failure
time was less than that predicted from the direct application of delayed failure data.

This finding stresses the importance of using a fracture mechanics theory for predictions of times-to-failure.

Davidge, et al. [14], explored the validity of the statistical method of design. Using data obtained by fracture mechanic techniques, they developed a diagram that related survival probability and fracture stress to the rate of loading. The diagram, which they termed an SPT diagram, was based on eq. (7) of the present paper; σ_{IC} was determined by Weibull statistics (eq. (10)). Strength data obtained on aluminum oxide ceramics (Al_2O_3) were found to fall close to the theoretically predicted line ($\tau = 1$ sec) of the SPT diagram (fig. 12).
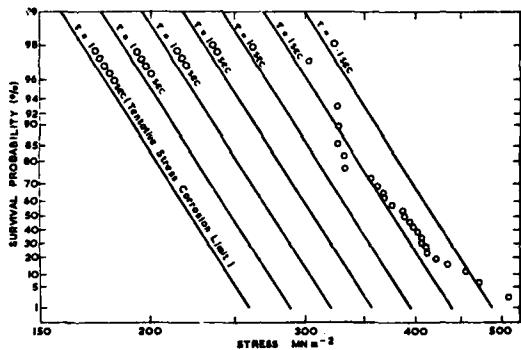

Figure 12. SPT diagram for Al_2O_3. Superimposed are delayed fracture data normalized to a failure time $\tau = 1$ sec [14].

Since the basic idea of proof testing is to truncate the stress distribution, and by so doing, eliminate all specimens that are weak, direct measurements can be conducted to test for truncation. This type of test procedure has been followed by a number of authors, Evans and Lange [22], for example (fig. 13), have shown that truncation occurs for silicon carbide that has been proof tested at 800 °C and tested for strength
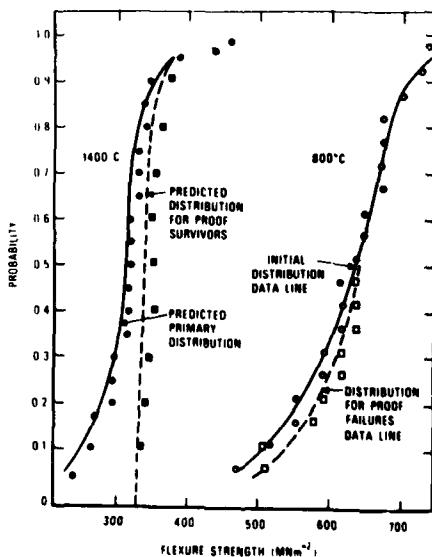

Figure 13. Effect of proof testing on the strength distribution of hot pressed silicon carbide [22].

at 1400 °C. Tighe [23] has demonstrated truncation for silicon nitride specimens that were proof tested at room temperature and similar results have been obtained for soda-lime-silicate glass [24,25]. The fact that truncation of the stress distribution is observed in these experiments reinforces the concept that proof testing can be used to establish design criteria for ceramic materials.

While the experiments described above support the theory presented in this paper, considerable additional experimentation is needed, both to further confirm the theory and to define the limits of application of the theory. Undoubtedly, there will be some systems which are not amendable to this approach, except perhaps in modified form: these include systems in which new flaws can be created after proof testing, or in which the flaw population changes with temperature. An example of the limitations of the approach was observed recently by Tighe on hot-pressed silicon nitride. Whereas truncation of the strength distribution of this material was obtained at room temperature, high temperature strength measurements after room temperature proof testing could discern no real difference between the silicon nitride that had been proof tested and that which had not been proof tested. For this material, proof testing at room temperature may not therefore be a viable procedure. However, elevated temperature proof testing, or proof testing of a pre-exposed sample may be applicable. There will undoubtedly be other materials for which similar problems can be expected. These materials can be identified only through extensive investigations that are designed to test these materials with regard to the theory presented in this paper.

7. Summary

This paper has presented a review of techniques that have been developed recently to assure the reliability of ceramic components in structural applications. Although fracture mechanics forms the basis of the failure prediction method, design diagrams that are developed through application of the method do not have to be obtained using fracture mechanics techniques. Instead, strength measurement techniques may be used to obtain these diagrams. To apply these methods of failure prediction, delayed failure in the ceramic components is first characterized either by crack propagation or strength measurement techniques. These basic data are then used to obtain failure diagrams. Three types of failure diagrams are obtained depending on whether the size of the critical flaw in the ceramic component is estimated by nondestructive evaluation, proof testing, or statistical evaluation. The three types of failure diagrams are used concurrently to evaluate the performance of a given component. The validity of the theory has been tested experimentally, and agreement between theory and experiment is generally satisfactory. However, additional experimentation is needed to fully evaluate the limits of the theory. Nevertheless, within its range of applicability, the theory provides a rational basis for design and is being used in a number of applications.

References

[1] L. Grenet, The Mechanical Strength of Glass, Bull. Soc. Encour. Ind. Mat. 4 (1899), p. 838; Translation in Glass Inc. 15 (1934), pp. 277-280.

[2] R. J. Charles, A Review of Glass Strength, in *Progress in Ceramic Science*, Vol. 1, J. E. Burke (Editor), New York, Pergamon Press (1961), pp. 1-38.

[3] S. M. Wiederhorn, Subcritical Crack Growth in Ceramics, in *Fracture Mechanics of Ceramics*, Vol. 2, R. C. Bradt, D. P. H. Hasselman, and F. F. Lange (Editors), New York, Pelnum Publishing Corporation (1974), pp. 613-646.

[4] R. J. Charles, Dynamic Fatigue of Glass, J. Appl. Phys. 29 (1958), pp. 1657-1662.

[5] A. G. Evans, Slow Crack Growth in Brittle Materials under Dynamic Loading Conditions, Int. J. Fracture, 10 (1974), pp. 251-259.

[6] P. C. Paris and G. C. Sih, Stress Analysis of Cracks, in *Fracture Toughness Testing and Its Applications*, ASTM Special Technical Publication No. 381 (1965) pp. 30-81.

[7] A. G. Evans and T. G. Langdon, Structural Ceramics, to be published in Progress in Materials Science.

[8] A. G. Evans, Fracture Mechanics Determinations, in *Fracture Mechanics of Ceramics*, Vol 1, R. C. Bradt, D. P. H. Hasselman, and F. F. Lange (Editors), New York, Plenum Publishing Corporation (1974), pp. 17-48.

[9] J. E. Ritter, Jr. and J. A. Meisel, Strength and Failure Predictions for Glass and Ceramics, J. Am. Ceram. Soc, Nov.-Dec. (1976).

[10] A. G. Evans and S. M. Wiederhorn, Proof Testing of Ceramic Materials--An Analytical Basis for Failure Prediction, Int. J. Fracture, 10 (1974), pp. 379-392.

[11] R. C. McMaster, *Nondestructive Testing Handbook*, Vol. II, New York, The Ronald Press Company (1959).

[12] A. G. Evans, B. R. Tittman, G. S. Kino, and P. Khuri-Yakub, Ultrasonic Flaw Detection in Ceramics, ARPA, AFML Report (Sept. 1976).

[13] C. F. Tiffany and J. N. Masters, Applied Fracture Mechanics, pp. 249-277, in reference 6.

[14] R. W. Davidge, J. R. McLaren, and G. Tappin, Strength-Probability-Time (SPT) Relationships in Ceramics, J. Mat. Sci. 8 (1973), pp. 1699-1705.

[15] W. Weibull, A Statistical Theory of the Strength of Materials, Ing. Vetenskaps. Akad. Handl., No. 151 (1939).

[16] J. R. Matthews, F. A. McClintock, and W. J. Shack, Statistical Determination of Surface Flaw Density in Brittle Materials, J. Am. Ceram. Soc., 59 (1976), pp. 304-308.

[17] S. M. Wiederhorn, E. R. Fuller, Jr., J. Mandel, and A. G. Evans, An Error Analysis of Failure Prediction Techniques Derived from Fracture Mechanics, J. Am. Ceram. Soc., Sept.-Oct. (1976).

[18] S. M. Wiederhorn, A. G. Evans, E. R. Fuller, Jr., and H. Johnson, Application of Fracture Mechanics to Space-Shuttle Windows, J. Am. Ceram. Soc. 57 (1974), pp. 319-323.

[19] S. M. Wiederhorn, Reliability, Life Prediction, and Proof Testing of Ceramics, in *Ceramics for High Performance Applications*, J. J. Burke, A. E. Gorum, and R. N. Katz (Editors), Chestnut Hill, Mass., Brook Hill Publishing Company (1974), pp. 633-663.

[20] A. G. Evans and H. Johnson, The Fracture Stress and Its Dependence on Slow Crack Growth, J. Mat. Sci. 10 (1975), pp. 214-222.

[21] J. E. Ritter, Jr. and R. P. LaPorte, Effect of Test Environment on Stress-Corrosion Susceptibility of Glass, J. Am. Ceram. Soc. 58 (1975), p. 265-267.

[22] A. G. Evans and F. F. Lange, Crack Propagation and Fracture in Silicon Carbide, J. Mat. Sci. 10 (1975), pp. 1659-1664.

[23] N. J. Tighe, unpublished results.

[24] E. R. Fuller and S. M. Wiederhorn, unpublished results.

[25] J. E. Ritter, Jr. and P. Oates, unpublished results.

[26] J. E. Ritter, Jr. and C. L. Sherburne, Dynamic and Static Fatigue of Silicate Glasses, J. Am. Ceram. Soc. 54 (1971), pp. 601-605.

AGARD

NATO ⊕ OTAN

7 RUE ANCELLE · 92200 NEUILLY-SUR-SEINE

FRANCE

Telephone 745.08.10 · Telex 610176

DISTRIBUTION OF UNCLASSIFIED AGARD PUBLICATIONS

AGARD does NOT hold stocks of AGARD publications at the above address for general distribution. Initial distribution of AGARD publications is made to AGARD Member Nations through the following National Distribution Centres. Further copies are sometimes available from these Centres, but if not may be purchased in Microfiche or Photocopy form from the Purchase Agencies listed below.

NATIONAL DISTRIBUTION CENTRES

BELGIUM
Coordonnateur AGARD – VSL
Etat-Major de la Force Aérienne
Caserne Prince Baudouin
Place Dailly, 1030 Bruxelles

CANADA
Defence Scientific Information Service
Department of National Defence
Ottawa, Ontario K1A OZ2

DENMARK
Danish Defence Research Board
Østerbrogades Kaserne
Copenhagen Ø

FRANCE
O.N.E.R.A. (Direction)
29 Avenue de la Division Leclerc
92 Châtillon sous Bagneux

GERMANY
Zentralstelle für Luft- und Raumfahrt-
dokumentation und -information
Postfach 860880
D-8 München 86

GREECE
Hellenic Armed Forces Command
D Branch, Athens

ICELAND
Director of Aviation
c/o Flugrad
Reykjavik

ITALY
Aeronautica Militare
Ufficio del Delegato Nazionale all'AGARD
3, Piazzale Adenauer
Roma/EUR

LUXEMBOURG
See Belgium

NETHERLANDS
Netherlands Delegation to AGARD
National Aerospace Laboratory, NLR
P.O. Box 126
Delft

NORWAY
Norwegian Defence Research Establishment
Main Library
P.O. Box 25
N-2007 Kjeller

PORTUGAL
Direccao do Servico de Material
da Forca Aerea
Rua de Escola Politecnica 42
Lisboa
Attn: AGARD National Delegate

TURKEY
Department of Research and Development (ARGE)
Ministry of National Defence, Ankara

UNITED KINGDOM
Defence Research Information Centre
Station Square House
St. Mary Cray
Orpington, Kent BR5 3RE

UNITED STATES
National Aeronautics and Space Administration (NASA),
Langley Field, Virginia 23365
Attn: Report Distribution and Storage Unit

THE UNITED STATES NATIONAL DISTRIBUTION CENTRE (NASA) DOES NOT HOLD
STOCKS OF AGARD PUBLICATIONS, AND APPLICATIONS FOR COPIES SHOULD BE MADE
DIRECT TO THE NATIONAL TECHNICAL INFORMATION SERVICE (NTIS) AT THE ADDRESS BELOW.

PURCHASE AGENCIES

Microfiche or Photocopy
National Technical
Information Service (NTIS)
5285 Port Royal Road
Springfield
Virginia 22151, USA

Microfiche
Space Documentation Service
European Space Agency
10, rue Mario Nikis
75015 Paris, France

Microfiche
Technology Reports
Centre (DTI)
Station Square House
St. Mary Cray
Orpington, Kent BR5 3RF
England

Requests for microfiche or photocopies of AGARD documents should include the AGARD serial number, title, author or editor, and publication date. Requests to NTIS should include the NASA accession report number. Full bibliographical references and abstracts of AGARD publications are given in the following journals:

Scientific and Technical Aerospace Reports (STAR),
published by NASA Scientific and Technical
Information Facility
Post Office Box 8757
Baltimore/Washington International Airport
Maryland 21240, USA

Government Reports Announcements (GRA),
published by the National Technical
Information Services, Springfield
Virginia 22151, USA